Unclassified

SECURITY CLASSIFICATION OF THIS PAGE

(2)

REPORT DOCUMENTATION PAGE

DTIC FILE COPY

Form Approved OMB No. 0704-0188

1a. REPORT SECURITY CLASSIFICATION Unclassified	1b. RESTRICTIVE MARKINGS
2a. SECURITY CLASSIFICATION AUTHORITY DTIC ELECTE NOV 16 1990 D	3. DISTRIBUTION/AVAILABILITY OF REPORT Approved for public release; distribution is unlimited.
2b. DECLASSIFICATION/DOWNGRADING SCHEDULE D	5. MONITORING ORGANIZATION REPORT NUMBER(S) AEOSR-TR- 90 1140
AD-A229 591	
6a. NAME OF PERFORMING ORGANIZATION Center for Propulsion Technology & Fluid Mechanics	6b. OFFICE SYMBOL (If applicable)
6c. ADDRESS (City, State, and ZIP Code) One Space Park Redondo Beach, CA 90278 TRW-Space Technology Group 213-812-4616	7a. NAME OF MONITORING ORGANIZATION AFOSR/NA
	7b. ADDRESS (City, State, and ZIP Code) Building 410, Bolling AFB, DC 20332-6448
8a. NAME OF FUNDING/SPONSORING ORGANIZATION AFOSR/NA	8b. OFFICE SYMBOL (If applicable) NA
8c. ADDRESS (City, State, and ZIP Code) Building 410, Bolling AFB, DC 20332-6448	9. PROCUREMENT INSTRUMENT IDENTIFICATION NUMBER F49620-87-C0081
	10. SOURCE OF FUNDING NUMBERS PROGRAM ELEMENT NO. 61102F; PROJECT NO. 2308; TASK NO. A2; WORK UNIT ACCESSION NO.

11. TITLE (Include Security Classification)
(U) Initiation and Modification of Reaction by Energy Addition: Kinetic and Transport Phenomena

12. PERSONAL AUTHOR(S)
Fendell, F. E., Chou, M. S., Zukowski, T. J., & Carrier, G. F.

13a. TYPE OF REPORT	13b. TIME COVERED	14. DATE OF REPORT (Year, Month, Day)	15. PAGE COUNT
Final	FROM 88-9-1 TO 90-9-1	90-10-1	150

16. SUPPLEMENTARY NOTATION

17. COSATI CODES		
FIELD	GROUP	SUB-GROUP

18. SUBJECT TERMS (Continue on reverse if necessary and identify by block number)
Laminar premixed flames; Photochemical ignition; Laser chemistry; Supersonic combustors; Oblique detonation wave engine

19. ABSTRACT (Continue on reverse if necessary and identify by block number)

Laboratory experiments, supplemented by approximate theoretical studies, have been carried out on the photochemical ignition of a flowing homogeneous gaseous fuel-oxidizer premixture by nonintrusive energy addition. In the experimental task, we have successfully demonstrated the ignition of H_2/O_2 and CH_4/O_2 mixtures with photolysis of NH_3, by use of an ArF laser at 193 nm. The minimum ignition energy density for a near-stoichiometric H_2/O_2 mixture is approximately 85 mJ/cm^3, which corresponds to an initial atomic-hydrogen concentration of about 8×10^{16} cm^{-3}. The OH emission monitored at three different locations in the irradiated volume suggests that the ignition occurs nearly homogeneously, with the ignition sites well distributed over the whole irradiated volume. The ignition-delay time based on the

20. DISTRIBUTION/AVAILABILITY OF ABSTRACT	21. ABSTRACT SECURITY CLASSIFICATION
☒ UNCLASSIFIED/UNLIMITED ☒ SAME AS RPT ☑ DTIC USERS	Unclassified
22a. NAME OF RESPONSIBLE INDIVIDUAL Julian M. Tishkoff	22b. TELEPHONE (Include Area Code) (202) 767-0465
	22c. OFFICE SYMBOL AFOSR/NA

DD Form 1473, JUN 86 Previous editions are obsolete.

SECURITY CLASSIFICATION OF THIS PAGE
Unclassified

216-5000 4/14/55

OH emission has been measured for several values of the incident laser energy, NH_3 concentration, and the fuel/oxidizer equivalence ratio. A typical ignition-delay time ranges from about 2 to 100 μs. The results of a computer-modeling calculation of the chemical kinetics suggest that the photolytically produced hot H atoms and vibrationally excited NH_2 play important roles in promoting the ignition chemistry.

The theory, by a combination of numerical and approximate analytic methods, examines the interaction of premixture stoichiometry, preferential diffusion (i.e., differing diffusivities for heat and species), and flame radius, with respect to the outward propagation of a laminar flame from a single spheroidal kernel (if a flame develops). Previously reported observations of the variation of the flame-front speed with flame radius, sometimes interpreted in terms of preferential-diffusion effects but probably better interpreted in terms of radiative heat loss, have been examined; the need exists for further spherical-flame-propagation experiments, with emphasis on measurements taken when the flame radius is more nearly comparable to the flame thickness.

The theory also considers the configuration of the (possibly multiply connected) unburned-gas/burned-gas interface that evolves when a train of rapidly repeated, brief pulses initiate a sequence of reacting kernels in a flowing mixture. Such nonintrusive deposition seems a means of stabilizing a combustion wave in a fast-flowing reactive mixture with minimal energy and power requirements. Many coplanar sites of energy deposition would be required to span (within a short downwind distance) a supersonic premixed stream with flame, if the lateral rate of flame propagation from each irradiated "blob" is typified by the modest deflagration-wave speed. However, if the nonintrusive energy deposition is rapid enough and substantial enough for the direct initiation of a detonation, then the lateral rate of effective flamespread is comparable to the streamwise supersonic speed of convection. The entire breadth of the premixed stream would be converted to product within a relatively very short distance downwind of a few coplanar sites of nonintrusive energy deposition. Thus, the direct photochemical initiation of detonation seems relevant to supersonic combustion with minimized entropy increase. The selfsimilar flow immediately downwind of a standing oblique (conical) detonation wave, and the subsequent expanding-nozzle configuration, have been discussed for a novel supersonic combustor.

PREFACE

The authors wish to thank Julian Tishkoff, the contract technical monitor, for helpful suggestions concerning future directions for the research, especially for comments during a visit to Redondo Beach, California in December 1988.

The following students have participated in research funded by this project as summer employees of TRW: Renee Chien, a mechanical engineering major entering the junior year at the University of California, Irvine; Scot Cook, an aeronautics major entering the junior year at the Massachusetts Institute of Technology; Michael Kezirian, a chemical engineering major entering the second year of graduate study at the Massachusetts Institute of Technology; Christopher Pallia, a chemistry major entering the senior year at the University of California, San Diego; and Monica Vazirani, a mathematics major entering the sophomore year at Harvard University.

TABLE OF CONTENTS

PROGRAM INFORMATION

Participants

George Carrier, professor of mechanical engineering, Harvard University, consultant

Renee Chien, mechanical engineering major, the University of California, Irvine, summer technical support (numerical analysis)

Mau-Song Chou, staff scientist, TRW, principal investigator, experimental task

Scot Cook, aeronautics major, Massachusetts Institute of Technology, summer technical support (numerical analysis)

Francis Fendell, staff engineer, TRW, principal investigator, theoretical task

Michael Kezirian, graduate student in chemical engineering, Massachusetts Institute of Technology, summer technical support (numerical analysis)

R. Daniel McGregor, senior project engineer, TRW, numerical analysis

Christopher Pallia, chemistry major, University of California, San Diego, summer technical support (numerical analysis)

Michael Petach, member of the technical staff, TRW, experiment construction and measurements

Michael Sheffield, member of the technical staff, TRW, numerical analysis

Monica Vazirani, mathematics major, Harvard University, summer technical support (numerical analysis)

Tmitri Zukowski, (former) member of the technical staff, TRW, experiment construction and measurements

Publications

Carrier, G. F., Fendell, F. E., and Sheffield, M. W. 1990 Stabilization of a planar flame by localized energy addition. AIAA Journal 28, 625-630.

Carrier, G., Fendell, F., Chen, K., and Pallia, C. 1990 Evaluating a simple model for laminar-flame-propagation rates. I. Planar geometry. Combustion Science and Technology, in review.

Carrier, G., Fendell, F., Chen, K. and Cook, S. 1990 Evaluating a simple model for laminar-flame-propagation rates. II. Spherical geometry. Combustion Science and Technology, in review.

Carrier, G., Fendell, F., McGregor, D., Cook, S., and Vazirani, M. 1990 Laser-initiated conical detonation wave for supersonic combustion. Journal of Propulsion and Power, in review. [Also, AIAA Paper 91-0578, 29th Aerospace Sciences Meeting, January 1991, Reno, Nevada.]

Chou, M.-S., and Zukowski, T. J. 1990 Ignition of $H_2/O_2/NH_3$, $H_2/Air/NH_3$ and $CH_4/O_2/NH_3$ premixed flow by excimer laser photolysis of NH_3. Combustion and Flame, in review.

Fendell, F. E., Kung, E. Y., and Sheffield, M. W. 1990 The flame configuration associated with localized energy addition to a combustible mixture. Journal of Propulsion and Power, in review.

Presentations

"Stabilization of premixed planar flame by localized energy addition," by F. E. Fendell, AIAA 27th Aerospace Sciences Meeting, January 1989, Reno, NV (Paper 89-0155).

"Ignition of $H_2/O_2/NH_3$, $H_2/Air/NH_3$ and $CH_4/O_2/NH_3$ premixed flows by excimer laser photolysis of NH_3," by M.-S. Chou, Fall Meeting, Western States Section, Combustion Institute, October 1989, Livermore, CA (Paper 89-94).

"Laser-initiated conical detonation wave for supersonic combustion," by F. E. Fendell, AIAA 29th Aerospace Sciences Meeting, January 1991, Reno, NV (Paper 91-0578).

Significant Interactions

Technical discussions with E. A. Lezberg, NASA Lewis Research Center, and G. B. Northam, NASA Langley Research Center, at the AFOSR Propulsion Contractors Meeting, June 1990, Atlanta, GA.

1.0 RESEARCH OBJECTIVES

In high-speed air-breathing combustion systems, a premium is placed on the complete release of chemical energy during the relatively brief residence time of reactants within combustors of practical length: mixing, ignition, and chemical reaction must be achieved in a relatively short time. We address, from a fundamental chemical-dynamics and fluid-transport point of view, the use of both alternative, photochemical ignition (by laser irradiation) and ignition-promoting additives, in order to alter chemical-reaction pathways to achieve rapid ignition and enhanced combustion rate. We address the influence of mixture inhomogeneity, and of departure from stoichiometric proportion in fuel/air mixtures, on the processes of ignition, flame development, and flame propagation. Chemical systems of particular interest include hydrogen/air and methane/air, often with trace amounts of carefully selected sensitizers. We identify, by irradiating premixtures flowing faster than the adiabatic flame speed, and by carrying out supporting approximate analyses of these experiments, optimal circumstances [minimal input energy, minimal amount of sensitizer(s), etc.] for achieving ignition and burnup with currently available optical sources.

A far more detailed exposition of the goals, background, and relevant literature may be found in the two earlier annual reports issued on this project (Fendell, Chou, Zukowski, and Carrier 1988, 1989). In the interest of brevity, for the discussion which follows, the reader is taken to be aware of the contents of those earlier reports.

2.0 ANALYSIS

The aerodynamics associated with flame stabilization in high-speed reactive flows, for propulsion objectives, has been the subject of the analytical efforts undertaken in this project. The novel flame-stabilization mechanism under study is based on the efficient absorption of energy nonintrusively deposited into combustible gaseous mixtures by use of modern optical sources (lasers). The experiments carried out with lasers in this project demonstrate the existing capability to initiate deflagration waves; the complete international literature on the use of lasers operating at many different frequencies to achieve ignition in sensitized or unsensitized mixtures of various reactants over a wide range of stoichiometries is now extremely voluminous. Further, the direct photochemical initiation of detonations in highly subatmospheric-pressure gaseous mixtures composed of various constituents was first reported a dozen years ago by use of xenon flashlamps (Lee et al. 1978). Here we attempt to elucidate by analysis a few of the new flame-stabilization possibilities (for high-speed air-breathing propulsion) that may become feasible as laser technology evolves. In particular, we anticipate that very rapidly repeatedly pulsed, energetic lasers that are both compact and reliable may be achieved within a couple of decades.

Attention was initially concentrated on the continuous nonintrusive deposition of laser radiation, efficiently absorbed by a uniform reactive mixture. The mixture is taken to be flowing very subsonically, but still supercritically, i.e., still faster than the deflagration-wave speed, so that a special provision such as energy deposition is required to preclude flame blowoff. The situation is the counterpart of the more familiar use (e.g., in a flat-flame burner) of energy extraction to preclude flashback in a subcritically flowing mixture. With energy deposition, the burned-gas temperature is in general in excess of the adiabatic flame temperature, whereas, with energy extraction, the burned-gas temperature is in general less than the adiabatic flame temperature. The early studies in this project concentrated on planar, line, and point radiant-energy sources, such that, respectively, one-dimensional, two-dimensional, and axisymmetric flames were stabilized (Carrier et al. 1990; Fendell et al. 1990). Only in the planar case is the solution analytically tractable for the large-heat-release conditions characteristic of combustion; for the line and point sources, analytic solution is tractable only for the limit of vanishingly small heat release, because large chemical exothermicity introduces aspects to the dynamics that necessitate numerical treatment. Such investment in numerical solution may not be warranted because stabilization by a continuous nonintrusive source is not

likely to be practically exploited, though such a demonstration in the laboratory may soon be feasible, and would mark a noteworthy, instructive milestone. The practical difficulty with a continuous deposition for flame stabilization is that the deposition is into burned mixture (since the flame is situated upwind of the deposition site), and needs to be relatively large (since every element of near-source mass throughput must be irradiated to preclude blowoff). For a planar flame, this means the energy deposition must be achieved uniformly across the entire deposition plane; for a line or point source, only that mass throughput passing near the source need be augmented in enthalpy, but the energy-deposition requirement is still demanding relative to that for a rapidly repeatedly pulsed source.

For the intermittent source, only enough radiant energy need be deposited to initiate discrete flame kernels; as each flame kernel is convected downwind by the flow, the flame evolving from the kernel propagates toward the flame evolving from the prior kernel and the flame evolving from the subsequent kernel, until the intervening reactive mixture is converted to product at some downwind distance. The flame of each kernel, then, envelopes already-burned mixture, and propagates into unburned mixture (see Appendices 1 and 2).[1] Since the same element of mixture cannot be burned twice, the initially multiply-connected

---

[1]The interplay of stoichiometry, differing diffusivities, and flame curvature in the early radially-outward propagation of a single spherical flame kernel in an unbounded expanse of combustible mixture has been the subject of experimental and theoretical inquiry over the last decade, but misinterpretations (Frankel and Sivashinsky 1983; Strehlow 1984) may have arisen. It is true that, if a reactant is both stoichiometrically deficient and relatively fast-diffusing, then theoretically the speed of a spherical flamefront may be greater at a smaller flamefront radius, at which curvature effects are significant, than at a larger flamefront radius, at which the propagation is effectively planar. What is less clear is whether such an effect occurs for parameter values arising in practice; what is even more doubtful is whether certain experiments (Palm-Leis 1966; Palm-Leis and Strehlow 1969) are evidence of such an effect, since the data are taken at flame radii much larger than the flame thickness; furthermore, the effect is observed only at sufficiently fuel-rich stoichiometries in propane-air mixtures (such that radiative heat loss seems an alternative explanation of the decrease of flamefront speed with increasing flamefront radius), and is not observed at any stoichiometry in methane-air mixtures (which have a smaller propensity to produce soot). At any stoichiometry tested, the observed flamefront speeds in the cited spherical-flame experiments either fail to approach an asymptote even at 8-9-cm radius, or approach an asymptote inconsistent with the density-ratio-adjusted laminar-planar-flame-speed value. There appears to remain a need for definitive spherical-flame-propagation experiments, with emphasis on data taken at small flamefront radii, in order to elucidate unresolved issues concerning flame-kernel development. These suggested combustion experiments are not concerned with the exotic photochemistry of energy deposition; in fact, ideally, no residuals of the ignition process would remain even at very early times in the spherical-flame-kernel evolution.

flames merge to form a "scalloped" reacting front circumscribed by the flame locus engendered by a continuous line or point source depositing energy at the same site as the intermittent (say, periodic) point or line source. Even if some of the kernels do not spawn flames, eventually all the intervening mixture is converted to product -- but the conversion occurs further downwind. However, if the convective speed of the flowing reactants far exceeds the propagation speed of the premixture (and, at one atmosphere, the laminar propagation speed of even a stoichiometric hydrogen/air mixture is but about 2 m/s), then significant lateral spread to span a stream with flame via deflagration occurs only far, far downwind. One might seek to deposit pulses at several lateral sites to shorten the streamwise distance for reactant conversion to product; this procedure not only incurs more complication with the source technology, but also may incur large pressure loss and high entropy rise owing to the possible initiation of a strong (normal) detonation!

Thus, the most viable procedure to span a supersonic stream of reactant with flame within a short streamwise distance of a site of nonintrusive energy deposition would appear to be the direct initiation of a detonation. As with the stabilization of a deflagration wave in a stream of mixture flowing at a modestly supercritical speed, so with the stabilization of a detonation in a stream of mixture flowing supersonically: the least energy and power requirement is associated with a very rapidly repeated source, rather than with a continuous source (which might lead to a locally normal detonation). Also, analogously, the spherical detonations initiated by a long train of pulses interact to form a scalloped detonation wave. As the interval between laser pulses vanishes, the pressure losses owing to the reflected shocks that arise from the interaction of neighboring spherical detonations also vanish, and a nearly conical detonation wave is formed. The word nearly is introduced in that a cellular structure arises in connection with spherical detonations (Lee 1977, 1984); however, the finite structure of this conical detonation seems a detail of minor practical consequence. The flow downwind of this (weak, oblique) conical detonation may be modeled as steady supersonic inviscid and axisymmetric; in fact, it is also selfsimilar and readily described in quantitative detail (see Appendix 3).

The concept of basing a supersonic combustor (i.e., a combustor in which the flow is everywhere supersonic) on a standing (i.e., stabilized) oblique detonation wave was first proposed decades ago (e.g., Gross and Chinitz 1960). The concept seems a viable alternative to the mixing-controlled supersonic-diffusion-flame designs that have received the preponderance of attention from supersonic-

combustor designers. However, previously, emphasis has been placed on the intrusion into the reacting stream of a symmetrically positioned right circular cone of finite length. The potential difficulties with such a design (or its two-dimensional analogue, the intrusion of a symmetrically positioned wedge of finite length) are many: additional frictional drag is incurred; all such bodies in practice will be somewhat blunted and subject to jitter, such that an at least locally normal detonation occurs, with associated pressure losses; and, for the high-altitude-flight conditions of interest, the pressure achieved even in the weakly shocked flow may be low enough that, in the absence of a positive ignition device, induction times for reaction may result in impracticable long combustors. Even if a conical detonation wave is supported by a pointed cone, the wave is likely to incur a larger entropy increase than the increase associated with a pulsed-laser-induced wave. Whenever a laser with the energy, power, and repetition rate is available, it seems clearly a superior alternative to the introduction of an intrusive cone.

Downwind of the axial plane at which the conical detonation wave intersects the surrounding container, the selfsimilar nature of the flow in the shocked and reacted gas no longer holds; that is, information is passed through the post-detonation flow of a finite physical length (the radius of the combustor wall). In fact, the container downwind of the detonation-wave/combustor-wall interaction must flare appropriately to accommodate an expansion: too great a flaring results in flow separation and effectively no thrust, and too little a flaring results in compressional shocks, regions of locally subsonic flow, and large pressure losses. Detailed refined design of a nozzle (to expand efficiently the shocked and reacted gas from the high-pressure levels of the selfsimilar flow to a flow that is laterally uniform at the ambient pressure) seems not properly the function of a basic inquiry into supersonic combustors. Nevertheless, it seems crucial to establish that one can design a short nozzle that can convert high-pressure conditions to high-flow-speed conditions, such that the associated thrust far exceeds the pressure drag incurred by the ambient streaming past the combustor. [At the hypersonic conditions of interest, the pressure drag does far exceed the frictional drag, and the pressure drag can be estimated simply but adequately by the Newtonian approximation (no rebounding of ambient-flow molecules that make contact with the enveloping combustor container)]. No proof of principle of the feasibility of a laser-initiated oblique-detonation-wave engine seems complete without evidence that such a properly flared nozzle can be identified. Thus, this inverse nozzle-flow exercise (given the "entrance" and "exit"

conditions, design a nozzle, so the flow can undergo the transition between the conditions within a short streamwise distance) is pursued by trail-and-error numerical calculations with candidate container configurations.

The laser-initiated oblique-detonation-wave engine presumes the prior formation of a fuel-air mixture. However, while there must be sufficiently large fraction of the flowing gaseous mixture that is detonable, there is no requirement that the entire mixture be so constituted. In fact, we have speculated that there may be performance advantages if one could so tailor the flowing mixture that a fraction would consist of millimeter-sized blobs of unmixed fuel and air in stoichiometric proportion. Such blobs would be compressed but unburned during passage through the conical detonation, in which the well-mixed portion of the mixture is converted to hot product gas. Downwind of the detonation the blobs would be converted in the hot surrounding gas, by a diffusionally controlled reaction.

On the basis of the above line of inquiry, we believe that one remaining task of high priority concerns the efficient mixing, without reaction or strong shocks, of fuels of interest (such as hydrogen) into a supersonic airstream; such a task is probably most productively pursued experimentally. Another task of high priority concerns systematic laboratory experimentation to establish what amount of energy, what time of deposition, and what focal volume permits the direct photochemical initiation of detonation in a (stagnant) mixture of a composition, and at a thermodynamic state, of interest. Also, the interaction of two such spherical detonations, set off in close proximity in space and time (but <u>not</u> precisely coincidentally or simultaneously) in a stagnant mixture, should be experimentally examined to be certain that no overlooked, large-entropy-producing phenomena would occur to frustrate the achievement of small-pressure-loss, low-entropy-rise supersonic combustion via the above-sketched laser-initiated oblique-detonation-wave engine. Further, for completeness, the interaction of a spherical detonation wave with a container wall might be worth laboratory examination to be certain that no here-unanticipated complications arise in connection with the accompanying noise, vibration, or reflected shock -- though we propose to flare the container wall to avoid detonation-wave/container-wall interaction.

3.0 EXPERIMENT

The results achieved under the experimental task are reported in Appendix IV.

REFERENCES

Carrier, G. F., Fendell, F. E., and Sheffield, M. W. 1990 Stabilization of a premixed planar flame by localized energy addition. AIAA Journal 28, 625-630.

Fendell, F. E., Chou, M.-S., Zukowski, T. J., and Carrier, G. F. 1988 Initiation and modification of reaction by energy addition: kinetic and transport phenomena. First annual report. Bolling Air Force Base, DC: Aerospace Sciences Directorate, Air Force Office of Scientific Research.

Fendell, F. E., Chou, M.-S., Zukowski, T. J., and Carrier, G. F. 1989 Initiation and modification of reaction by energy addition: kinetic and transport phenomena. Second annual report. Bolling Air Force Base, DC: Aerospace Sciences Directorate, Air Force Office of Scientific Research.

Fendell, F. E., Kung, E. Y., and Sheffield, M. W. 1990 The flame configuration associated with localized energy addition to a combustible mixture. Journal of Propulsion and Power, in review.

Frankel, M. L., and Sivashinksy, G. I. 1983 On effects due to thermal expansion and Lewis number in spherical flame propagation. Combustion Science and Technology 31, 131-138.

Gross, R. A., and Chinitz, W. 1960 A study of supersonic combustion. Journal of the Aero/Space Sciences 27, 517-524, 534.

Lee, J. H. S. 1977 Initiation of gaseous detonations. Annual Review of Physical Chemistry 28, 75-104.

Lee, J. H. S. 1984 Dynamic parameters of gaseous detonations. Annual Review of Fluid Mechanics 16, 311-336.

Lee, J. H., Knystautas, R., and Yoshikawa, N. 1978 Photochemical initiation of gaseous detonations. Acta Astronautica 5, 971-982.

Palm-Leis, A. 1966 Transient behavior of free flames in laminar and turbulent media. Ph.D. thesis. Urbana, IL: Department of Aeronautical and Astronautical Engineering, University of Illinois.

Palm-Leis, A., and Strehlow, R. A. 1969 On the propagation of turbulent flames. Combustion and Flames 13, 111-129.

Strehlow, R. A. 1984 Combustion Fundamentals. New York, NY: McGraw-Hill.

APPENDIX I.

Evaluating a Simple Model for Laminar-Flame-Propagation Rates. I. Planar Geometry

G. Carrier, F. Fendell, K. Chen, and C. Pallia

TRW Space and Technology Group
Redondo Beach, CA 90278

(Submitted to Combustion Science and Technology)

A comparison with experimental flame-speed data is made for results from a simple formulation, conveniently reducible to quadrature, of laminar isobaric flame propagation in an initially homogeneous gaseous mixture. A direct one-step irreversible bimolecular second-order chemical reaction with large Arrhenius activation energy is adopted, but account is taken of the modified exothermicity owing to partial dissociation of the product species and to other causes of incomplete oxidation. The effects arising from differing diffusivities for heat transfer and reactant-species transport are developed to within the limitations of the model. A tractable general expression is obtained for the steady-laminar-flame-propagation speed, by exploitation of the two-zone (convective-diffusive, diffusive-reactive) deflagration-wave structure. For simple-fuel/air mixtures, the predicted variation of flame speed with equivalence ratio ϕ agrees fairly well with experimental data, with the provision that (1) the cold-mixture transport properties are evaluated for the pertinent value of ϕ, and (2) the overall activation energy, taken to be invariant with ϕ, is ascribed values in the 10-15 kcal/mole range. In particular, the experimentally observed off-stoichiometric (often fuel-rich) condition for peak flame speed in simple-fuel/air premixtures is recovered. However, for simple-fuel/oxygen mixtures, the predictions deviate from the data, although the sense of the stoichiometry for which the peak speed occurs is recovered. Finally, observations concerning the transient planar deflagration wave are made, as background useful for a study of spherical flame propagation, to be reported separately.

1. INTRODUCTION

1.1 Objectives

This work stems from an interest in the multiparameter dependence of the flame speed of a spherical flame on its radius, on the transport properties of the reactants, and on the stoichiometry of the combustible mixture (Strehlow 1984). For the ease of interpretation of results, in view of this multiparameter dependence, it is advantageous first to present an analysis of (planar) one-dimensional flames; spherically propagating flames are then treated in a companion study (Carrier et al. 1990).

We adopt a basic, well-established but approximate formulation. It does not serve our purpose to dwell at length on identifying the most general formulation tractable for a reduction to quadratures, the form to which we seek to express the solution; thus, the model could be generalized at several turns. We note

that, for the convenience of nondimensionalization, we refer temperature, density, and several parameters to their ambient (unburned) values, because we are interested in a comparison of the predicted flame-propagation speed with families of experiments wherein the individual members of each family involve a (mostly) common initial (unburnt) thermodynamic state.

We assign parameters observed or plausible values and then evaluate the predictive accuracy for simple-fuel/oxidizer mixtures. For example, we do not assign the orders of reaction to have fractional, even negative values, in order to try to match flammability-limit data (an adiabatic model inherently cannot predict such limits -- cf. Westbrook and Dryer 1981). Neither do we assign the activation energy a variation with equivalence ratio to curve fit the results of an equal-diffusion-coefficient model to flame-propagation-speed data (cf. Coffee et al. 1983,1984).

1.2 Formulation

We adopt a direct one-step bimolecular second-order irreversible chemical reaction. The entirely gaseous product species are formed by burning a pure gaseous fuel F (e.g., hydrogen or a simple hydrocarbon) either in oxygen or in air (while nitrogen could be replaced by some other inert gas for purposes of inquiry, we develop in terms of nitrogen)

$$\nu_F \, F + \nu_O \, O \rightarrow \text{product(s)} + Q, \tag{1.1}$$

where Q is the heat evolved from burning with oxygen O, with ν_i denoting the stoichiometric coefficient of species i for complete oxidation of the fuel to CO_2 and H_2O. In fact, the products vary appreciably as conditions change (e.g., from significantly fuel-rich to significantly fuel-lean), so the value of Q is permitted to be stoichiometrically dependent. The heat Q is assigned to reflect the exothermicity consistent with an adequate accounting of the species actually present in the burned mixture at equilibrium (Coffee et al. 1983). If $m = m_O \nu_O + m_F \nu_F$, where m_i is the molecular weight of species i, and u_{ref} is a reference speed, to be identified later,

$$\vec{x} = \frac{\vec{x}^*}{\ell} \, , \; t = \frac{t^*}{t_o} \, , \text{ where } \ell^2 = \kappa_u \, t_o \, , \; t_o = \kappa_u / u_{ref}^2 \, ; \tag{1.2}$$

$$\theta = \frac{T}{T_u} \, , \; \rho = \frac{\rho^*}{\rho_u} \, , \; \vec{u} = \frac{\vec{u}^*}{u_{ref}} \, , \text{ where } \rho \, \theta = 1 \, ; \tag{1.3}$$

$$Y = \frac{Q\, Y_F}{m\, c_p\, T_u}\,,\quad Y_F = \frac{m\, \nabla_F}{m_F\, \nu_F}\,;\quad X = \frac{Q\, Y_O}{m\, c_p\, T_u}\,,\quad Y_O = \frac{m\, \nabla_O}{m_O\, \nu_O}\,. \tag{1.4}$$

Here, a superasterisk is used to designate a dimensional quantity if there otherwise would arise an ambiguity with its dimensionless counterpart. The dimensional spatial coordinates are designated $\vec{x}^*$, although below we shall restrict attention to one-velocity-component flows spatially dependent on only one spatial coordinate (designated x^* in a planar flow, r^* in a spherically symmetric flow); the reference length scale ℓ is defined in terms of the reference thermal diffusivity κ_u and a reference speed u_{ref}, to be assigned below. The thermal diffusivity κ_u is defined (as usual) in terms of the thermal conductivity k_u, the density ρ_u, and the specific heat capacity at constant pressure c_p, where subscript u refers to the (uniform) state of the cold (unburned) premixture and c_p is approximated as a constant throughout the flow. If we anticipate that, for a given "pair" of reactants (such as a pure hydrocarbon and air, the quantity u_{ref} is assigned a value which does not vary with the mixture composition, then we note that, since κ_u does vary with the mixture composition, the length scale and the time scale adopted in (1.2) vary with mixture composition. Also, T signifies temperature and ρ, density, and both are normalized against their values in the cold premixture. The molecular weights of the dominant species (in terms of mass fraction) are taken to be comparable throughout the flow, so that the equation of state for the highly subsonic, effectively isobaric flows of interest here is taken in (1.3) to be $\rho\,\theta = 1$. If ∇_i denotes the mass fraction of species i, (1.4) reflects the standard practice of introducing the stoichiometrically adjusted mass fractions ∇_F, equal to $(m\,\nabla_F)/(m_F\,\nu_F)$, and Y_O, equal to $(m\,\nabla_O)/(m_O\,\nu_O)$; for a fuel-lean condition, the excess oxygen in the burned gas $Y_{Ob} = Y_{Ou} - Y_{Fu} = Y_{Ou}(1 - \phi)$, where the fuel-to-oxidizer equivalence ratio $\phi = Y_{Fu}/Y_{Ou}$, $Y_{Fu} = (m\,\nabla_{Fu})/(m_F\,\nu_F)$, $Y_{Ou} = (m\,\nabla_{Ou})/(m_O\,\nu_O)$. Equivalently, $\phi = (\nabla_{Fu}/\nabla_{Ou})/r$, $r = (m_F\,\nu_F)/(m_O\,\nu_O)$; equivalently, if ∇_N is the mass fraction of nitrogen, $\phi = [\nabla_{Fu}/(\nabla_{Ou} + \nabla_{Nu})]/(r\,N)$, since $[\nabla_{Ou}/(\nabla_{Ou} + \nabla_{Nu})] = N$, a const.($\approx 0.23$ for air) -- so ϕ also can be defined in terms of the fuel-to-air ratio. For simplicity here, attention is limited to cold premixtures consisting only of fuel, oxygen, and (sometimes) nitrogen, so $\nabla_{Ou} + \nabla_{Nu} + \nabla_{Fu} = 1$; further, attention is limited to the cases $N = 0.23$ (pure-fuel/air mixture) and $N = 1$ (pure-fuel/oxygen mixture).

In (1.4) we also choose to introduce the energetically adjusted mass fraction for fuel Y and for oxygen X; these are so defined that the increase of one unit of θ is effected by the decrease of one unit of (say) Y, with the understanding that the decrease is owing to chemical conversion in accord with the reaction

(1.1). In particular, if $Y_u = (Q\ Y_{Fu})/(m\ c_p\ T_u) = a$, then (for a fuel-lean situation, $1 > \phi > 0$), in the fully burned ("hot") gas, in which $Y = 0$, θ would have increased from a value of unity in the unburned gas to a value of $(1 + a)$ in the burned gas, in the absence of heat losses. The quantity $(1 + a)$ is termed the adiabatic flame temperature θ_f, and a, sometimes termed the second Damkohler number and given the symbol D_2, is the ratio of chemical exothermicity per mass of fuel $(Q\ Y_{Fu}/m)$ to the cold premixture enthalpy $c_p\ T_u$. In the absence of a significant occurrence of soot (so that, with reservations discussed in a spherical flame context, the radiative transfer of heat is negligible for most purposes, in accounting for the conservation of energy), this formulation holds for the case of a fuel-rich mixture by noting that in the burned gas, in which now $X = 0$ and $Y = (a - b) > 0$, $\theta_f = (1 + b)$, where $X_u = (Q\ Y_{Ou})/(m\ c_p\ T_u) = b$. The stoichiometric case ($\phi = 1$) is $a = b = a^+$, where henceforth the superscript + denotes evaluation at stoichiometric conditions. Note that a^+ may take on a range of values for the same pair of reactants with invariant cold-premixture pressure and temperature, because of variable dilution with chemically inert species.

For the transport coefficients, if D_i^* is the (binary) diffusion coefficient of species i, and k^* is the thermal conductivity, then it is useful to introduce dimensionless counterparts (σ_i is the Lewis-Semenov number of species i):

$$\frac{D_i^*}{\ell^2/t_o} = \frac{D_i^*}{\kappa_u} = D_i = \left[\frac{D_i^*}{D_{iu}}\right]\left[\frac{D_{iu}}{\kappa_u}\right] = \bar{D}_i\ \sigma_i,\ i = O,F, \tag{1.5}$$

where D_{iu} is the (dimensional) value of D_i^* in the cold premixture, and $\bar{D}_i$ is dimensionless;

$$\frac{k^*}{c_p} = \left[\frac{k_u\ k}{c_p}\right]\left[\frac{\rho_u}{\rho_u}\right] = \kappa_u\ k\ \rho_u, \tag{1.6}$$

where (again) k_u is the (dimensional) value of k^* in the cold premixture, and k is dimensionless. The transport coefficients $\bar{D}_i$ and k are taken to be functions of θ only.

For the chemical kinetics, a direct one-step irreversible bimolecular second-order reaction, subject to an Arrhenius-type specific rate constant (adjusted to obviate the cold-boundary difficulty). Specifically, the specific rate constant is taken in the form

$$B_f\ T^\alpha \exp\left[-\frac{T_a}{T - T_u}\right] = B_f\ T_u^\alpha\ \theta^\alpha \exp\left[-\frac{E}{\theta - 1}\right], \tag{1.7}$$

where T_a is activation temperature; the effective frequency factor B_f has units of $m^3/(s\ mole^2\ K^\alpha)$; and the dimensionless activation energy $E = (T_a/T_u)$, a large quantity for premixtures of interest here.

2. THE ONE-DIMENSIONAL ANALYSIS

We consider the one-dimensional structure of a steady flame that sits at $x = 0$ in a coordinate system in which the flow is in the positive x direction. We consider only isobaric phenomena so that the conservation of momentum is not at issue; mass conservation requires merely that $\rho\ u = u(-\infty) = \text{const.}$ and, as is well known, $\rho\ u$ will be an eigenvalue of the mathematical problem.

The equations describing the conservation of energy and of chemical species are, in accord with the discussion of Section 1,

$$\rho\ u\ \theta_x - \left[k(\theta)\ \theta_x\right]_x = \frac{J^*}{u_{ref}^2}\ \theta^{\alpha-2}\ Y\ X \exp\left[-\frac{E}{\theta - 1}\right] = \theta^{\alpha-2}\ RR\ , \tag{2.1}$$

$$\rho\ u\ Y_x - \sigma_F\ \left[\theta^{-1}\ \bar{D}_F(\theta)\ Y_x\right]_x = -\theta^{\alpha-2}\ RR\ , \tag{2.2}$$

$$\rho\ u\ X_x - \sigma_O\ \left[\theta^{-1}\ \bar{D}_O(\theta)\ X_x\right]_x = -\theta^{\alpha-2}\ RR\ . \tag{2.3}$$

Henceforth, we adopt a common temperature dependence of the reactant-species diffusion coefficients, conditions consistent in accuracy with previous approximations:

$$k(\theta) = \theta^{-1}\ \bar{D}_F(\theta) = \theta^{-1}\ \bar{D}_O(\theta)\ . \tag{2.4a}$$

The Lewis-Semenov numbers σ_O, σ_F are known input quantities. The numerator of the first Damkohler number (J^*/u_{ref}^2) is defined as follows:

$$J^* = \kappa_u\ B_f\ \rho_u\ T_u^{\alpha+1}\ \nu_F\ \nu_O/(Q/c_p)\ . \tag{2.4b}$$

The equations (2.1)-(2.3) involve dimensionless quantities only, except for the factors J^* and u_{ref}^2.

The foregoing equations can be reduced without further approximation to their constant-diffusivity forms by use of the definition

$$\xi = \int_0^x [k(\theta)]^{-1}\ dx. \tag{2.4c}$$

With that substitution, (2.1) - (2.3) become

$$\rho u \theta_\xi - \theta_{\xi\xi} = \sigma(\theta)\, RR\ ,\ \sigma(\theta) = \theta^{\alpha-2}\, k(\theta)\ ; \tag{2.5}$$

$$\rho u Y_\xi - \sigma_F Y_{\xi\xi} = -\sigma(\theta)\, RR\ , \tag{2.6}$$

$$\rho u X_\xi - \sigma_O X_{\xi\xi} = -\sigma(\theta)\, RR\ . \tag{2.7}$$

As noted earlier, we confine our attention to mixtures for which E is large enough to imply that the thickness of the zone in which reactions cannot be ignored, $(\rho u E)^{-1}$, is small compared to the thickness, $(\rho u)^{-1}$, of the diffusive-convective (preheating) zone (Bush and Fendell 1970; Fendell 1972). It is implied in all large-activation-energy treatments of gaseous deflagrations that the temperature to be assigned to the hot end of the convective-diffusive zone is the same as that assigned to the hot end of the reaction zone. With this constraint we note that, both in the reaction zone and in the downstream zone where $\theta = \theta_f = \text{const.}$, (2.5)-(2.7) imply

$$(\theta + \sigma_F Y)_{\xi\xi} = 0\ , \tag{2.8}$$

$$(\theta + \sigma_O X)_{\xi\xi} = 0\ . \tag{2.9}$$

When the fuel content of the cold premixture $Y_u (= a$, for brevity) is smaller than the oxygen content of the cold premixture $X_u (= b)$, it is recalled that the burnt state of the gas is one for which $Y(\infty) = 0$, $X(\infty) = (b - a)$, $\theta(\infty) = \theta_f = (1 + a)$. Accordingly, (2.8) and (2.9) imply

$$Y = (1 + a - \theta)/\sigma_F\ , \tag{2.10}$$

$$X = b - a + (1 + a - \theta)/\sigma_O\ . \tag{2.11}$$

We shall continue the analysis as though $a \leq b$, but recall that when $b \leq a$, the description displayed will be valid provided that, in each recipe, one interchanges a and b, and also interchanges the subscripts F and O. It is reiterated that the value of Q/c_p (which is a factor that enters in b, a, and other quantities) is permitted to vary with stoichiometry and dilution because in practice the burnt-gas composition changes; standard computerized equilibrium calculations (e.g., Gordon and McBride 1976) permit the product species, and hence Q/cp, to be identified.

Also in the reaction zone and downstream thereof, we have, from (2.5), (2.10), and (2.11),

$$-\theta_{\xi\xi} = \sigma(\theta)\, \frac{J^*}{u_{ref}^2}\, \frac{(1 + a - \theta)}{\sigma_F} \left[(b - a) + \frac{1 + a - \theta}{\sigma_O}\right] \exp\left[-\frac{E}{\theta - 1}\right]. \tag{2.12}$$

It follows that, upon multiplication by θ_ξ and integration,

$$\theta_\xi^2(\xi) = 2\,\sigma(1+a)\,\frac{J^*}{u_{ref}^2}\int_\theta^{1+a}\frac{(1+a-T)}{\sigma_F}\left(b-a+\frac{1+a-T}{\sigma_0}\right)\exp\left[-\frac{E}{T-1}\right]dT, \tag{2.13}$$

where the integral is designated $H(\theta)$ and the temperature distribution is implicit in

$$d\xi = d\theta/\left[2\,\sigma(1+a)\,\frac{J^*}{u_{ref}^2}\,H(\theta)\right]^{1/2}. \tag{2.14}$$

The details of $\theta(\xi)$ are of no real interest, especially in the absence of a chemically more accurate model for the reaction rate RR, but, in particular, the downstream behavior is given by $\theta(\infty) = (1+a)$ and $u(\infty) = (1+a)\,u(-\infty)$.

We do need, from (2.13), the value of θ_ξ at the upstream end of the reaction zone. When $a \le b$, $\theta_\xi(0-)$ is given by

$$\theta_\xi^2(0-) = 2\,\sigma(1+a)\,\frac{J^*}{u_{ref}^2}\,H(1) = 2\,\sigma(1+a)\,\frac{J^*}{u_{ref}^2}\,G(a,b-a,E,\sigma_0,\sigma_F)$$

$$= 2\,\sigma(1+a)\,\frac{J^*}{u_{ref}^2}\int_1^{1+a}\left[\frac{(b-a)(1+a-T)}{\sigma_F}+\frac{(1+a-T)^2}{\sigma_0\,\sigma_F}\right]\exp\left[-\frac{E}{T-1}\right]dT\,. \tag{2.15}$$

Alternately, when $b \le a$, $\theta_\xi(0-)$ has the value

$$\theta_\xi^2(0-) = 2\,\sigma(1+b)\,\frac{J^*}{u_{ref}^2}\int_1^{1+b}\left[\frac{(a-b)(1+b-T)}{\sigma_0}+\frac{(1+b-T)^2}{\sigma_0\,\sigma_F}\right]\exp\left[-\frac{E}{T-1}\right]dT\,. \tag{2.16}$$

In these equations the use of the lower limit, $T = 1$, in the integral H can be justified mathematically using conventional singular-perturbation techniques. Physically, the justification stems from the fact that, in (2.13), changes in the value of $H(\theta)$ associated with changes of θ in the range $1 < \theta < [1 + a - (\bar{A}/E)]$, where $\bar{A} = O(1)$, are smaller than the inaccuracies inherent in the asymptotic procedures invoked in these flame-propagation problems.

Even at this stage of the analysis, one can see, by comparing (2.15) and (2.16), that if (for example) a deflagration wave advances through a fuel-lean mixture of hydrogen ($\sigma_F \doteq 3.5$) and air ($\sigma_0 \doteq 0.85$) with a stoichiometry given by $a_1 = 0.8\,b_1$, the value of $\theta_\xi(0-)$ will differ significantly from that of a second fuel-rich experiment in which $a_2 = b_1$, and $b_2 = a_1$; here the subscripts on

a and b merely distinguish the values of a and b in the first experiment from those characterizing the second experiment. This asymmetry is clearly apparent in the laminar-flame-speed data, given as a function of stoichiometric ratio ϕ by Glassman (1987, p. 137, Fig. 14, and pp. 461-464), who presents results not only for hydrogen/air mixtures, but also for a variety of simple mixtures of other gaseous fuel species with air. The data are mainly from Gibbs and Calcote (1959). Zabetakis (1965) presents a limited amount of data for fuel/oxygen mixtures. We shall compare our theoretical results with this data in the next section.

In the region where θ is so small that reactions can be ignored [most of the region in which $\theta < (1 + a)$], (2.5) implies that

$$\theta_{\xi\xi} - \rho u \theta_{\xi} = 0 . \tag{2.17}$$

Accordingly, in that region, if A is a constant of integration,

$$\theta = 1 + A \exp(\rho u \xi) . \tag{2.18}$$

Whenever E is sufficiently large that θ_{ξ}, as defined by (2.13), gets reasonably close to its asymptotic value (that at $\theta = 1$) while θ is still sensibly close to the value (1 + a), one can match θ_{ξ} of the "inner approximation", given by (2.13), to the θ_{ξ} of the "outer approximation", obtainable from (2.18). Mathematically, this step again is justified by an appeal to the asymptotic formalities referred to earlier in this section; the fact is that the foregoing approximation gives correct qualitative descriptions, and, over a broad range of parameter values of practical interest, it gives quantitative descriptions of very acceptable and informative accuracy. Therefore, using this matching specification, (2.18) becomes

$$\theta = 1 + a \exp(\rho u \xi) , \tag{2.19}$$

and

$$\theta_{\xi}(0-) = \rho u a = a u(-\infty) , \tag{2.20}$$

where $\theta_{\xi}(0-)$ is given by (2.15) or (2.16), in accord with the magnitudes of a and b. In (2.19) and (2.20), the factor a is replaced by b when $a > b$.

This is a particularly convenient point at which to choose the dimensional parameter u_{ref} to be the actual flame speed for equivalence ratio unity. More formally, u_{ref} is the velocity which [for any pair of reactants in stoichiometric proportion, with specified dilution by a chemical species nominally neutral] gives $u(-\infty) = 1$. Hence, u_{ref}^2 for a given pair of reactants with specified dilution is given by

$$u^2_{ref} = \frac{2\, J^*(1,N_{ref})\, \sigma(1+a^+)}{(a^+)^2}\, G(a^+,0,E,\sigma_0,\sigma_F)\ , \tag{2.21}$$

where it is recalled that a^+ is the value of a, and also the value of b, that defines the stoichiometric mixture of specified dilution. We have already anticipated below (2.4b) that, through the factors κ_u and (Q/c_p), the quantity J^*, defined in (2.4b), is a function of the equivalence ratio ϕ and the dilution ratio N, both previously defined in Section 1 and taken as specified input; thus, in general, we henceforth write $J^*(\phi,N)$, and, in particular, for the stoichiometric conditions upon which (2.21) is predicated, we write $J^*(1,N_{ref})$. While in general $N \neq N_{ref}$ because it is possible to conceive of various comparisons in numerical calculations presented below, we shall concentrate on cases in which $N = N_{ref}$, i.e., both the degree of oxygen dilution by nitrogen (and the examined pair of reactants) are fixed while the equivalence ratio ϕ is altered. It follows that $u^2(-\infty)$ for other mixtures of the same reactants (whether diluted or not) is given by, from (2.15), (2.16) (2.20), and (2.21),

$$u^2(-\infty) = \frac{\sigma(1+a)}{\sigma(1+a^+)}\ \frac{J^*(\phi,N)}{J^*(1,N_{ref})} \left[\frac{a^+}{a}\right]^2 \frac{G(a,b-a,E,\sigma_0,\sigma_F)}{G(a^+,0,E,\sigma_0,\sigma_F)}\ ,\ b > a; \tag{2.22a}$$

or by

$$u^2(-\infty) = \frac{\sigma(1+b)}{\sigma(1+a^+)}\ \frac{J^*(\phi,N)}{J^*(1,N_{ref})} \left[\frac{a^+}{b}\right]^2 \frac{G(b,a-b,E,\sigma_F,\sigma_0)}{G(a^+,0,E,\sigma_F,\sigma_0)}\ ,\ a > b. \tag{2.22b}$$

The quantity $u(-\infty)$ is the ratio of the flame speed of the mixture with a,b stoichiometry to the flame speed of the stoichiometric (reference) mixture. In (2.2a) and (2.22b), if $\bar{Q} = Q/c_p$,

$$\frac{J^*(\phi,N)}{J^*(1,N_{ref})} = \frac{\kappa_u(\phi,N)}{\kappa_u(1,N_{ref})}\ \frac{\bar{Q}(1,N_{ref})}{\bar{Q}(\phi,N)} \to \frac{\bar{Q}(1,N_{ref})}{\bar{Q}(\phi,N)} \tag{2.22c}$$

<u>if</u> one ignores the variation of the thermal diffusivity with stoichiometry. Also, in (2.22a) and (2.22b), the factors a,b involve $\bar{Q}(\phi,N)$, whereas the factors a^+,b^+ involve $\bar{Q}(1,\bar{N}_{ref})$.

Equations (2.22) give the square of the ratio (of the flame speed at general equivalence ratio to the flame speed at stoichiometry) in the thermal-conductivity-distorted ξ coordinate, defined by (2.4c). To express the same square of the ratio in the (nondimensionalized) coordinate x, we multiply the right-hand

side of (2.22a) by the square of the ratio $k(1 + a)/k(1 + a^+)$, and the right-hand side of (2.22b) by the square of the ratio $k(1 + b)/k(1 + a^+)$, since $dx/dt = (dx/d\xi)(d\xi/dt)$. Thus, if $k(\theta) \sim \theta^\delta$, δ being a given constant, then, in (2.22a), for the square of the velocity ratio pertinent to the x coordinate, the ratio $\sigma(1 + a)/\sigma(1 + a^+)$ is replaced by the factor $\left[(1 + a)/(1 + a^+)\right]^{\alpha-2+3\delta}$.

Now that we have obtained an expression for $u(-\infty)$, we recall that

$$\theta(\xi) = 1/\rho(\xi) = u(\xi)/u(-\infty), \tag{2.23}$$

and that: downstream of the reaction zone,

$$\theta(\xi) = \begin{cases} 1 + a, & a < b \\ 1 + b, & a > b \end{cases}; \tag{2.24a}$$

in the reaction zone,

$$\theta(\xi) \text{ is implicit in (2.14)} ; \tag{2.24b}$$

and upwind of the reaction zone,

$$\theta(\xi) = \begin{cases} 1 + a \exp[\xi\, u(-\infty)] , & a < b \\ 1 + b \exp[\xi\, u(-\infty)] , & a > b . \end{cases} \tag{2.24c}$$

3. CALCULATIONS OF THE FLAME SPEED AS A FUNCTION OF THE EQUIVALENCE RATIO

3.1 Preliminary Remarks

By use of the simple theory presented in Section 2, especially in (2.15), (2.16), and (2.22a-c), results were calculated for the dozen fuel/air mixtures $\left\{N = \left[\nu_{Ou}/\left[\nu_{Ou} + \nu_{Nu}\right]\right] = 0.23\right\}$ and fuel/oxygen mixtures (N = 1) listed in Table 1. In Table 1, the Lewis-Semenov numbers for the cold premixture have been presented as if they were constants invariant with stoichiometry, as is done in some simple developments (e.g., Frankel and Sivashinsky 1983). This is a very rough approximation, since the thermal diffusivity of the cold premixture varies with the equivalence ratio, even if the species binary-diffusion coefficients are sometimes reasonably approximated to be fixed as the equivalence ratio changes (Reid et al. 1977, pp. 547-548; Westbrook and Dryer 1981, p. 32). The density, heat capacity, and thermal conductivity, and thermal conductivity of the cold mixture vary with the mole fractions of the constituents (Penner 1957, p. 250). If we limit attention to $0 \le \phi \le 2$ in a simple-hydrocarbon/air mixture, then the mole fraction of fuel in the cold premixture does not much exceed 0.12 in the case of

(for example) ethane, though the mole fraction for hydrogen does reach 0.44 over the range of ϕ just cited. Since the molecular weight, heat capacity, and thermal conductivity of oxygen and nitrogen are similar in value, if the cold mixture has modest fuel content (as for fuel-lean mixtures), taking the thermal diffusivity as constant at the value appropriate for N_2 (as in Table 1) might be acceptable for pure-fuel/air mixtures -- such a procedure was discussed in (2.22c). But the approximation fails for pure-fuel/oxygen mixtures (since, as $\phi \to 2$, the ethane mole fraction approaches 0.36 for ethane/oxygen mixtures, and 0.8 for a hydrogen/oxygen mixture); erroneous values for the thermal diffusivity result in erroneous values for the Lewis-Semenov numbers, and hence for the flame speed.

In the calculations to be reported, the pre-exponential temperature dependence of the reaction rate, α, is taken to be 2.0, and the power-law temperature dependence of the thermal conductivity δ is taken to be 0.5, unless otherwise stated. Calculation shows that for fixed N, increasing the algebraic value of the exponent of the function $\sigma(\theta_f) = (\theta_f)^{\alpha-2+3\delta}$ [see (2.5) and just above (2.23)] gives a slightly greater peak value for the normalized flame speed $u(-\infty)$, and the peak value occurs for slightly richer stoichiometry. In fact, the ratio $u(-\infty)$ is augmented in value for all ϕ. However, since the appropriate value of α is O(1) and not well established, and $\delta \doteq 0.5$, the factor does not contribute significantly and is not discussed further.

It has already been noted below (2.11) that a standard computer code (e.g., Gordon and McBride 1976) yields the equilibrium (burned-gas) temperature, for a given combustible mixture which is initially at standard conditions and which undergoes an isobaric process. By this means, the dimensionless burned-gas temperature T_f is ascribed a physically suitable value, despite the adoption of the one-step pseudo-mechanism (1.1). Since $T_f = (1 + a)$ for $\phi \leq 1$ and $T_f = (1 + b)$ for $\phi \geq 1$, self-consistency of the simplistic theory with a detailed treatment (Gordon and McBride 1976) of equilibrium in the burned gas is achieved at any stoichiometry by assigning the appropriate value for the ratio (Q/c_p). The implications of differing diffusivities on laminar-flame-propagation speed as a function of stoichiometry were noted by Sen and Ludford (1979). However, even their ultimate model (Sen and Ludford 1982) involves only a single product species, which is allowed to dissociate (but weakly) to the original fuel and oxygen only. Such a model seems quantitatively inapplicable over the range of interesting stoichiometries to any real chemical system, certainly to any system used in practical applications, and indeed no comparison with flame-speed data was undertaken in that work.

For a given chemical system of a pure fuel and oxidizer (either air or pure oxygen) at fixed initial temperature and pressure, results are presented in terms of the ratio $u(-\infty)$, which is the flame speed at a general value of the equivalence ratio ϕ divided by the flame speed for $\phi = 1$. Since the frequency factor B_f [see (2.46)] can be assigned so that the calculated flame speed recovers the value experimentally observed for stoichiometric proportions of fuel and oxygen, for any ambient pressure and temperature, no compromise is involved in dealing with the normalized flame speed for purposes of comparison with experimental data. Effectively equivalent normalization was adopted by Westbrook and Dryer (1981).

Generally, for a given system, although according to the equilibrium code the peak burned-gas temperature lies near stoichiometric conditions (meticulously, slightly on the fuel-rich side), the inferred value of (Q/c_p) decreases monotonically with increasing ϕ for fuel-air systems. For fuel-oxygen systems ($N = 1$), the decrease of (Q/c_p) with increasing ϕ is appreciably more modest on the fuel-rich side, and for methanol (Q/c_p) increases slightly with ϕ for $\phi > 1$; the behavior for $N = 1$ is a consequence of the much "broader" maximum of the burned-gas temperature T_f as function of ϕ, in comparison with the more sharply defined peak for fuel-air ($N = 0.23$) systems.

From (2.15), (2.16), and (2.22a-c), the asymmetric behavior about stoichiometry of the flame speed as a function of equivalence ratio ϕ for a pure-fuel/air mixture is owing to (1) the difference in molecular weights and stoichiometric coefficients of the fuel and oxygen in the stoichiometric balance (for which CO_2 and H_2O are the products); (2) the variation in the equilibrium product species (i.e., the effective exothermicity of the reaction) with equivalence ratio; (3) the nitrogen content of air, which distinguishes it from a pure fuel (except for cases in which pure oxygen is the oxidizer); and (4) the difference in values of the (stoichiometrically varying) Lewis-Semenov numbers for fuel and oxygen. Only in purely academic cases in which no distinction between fuel and oxidizer arises on the basis of either of the first two items, and in which pure fuel and oxygen are the reactants, is the source of the asymmetric response of the flame speed as a function of equivalence ratio owing entirely to a difference between the values of the Lewis-Semenov number for fuel and the Lewis-Semenov number for oxygen. In particular, in such academic cases, if either the Lewis-Semenov number significantly exceeds unity, then the flame speed has a pronounced maximum at an equivalence ratio on the fuel (or oxygen) side of stoichiometry; in fact, if both Lewis-Semenov numbers appreciably exceed unity, there is an evident

local flame-speed maximum at a fuel-lean equivalence ratio and at a fuel-rich equivalence ratio, and the absolute maximum occurs at a value of ϕ corresponding to the larger of the two Lewis-Semenov numbers. In academic cases in which no asymmetries about stoichiometry arise on the basis of any of the four just-listed considerations, then increasing the dimensionless activation temperature E results in a more rapid decay of $u(-\infty)$ as ϕ increases or decreases from unity. Of course, in practice, the first two of the four above-listed considerations do lead to asymmetry, and most combustion processes occur in air, rather than pure oxygen, to add further asymmetry.

It seems useful to anticipate that the magnitude of the normalized laminar flame speed, and the stoichiometry of the mixture for which that maximum occurs (often at slightly fuel-rich conditions), are fairly well recovered for fuel/air mixtures, under the provision that one adopts somewhat lower values for the dimensionless activation temperature E than are sometimes cited. However, for simple overall mechanisms, the conventional values of E often are established on the basis of ignition-delay measurements (Mullins and Penner 1959, pp. 197-202), whereas appreciably lower activation temperatures have been adopted in the past by several theoretical modelers to recover measured flame-propagation-speed data (Dugger 1951; Fenn and Calcote 1953; Gaydon and Wolfhard 1979, pp. 118-121; Coffee et al. 1983). Also, typically about a 15% reduction is appropriate for the value of E used here, relative to the more conventionally assigned value, owing to the approximation adopted in (1.7) to resolve the cold-boundary difficulty. Explicitly, the dimensionless activation temperature E here is ascribed values of 15, 25, and 66, corresponding to activation temperatures of about 4500 K, 7500, and 20,000 K, respectively; the value $E \doteq 15$ gives results closer to the experimental data (e.g., Gibbs and Calcote 1959). This value is marginal but acceptable for the application of asymptotic analysis.

In the absence of heat-loss mechanisms, the theory continues to give finite values for $u(-\infty)$ for values of the equivalence ratio ϕ well outside the typically observed flammability limits. Others have postulated that prediction of a propagation rate below some small value is tantamount to a prediction of extinction in practice (Penner and Mullins 1959, p. 143), but attempting such rough rules of thumb goes beyond our objectives.

3.2 Computational Results

For the propane-air system, Figure 1 presents both the equilibrium-code-calculated values of T_f and the inferred values of (Q/c_p) vs. ϕ; Figure 2 presents,

for several assignments for the parameter E, the resulting values of $u(-\infty)$ vs. ϕ, together with the observed values. Corresponding graphs for the hydrogen-air system appear as Figures 3 and 4; and for the ethane-air system, as Figures 5 and 6. In all these results the Lewis-Semenov numbers have been held constant (at values given in Table 1) over the equivalence ratios examined. On Figure 2 are also presented numerical results obtained by Warnatz (1985) from a 93-step mechanism; this particular result is included because it is obtained from a scheme that has been extended to alkanes from propane through octane, so it seems indicative of the performance of a more widely applicable detailed-chemistry scheme (not a scheme limited either conceptually or practically to just exceedingly simple fuels). Even with 93 reactions, the scheme is deemed by Warnatz to be nonapplicable to mixtures richer than those included on Figure 2.

Flame speeds calculated with the Lewis-Semenov numbers permitted to vary with cold-mixture stoichiometry are more consistent with the data for propane-air (Figure 7) and hydrogen-air (Figure 8). For the propane-oxygen system, Figures 9 and 10 are the counterparts of Figures 1 and 2, which pertain to the propane-air system; for the hydrogen-oxygen system, Figures 11 and 12 are the counterparts of Figures 3 and 4, which pertain to the hydrogen-air system; in Figures 10 and 12, the cold-mixture Lewis-Semenov numbers are permitted to vary with the stoichiometry.

The results make a point apparently not previously noted: whereas one-step models can approximately predict flame speeds for simple-fuel/air flames (if the variability of the Lewis-Semenov numbers with stoichiometry is retained, and if the appropriate exothermicity is assigned by use of an equilibrium calculation for the burned gas), the adequacy of one-step models deteriorates badly for simple-fuel/oxygen flames. About all the models can do for the pure-oxygen case is to predict on which side of stoichiometry the peak flame speed occurs. For the hydrogen/oxygen case, results for the flame speed seem improved notably if one adopts a cold-mixture diffusivity for the fuel species (and hence for the oxidizer species) which is decremented appreciably. This observation suggests that regarding the effective fuel species to be an intermediate, appreciably heavier species containing both hydrogen and oxygen is appropriate for estimating the flame speed; i.e., use of molecular hydrogen as the fuel species is inappropriate for the relatively hot hydrogen/oxygen flame, even if it crudely suffices to retain molecular hydrogen as the fuel species for not-too-rich hydrogen/air flames. Decreasing the diffusion coefficients for the cold-mixture reactants in a propane/oxygen flame also helps bring the results more in line

with observations, but in this case it is difficult to envision how species with diffusion coefficients larger than those of the original reactants may arise. While the onset of soot formation may be deferred to slightly higher equivalence ratio [because the soot-precursor-oxidation rates rise more quickly with temperature than the pyrolytic, soot-precursor-formation rates (Glassman 1988)], once past the onset-of-sooting equivalence ratio, the soot yield may be enhanced in higher-temperature, hydrocarbon/oxygen flames over the soot yield in the same-hydrocarbon/air flame, with all else held fixed. Thus the overestimate of observed hydrocarbon/oxidizer-flame speed at quite rich stoichiometries by a theory that omits radiative heat loss is to be anticipated (Gaydon and Wolfhard 1979, p. 205; Haynes and Wagner 1981, pp. 232-234). The overestimation is likely to be pronounced if the oxidizer is oxygen rather than air. Despite these caveats, and despite the fact that empirically-guided altering of the orders of reaction in a one-step-kinetics theory might be of some avail, probably the one-step model itself needs generalization for flame-speed estimation for fuel/oxygen mixtures.

For completeness, we note that elaborate numerical calculations with multi-component-diffusion and detailed-chemical-kinetic models (Warnatz 1981) can very accurately yield the flame speed as a function of the equivalence ratio for various pure-hydrocarbon/air mixtures ("up to butane") and for hydrogen mixtures with various ratios of nitrogen to oxygen. What is less clear to the present authors is the degree to which the success is attributable to "tuning" some of the many available chemical-kinetic parameters purposely to fit the particular finite set of experimental data. Further, Egolfopoulos et al. (1989) document, for methane-air mixtures initially at room conditions, the highly variable success of different formulations that adopt (still-large) subsets of the full-chemical-kinetic models. For example, one seriously proposed, plausible subset involving fourteen species and eighteen reactions performed no better than the one-step scheme proposed here, yet the solution for a single stoichiometry for this type of scheme is reported to require about 130-145 minutes CPU time on a VAX 11/785 computer.

4. THE TRANSIENT ONE-DIMENSIONAL PROBLEM

It is useful, in anticipation of a companion study of spherical-flame propagation (Carrier et al. 1990), to conclude with remarks on the one-dimensional counterpart: the flame propagation that would ensue when, in a gas mixture at rest in $-\infty < y < \infty$, a flame is initiated in a small region $-y_0 < y < y_0$, so that

it subsequently evolves as two flames propagating symmetrically away from $y = 0$. One such configuration (again with $a < b$) can be constructed as follows.

Define

$$x = y + (1 + a)\, u(-\infty)\, t \tag{4.1a}$$

and write for $y < 0$, in view of (2.23),

$$u_{transient} = -(1 + a)\, u(-\infty) + u(x)$$

$$= [\theta(x) - (1 + a)]\, u(-\infty)\ . \tag{4.1b}$$

The coordinates ξ and x are related through (2.4c), and $\theta(\xi)$ is displayed in (2.24).

In $y > 0$ the configuration is the mirror image of that in $y < 0$; more precisely, u is odd in y, whereas ρ and θ are even in y.

The matchup at $y = 0$ of the state variables, including velocity, is fully consistent with first principles and each flow is merely that derived in Section 2, except for the fact that, here, each is translating relative to the laboratory coordinates at a constant speed of magnitude $(1 + a)\, u(-\infty)$. The only feature of this composite flow that is inconsistent with initiation at $t = 0$ is the nonzero velocity at large y. Mass conservation requires, of course, that there be a non zero flow velocity on the cold side of each reaction zone, but it should not extend outside of $|y| = Y(t)$, where $\dot{Y}(t)$ is the speed of the very weak shock (an acoustic wave, for all practical purposes) that is consistent with the flow speed behind the wave front. Thus, we expect the flow described above to be valid in $|y| < Y(t) < a_0\, t$, where $a_0 = a_0^*/u_{ref}$, and a_0^* is the (dimensional) speed of sound in the ambient premixture and the reference speed u_{ref} has been chosen to be the stoichiometric-mixture adiabatic flame speed, typically less than 4 m/s. Outside of these "precursors", i.e., in $|y| > a_0\, t$, the motionless state of the gas differs from that of the cold gas in the foregoing analysis. The distinction is completely negligible, even for vigorous flames. For example, the pressure change across the acoustic-wave front is given by

$$\frac{\Delta p}{p_0} = \gamma(a - 1)/a_0 = O(10^{-2})\ . \tag{4.2}$$

No independent treatment of the time-dependent equations is needed to justify the foregoing construction, but, for comparisons with spherical-flame propagation, we note that the appropriate conservation laws are [with $k(\theta) = \theta^{-1}\, \bar{D}_F(\theta) = \theta^{-1}\, \bar{D}_O(\theta) = 1$, $\alpha = 2$]

$$\rho\,\theta_t + \rho\,u_{transient}\,\theta_y - \theta_{yy} = RR,\quad RR = RR\left[X, Y, \theta, E, \frac{J^*}{u_{ref}^2}\right] \tag{4.3a}$$

$$\rho\,Y_t + \rho\,u_{transient}\,Y_y - \sigma_O\,Y_{yy} = -RR\ , \tag{4.3b}$$

$$\rho\,X_t + \rho\,u_{transient}\,X_y - \sigma_F\,X_{yy} = -RR\ . \tag{4.3c}$$

Further, with $s = y + \zeta(t)$ and $\theta(y,t) \to \theta(s,\zeta)$, $Y(y,t) \to Y(s,\zeta)$, and $X(y,t) \to X(s,\zeta)$, the equations become

$$\xi\,\rho\,\theta_\zeta + \rho\,\xi\,\theta_s + \rho\,u_{transient}\,\theta_s - \theta_{ss} = RR\ , \tag{4.4a}$$

$$\xi\,\rho\,Y_\zeta + \rho\,\xi\,Y_s + \rho\,u_{transient}\,Y_s - Y_{ss} = -RR\ , \tag{4.4b}$$

$$\xi\,\rho\,X_\zeta + \rho\,\xi\,X_s + \rho\,u_{transient}\,X_s - X_{ss} = -RR\ . \tag{4.4c}$$

We omit the supporting manipulations, but we note that, for the transient phenomenon described in the foregoing, $\theta_\zeta = Y_\zeta = X_\zeta = 0$. It is also useful to note that this transient wave field is one for which no enthalpy except that of the ambient gas was involved in the ignition process. We explicitly point out that $u_{transient} = 0$ in the burned gas.

ACKNOWLEDGMENT

The authors are pleased to acknowledge that this research was sponsored by the Air Force Office of Scientific Research, Systems Command, USAF, under contract F49620-87-C-0081, monitored by Dr. Julian Tishkoff. The U.S. Government is authorized to reproduce and distribute reprints for Governmental purposes.

REFERENCES

Bush, W., and Fendell, F. (1970). Asymptotic analysis of laminar flame propagation for general Lewis numbers. Combustion Science and Technology 1, 421-428.

Carrier, G., Fendell, F., Chen, K., and Cook, S. (1990). Evaluating a simple model for laminar-flame-propagation rates. II. Spherical geometry. In preparation.

Coffee, T. P., Kotlar, A. J., and Miller, M. S. (1983). The overall reaction concept in premixed, laminar, steady-state flames. I. Stoichiometries. Combustion and Flame 54, 155-169.

Coffee, T. P., Kotlar, A. J., and Miller, M. S. (1984). The overall reaction concept in premixed, laminar, steady-state flames. II. Initial temperatures and pressures. Combustion and Flame 58, 59-67.

Dugger, G. (1951). Effect of initial mixture temperature on burning velocity. The Journal of the American Chemical Society 73, 2398.

Eckert, E. R. G., and Drake, Jr., R. M. (1972). Analysis of Heat and Mass Transfer. New York, NY: McGraw-Hill.

Egolfopoulos, F. N., Cho, P., and Law, C. K. (1989). Laminar flame speeds of methane-air mixtures under reduced and elevated pressures. Combustion and Flame 76, 375-391.

Fendell, F. (1972). Asymptotic analysis of premixed burning with large activation energy. Journal of Fluid Mechanics 56, 81-96.

Fenn, J. B., and Calcote, H. F. (1953). Activation energies in high temperature combustion. Fourth Symposium (International) on Combustion, 231-238. Baltimore, MD: Williams and Wilkins.

Frankel, M. L., and Sivashinsky, G. I. (1983). On effects due to thermal expansion and Lewis number in spherical flame propagation. Combustion Science and Technology 31, 131-138.

Gaydon, A. G., and Wolfhard, H. G. (1979). Flames -- Their Structure, Radiation and Temperature, 4th ed. London, England: Chapman and Hall.

Gibbs, G. J., and Calcote, H. F. (1959). Effect of molecular structure on burning velocity. Journal of Chemical and Engineering Data 5, 226-237.

Glassman, I. (1987). Combustion, 2nd ed. New York, NY: Academic.

Glassman, I. (1988). Soot formatin in combustion processes. Twenty-Second Symposium (International) on Combustion, 295-311. Pittsburgh, PA: Combustion Institute.

Gordon, S., and McBride, B. J. (1976). Computer program for calculation of complex chemical equilibrium compositions, rocket performance, incident and reflected shocks, and Chapman-Jouguet detonations. NASA SP-273, interim revision. Washington, DC: National Aeronautics and Space Administration.

Haynes, B.S., and Wagner, H. G. (1981). Soot formation. Progress in Energy and Combustion Science 7, 229-273.

Hirschfelder, J. O., Curtiss, C. F., and Bird, R. B. (1954). Molecular Theory of Gases and Liquids. New York, NY: John Wiley.

Lewis, B., and von Elbe, G. (1951). Combustion, Flames and Explosions of Gases. New York, NY: Academic.

Penner, S. S. (1957). Chemistry Problems in Jet Propulsion. London, England: Pergamon.

Penner, S. S., and Mullins, B. P. (1959). Explosions, Detonations, Flammability and Ignition. New York, NY: Pergamon.

Reid, R. C., Prausnitz, J. M., and Sherwood, T. K. (1977). The Properties of Gases and Liquids, 3rd ed. New York, NY: McGraw-Hill.

Sen, A. K., and Ludford, G. S. S. (1979). The near-stoichiometric behavior of combustible mixtures. Part 1. Diffusion of the reactants. Combustion Science and Technology 21, 15-23.

Sen, A. K., and Ludford, G. S. S. (1982). Maximum flame temperature and burning rate of combustible mixtures. Nineteenth Symposium (International) on Combustion, 267-274. Pittsburgh, PA: Combustion Institute.

Strehlow, R. A. (1984). Combustion Fundamentals. New York, NY: McGraw-Hill.

Warnatz, J. (1981). The structure of laminar alkane-, alkene-, and acetylene flames. Eighteen Symposium (International) on Combustion, 369-381. Pittsburgh, PA: Combustion Institute.

Warnatz, J. (1985). Chemistry of high temperature combustion of alkanes up to octane. Twentieth Symposium (International) on Combustion, 845-856. Pittsburgh, PA: Combustion Institute.

Westbrook, C. K., and Dryer, F. L. (1981). Simplified reaction mechanisms for the oxidation of hydrocarbon fuels in flames. Combustion Science and Technology 27, 31-43.

Yu, G., Law, C. K., and Wu, C. K. (1986). Laminar flame speeds of hydrocarbon plus air mixtures with hydrogen addition. Combustion and Flame 63, 339-347.

Zabetakis, M. G. (1965). Flammability characteristics of combustible gases and vapors. U.S. Bureau of Mines Bulletin 627. Washington, DC: U.S. Government Printing Office.

Table 1. Data Relating to the Flame Speeds of Fuel-Air Mixtures

Fuel Species	m_F (g/mole)	ν_F (moles)	ν_O (moles)	D_{Fu} (cm^2/s)	σ_F	ϕ at $u_m^*(-\infty)$	$u_m^*(-\infty)$ (cm/s)
hydrogen, H_2	2	2	1	0.777	3.506	1.80	325
methane, CH_4	16	1	2	0.23	1.004	1.08	44.8
acetylene, C_2H_2	26	2	5	0.17	0.767	1.25	155
ethylene, C_2H_4	28	1	3	0.16	0.722	1.13	73.5
ethane, C_2H_6	30	2	7	0.156	0.703	1.14	47.6
methanol, CH_3OH	32	2	3	0.133	0.600	1.08	50.4
butane, C_4H_{10}	58	2	13	0.096	0.433	1.03	44.9
cis-2-butene, C_4H_8	56	1	6	0.095	0.429	no data	no data
propane, C_3H_8	44	1	5	0.088	0.397	1.06	46.4
acetone, C_3H_6O	58	1	4	0.082	0.373	0.93	44.4
benzene, C_6H_6	78	2	15	0.075	0.338	1.00	47.6
heptane, C_7H_{16}	100	1	11	0.075	0.338	1.05	42.8

Notes. The maximum adiabatic flame speed $u_m^*(-\infty)$, and the equivalence ratio ϕ at which it occurs, are for a gaseous mixture initially at 298 K and one atmosphere (Gibbs and Calcote 1959). Acetone, benzene, and methanol have normal boiling points just slightly above room temperature. For the evaluation of Lewis-Semenov number for fuel, σ_F, the ambient thermal diffusivity $\kappa_u = 0.222\ cm^2/s$; the Lewis-Semenov number for oxygen, σ_O, is taken to be 0.83. The stoichiometric coefficients for fuel and oxygen (ν_F and ν_O, respectively) are for complete oxidation to CO_2 and H_2O. The fuel molecular weight is m_F. The ambient diffusion coefficients for the fuel species are mainly from Eckert and Drake (1972) and Hirschfelder et al. (1954). The diffusion coefficient for propane was estimated and, in retrospect, the value may be about 13% too small.

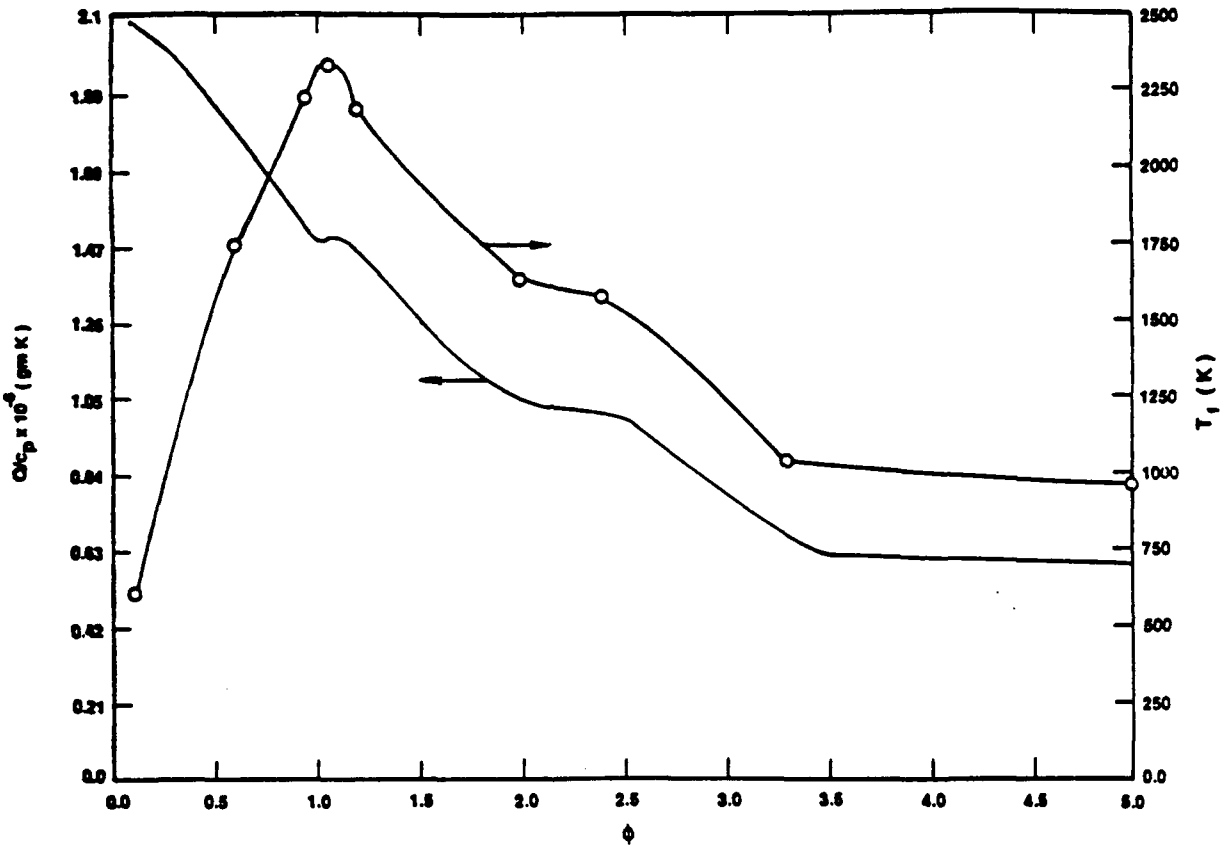

Figure 1. For a propane-air mixture initially at room conditions, the equilibrium temperature T_f achieved after isobaric burning, and the consistent effective chemical exothermicity (Q/c_p), vs. the equivalence ratio ϕ.

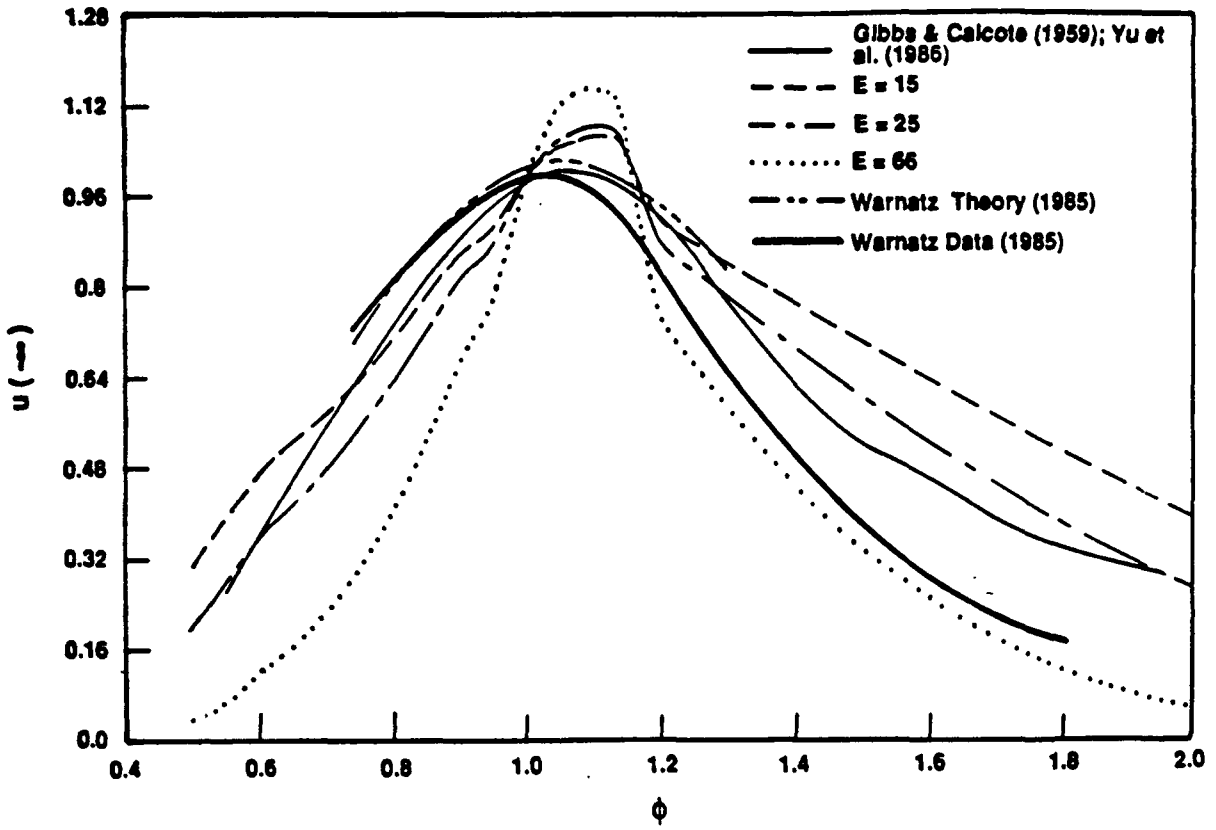

Figure 2. The laminar adiabatic flame speed $u(-\infty)$, normalized so its value is unity for a stoichiometric mixture ($\phi = 1$), vs. the equivalence ratio ϕ, for a propane-air mixture initially at room conditions. The activation temperature, nondimensionalized against the ambient temperature T_u, is denoted E. Results for E = 15 are closest to the experimental observations (Gibbs and Calcote 1959; Yu et al. 1986; Glassman 1987). Without inclusion of heat losses, the simple model predicts no flammability limits. Some of the parametric assignments for the theoretical model are given in Table 1. Also plotted are results calculated with an "abbreviated" detailed-chemistry model (Warnatz 1985).

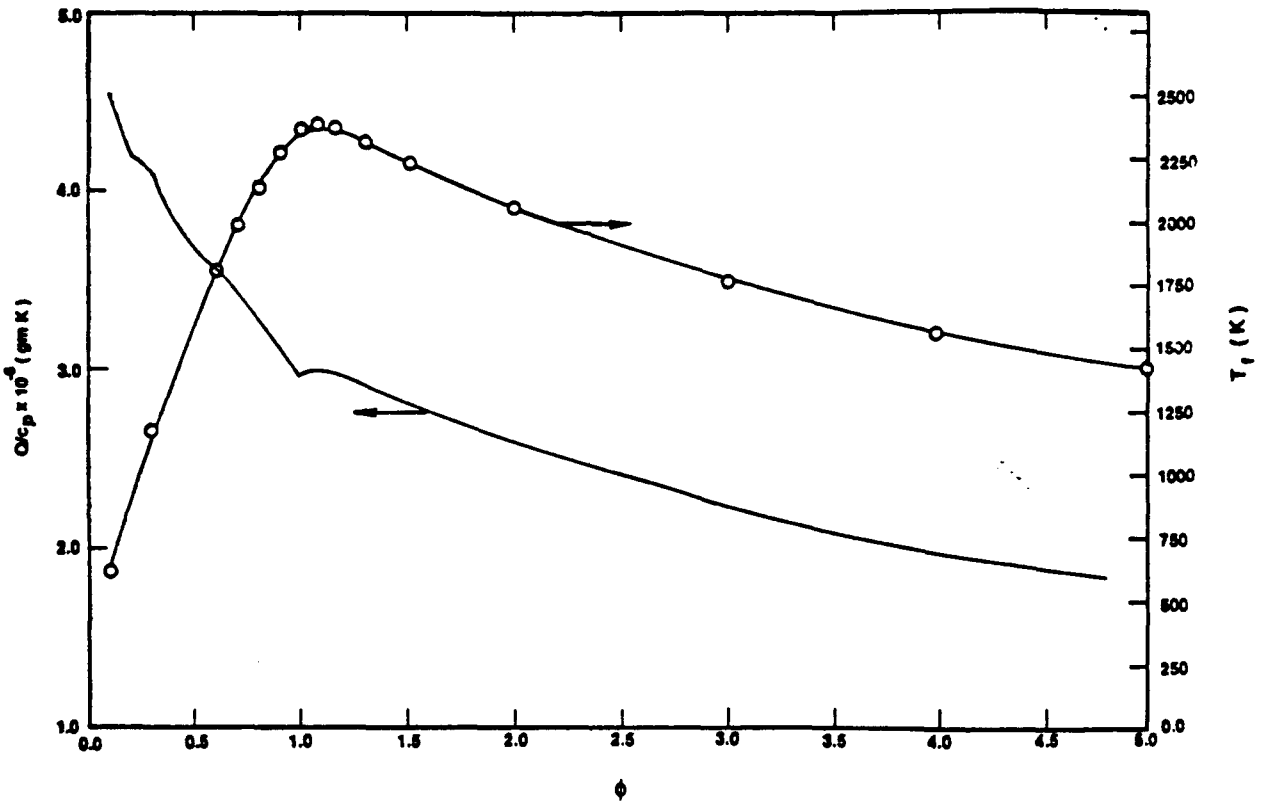

Figure 3. Same as Figure 1, but for a hydrogen-air mixture.

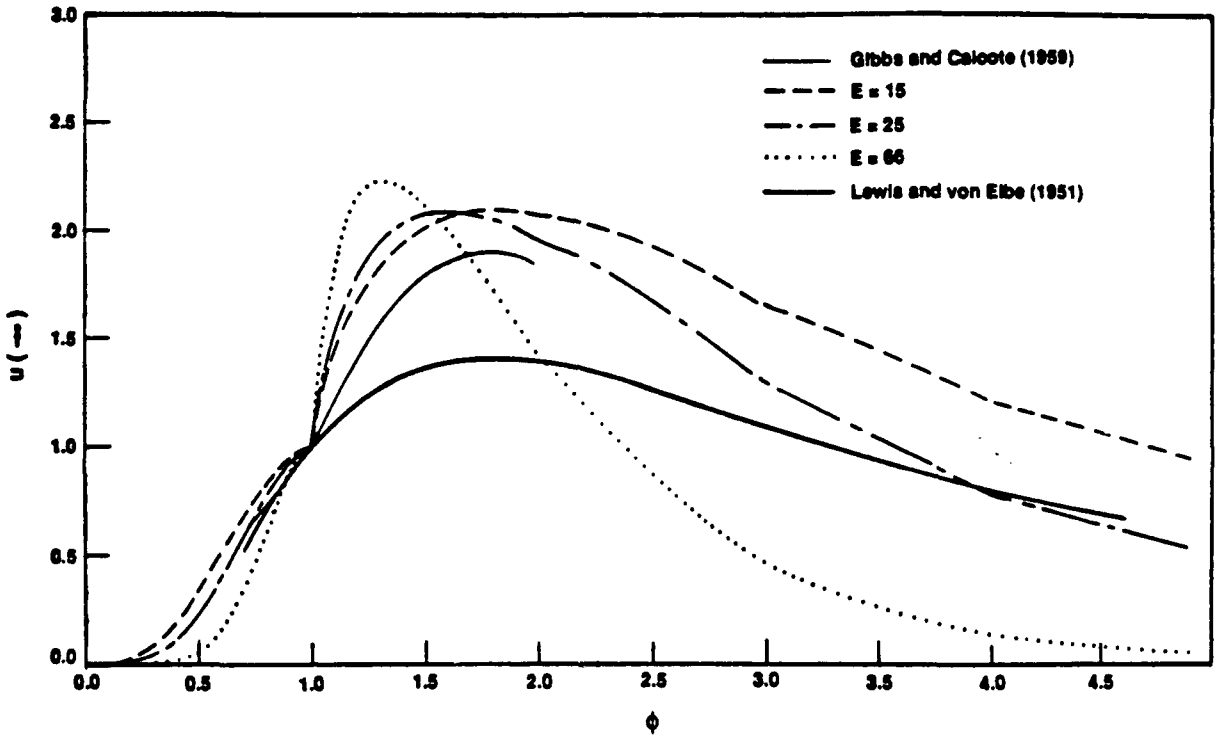

Figure 4. Same as Figure 2, but for a hydrogen-air mixture. The experimental observations are from Gibbs and Calcote (1959) and from Lewis and von Elbe (1951).

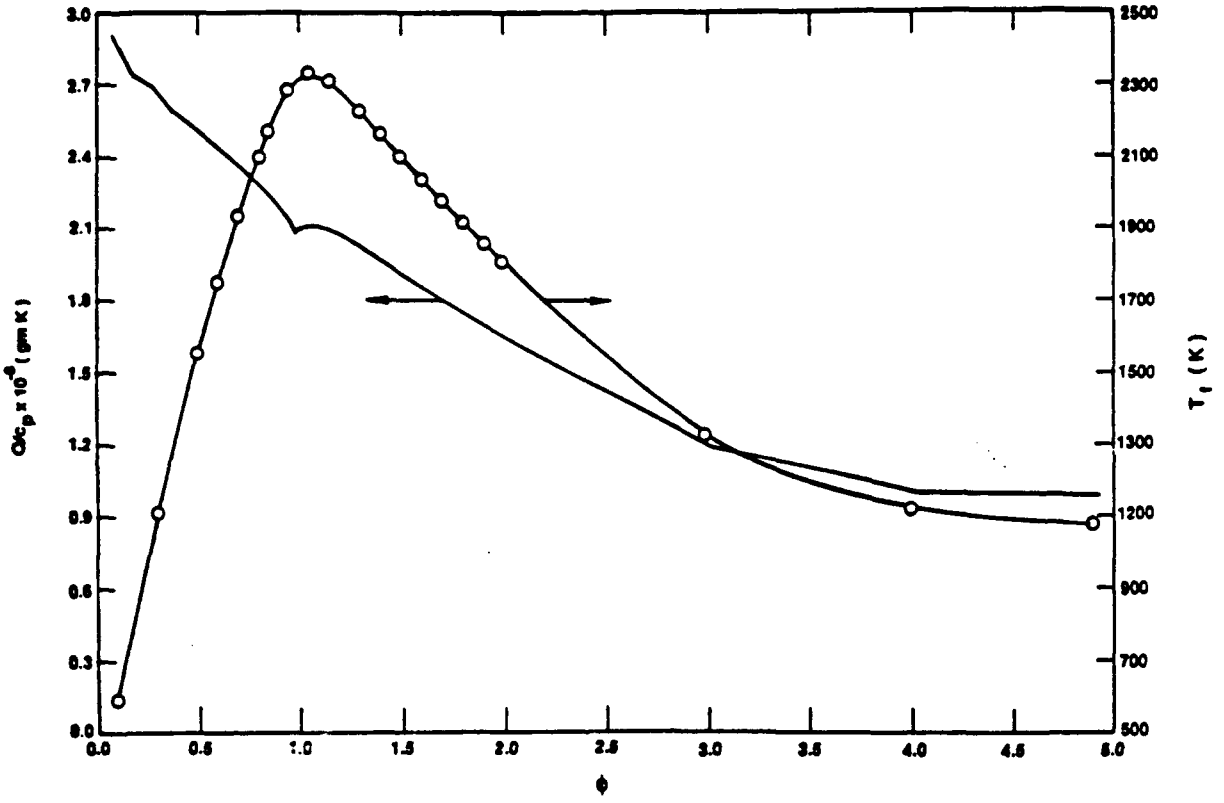

Figure 5. Same as Figure 1, but for an ethane-air mixture.

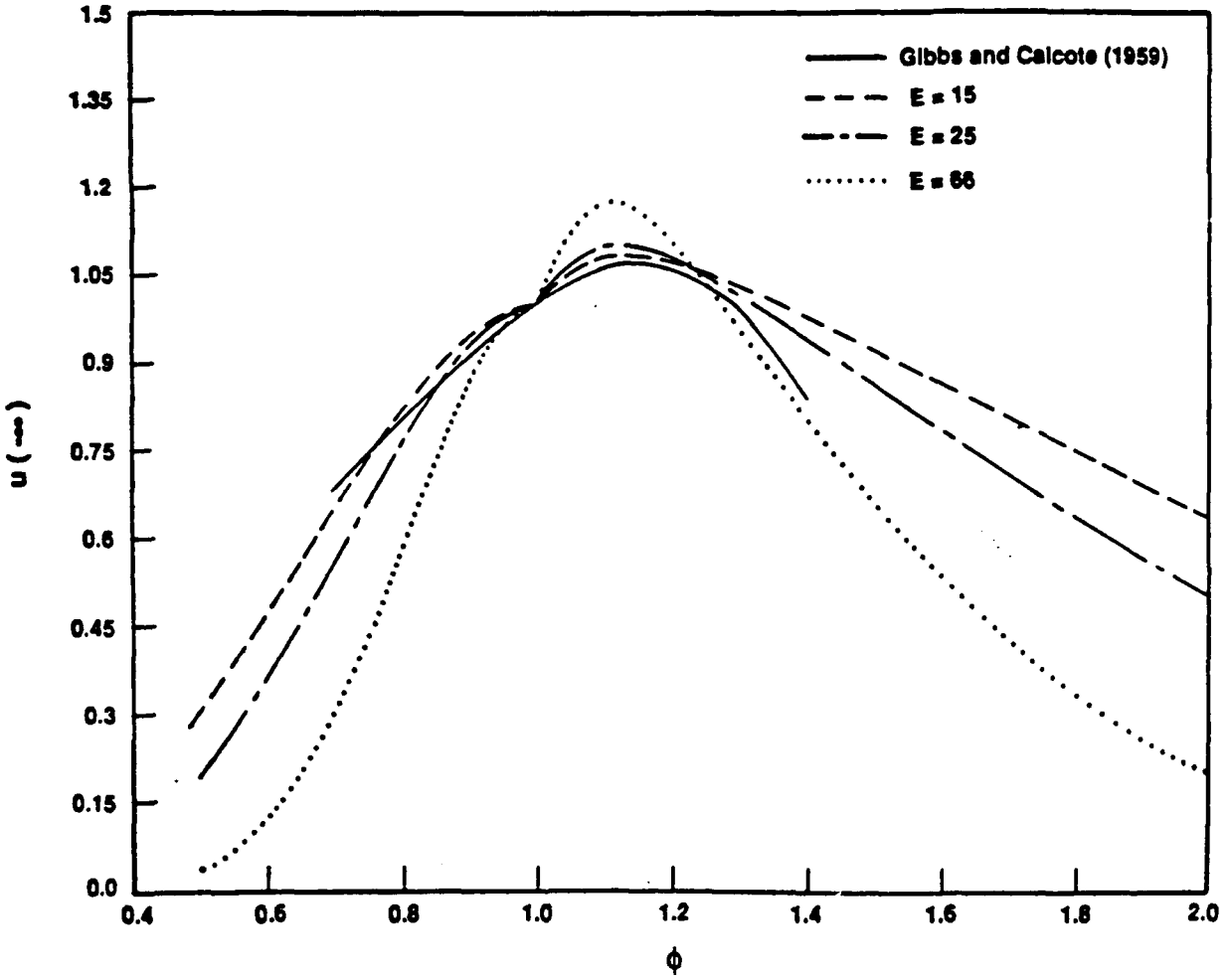

Figure 6. Same as Figure 2, but for an ethane-air mixture. The experimental observations are reported by Gibbs and Calcote (1959).

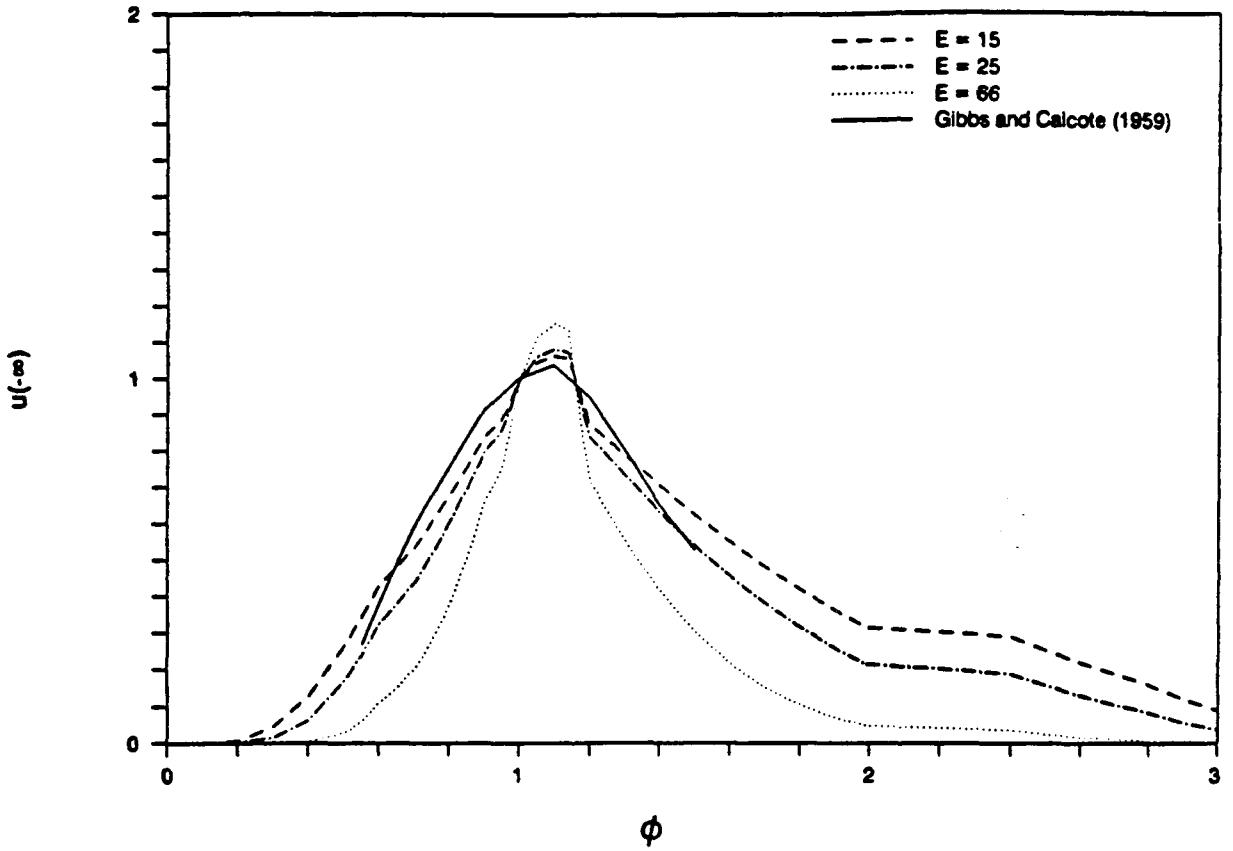

Figure 7. Same as Figure 2, except that the thermal diffusivity, and hence the Lewis-Semenov numbers, are permitted to vary with the stoichiometry of the cold propane/air mixture.

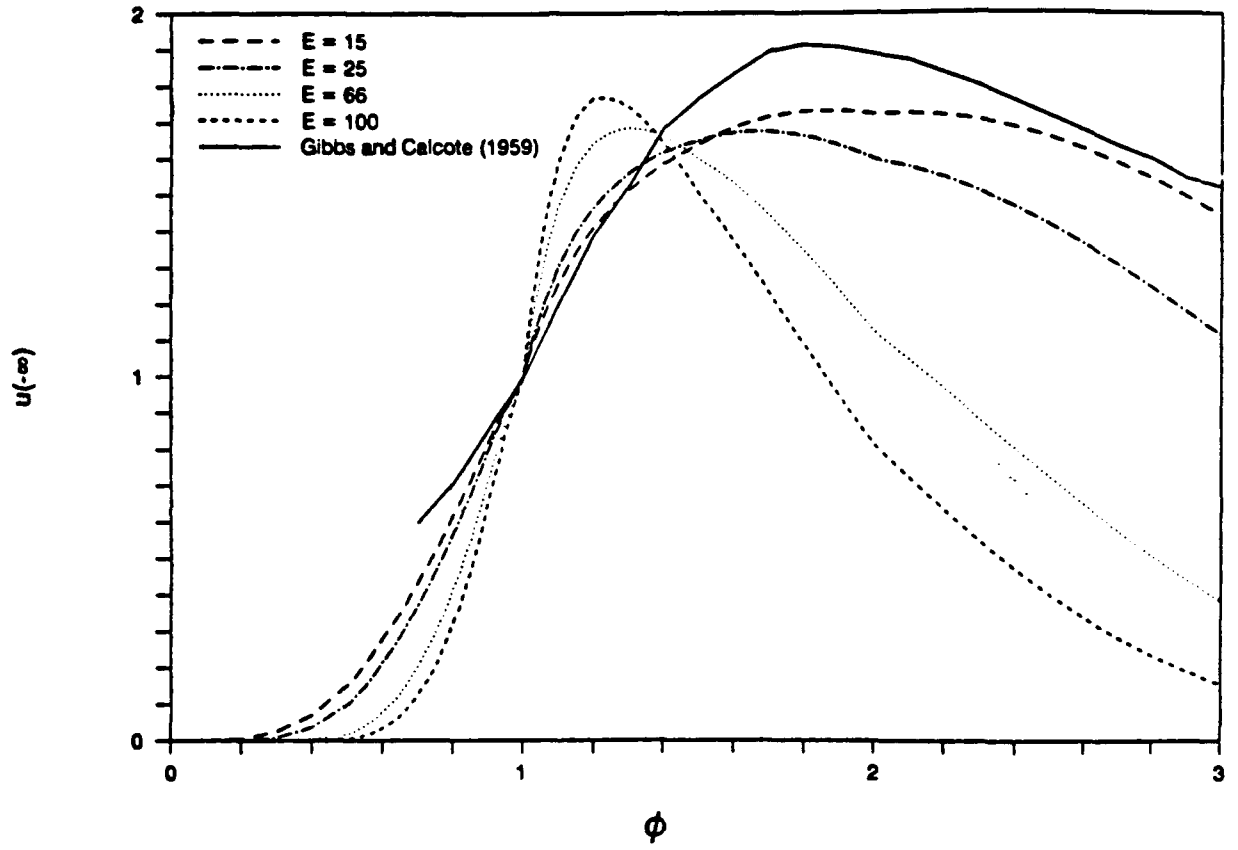

Figure 8. Same as Figure 4, except that the thermal diffusivity, and hence the Lewis-Semenov numbers, are permitted to vary with the stoichiometry of the cold hydrogen/air mixture.

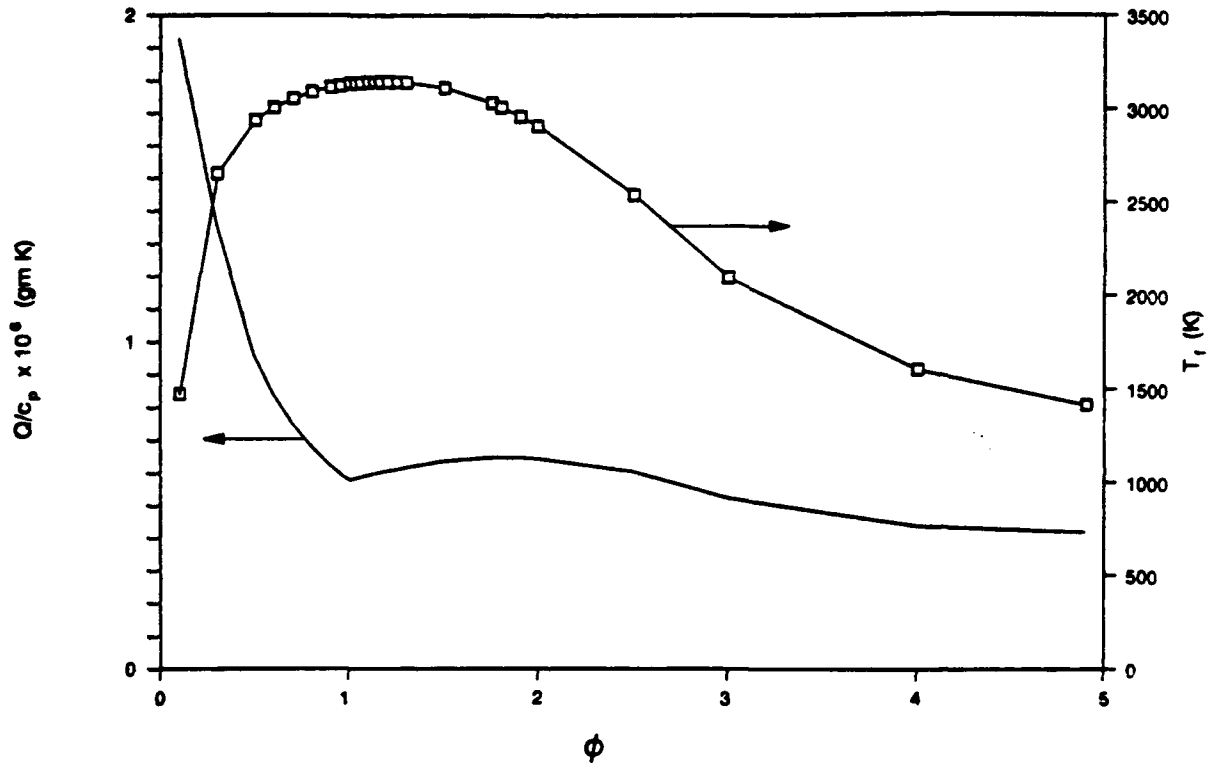

Figure 9. Same as Figure 1, except for a propane-oxygen mixture.

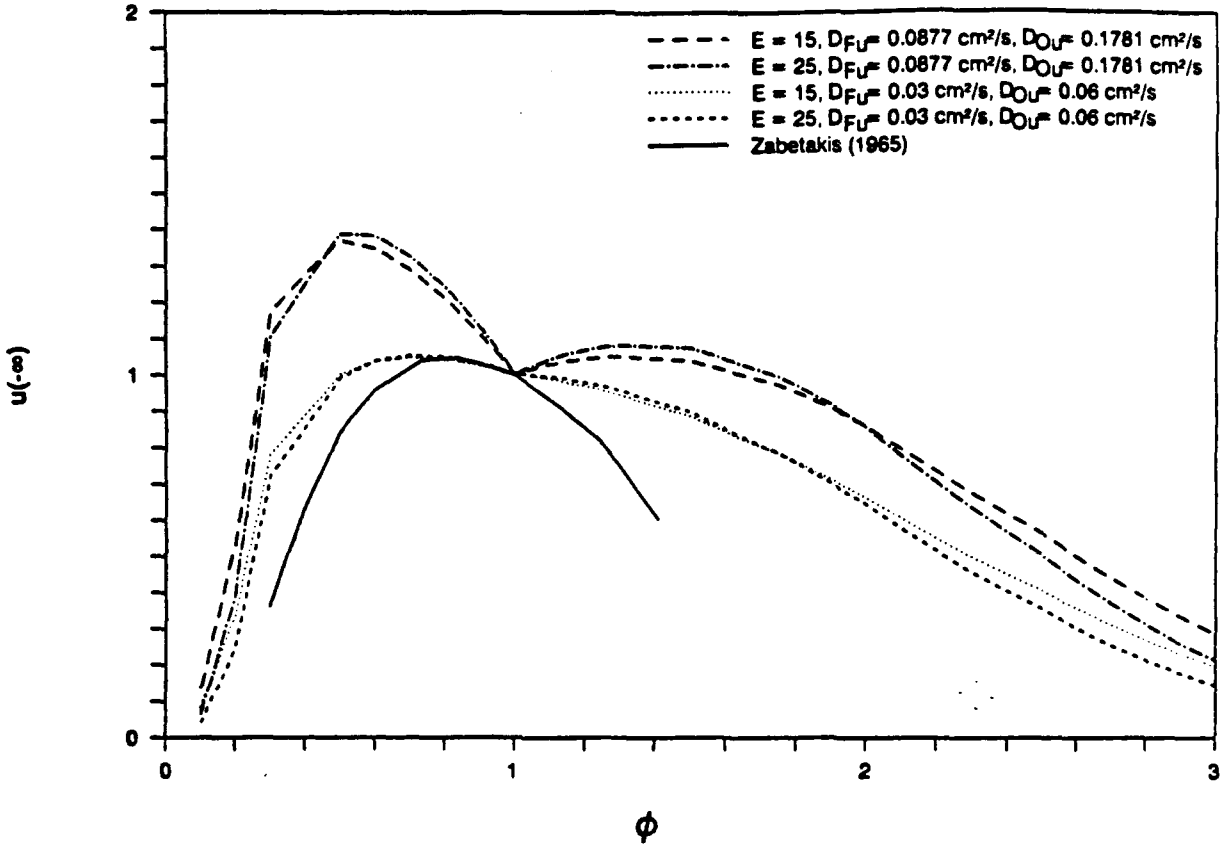

Figure 10. The laminar adiabatic flame speed $u(-\infty)$, normalized so its value is unity for a stoichiometric mixture ($\phi = 1$), vs. the equivalence ratio ϕ, for a propane-oxygen mixture initially at room conditions. Results for E = 15 are closest to experimental observations (Zabetakis 1965). The thermal diffusivity, and hence the Lewis-Semenov numbers, are permitted to vary with the stoichiometry of the cold mixture. Whereas $D_{Fu} \doteq 0.088$ cm^2/s and $D_{Ou} \doteq 0.18$ cm^2/s, it is noted that arbitrarily assigning the smaller values $D_{Fu} \doteq 0.03$ cm^2/s and $D_{Ou} \doteq 0.06$ cm^2/s does better recover the data; however, the need for such difficult-to-justify values suggests that the one-step kinetic mechanism needs generalization.

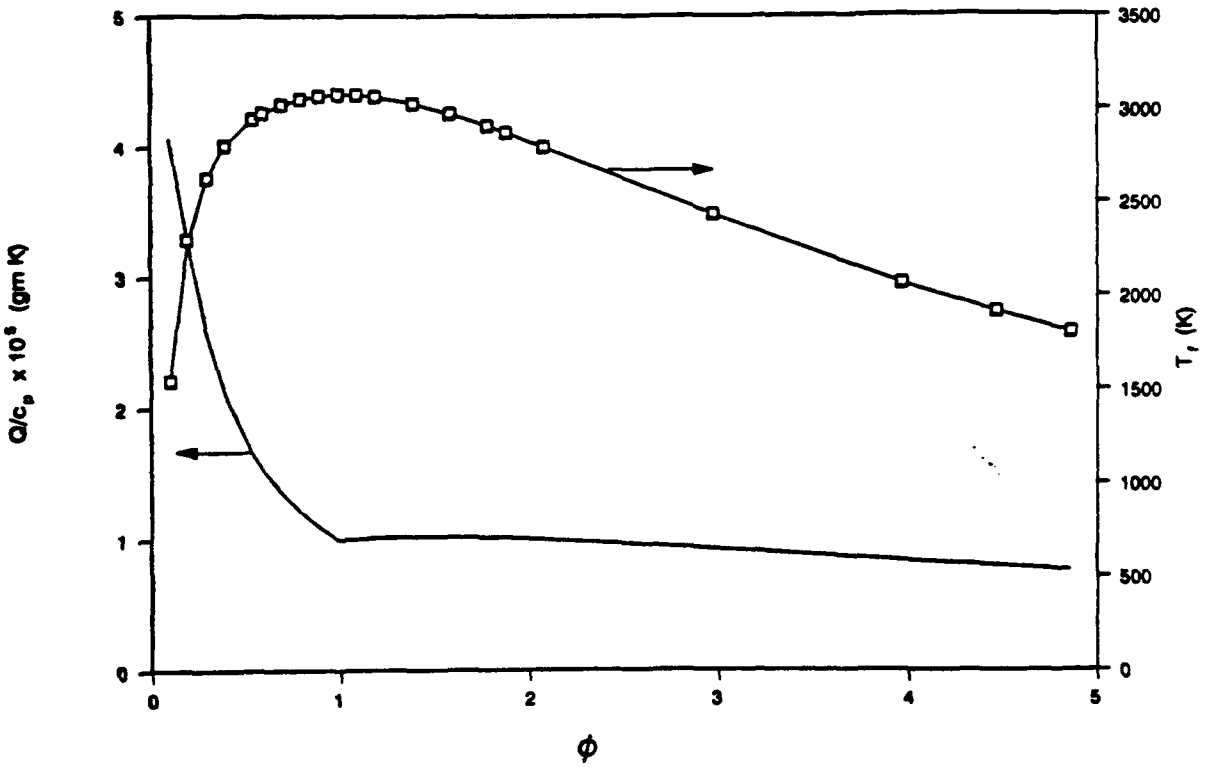

Figure 11. Same as Figure 1, except for a hydrogen-oxygen mixture.

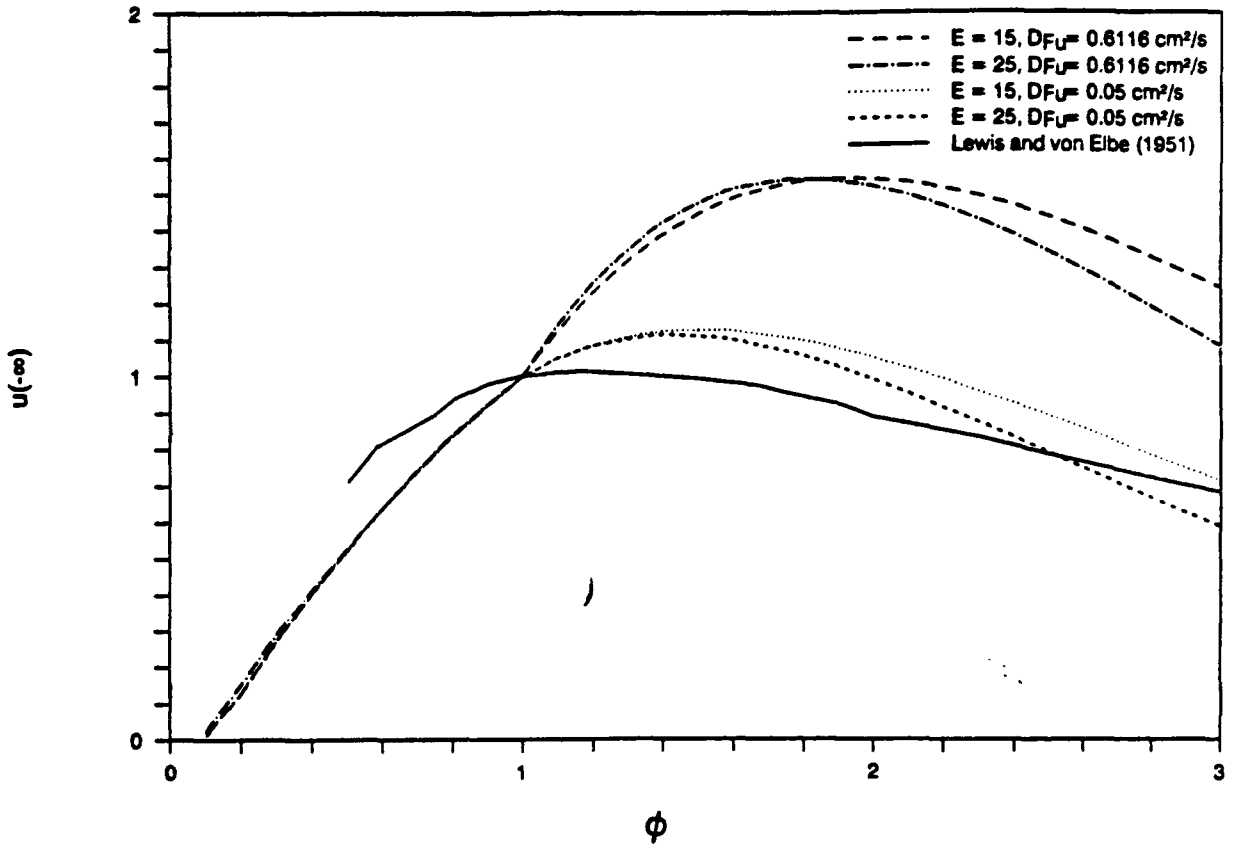

Figure 12. Same as Figure 10, except for a hydrogen-oxygen mixture. Again, decrementing the value of the fuel diffusivity ($D_{FU} \doteq 0.61$ cm^2/s is the observed value) better recovers the data (Lewis and von Elbe 1951). For hydrogen-oxygen mixtures, such decrementing may suggest a crucial transport role in flame spread for a hydrogen-containing radical appreciably heavier than the hydrogen molecule.

APPENDIX II.

Evaluating a Simple Model for Laminar-Flame-Propagation Rates. II. Spherical Geometry

G. Carrier, F. Fendell, K. Chen, and S. Cook

TRW Space and Technology Group
Redondo Beach, CA 90278

(Submitted to Combustion Science and Technology)

The propagation of a spherical flame radially outward (from an unspecified ignition with purely local and transient consequences) is examined by approximate analysis for an initially homogeneous gaseous premixture. A direct one-step irreversible bimolecular second-order chemical reaction with large Arrhenius activation energy is adopted, but account is taken of the modified exothermicity owing to the partial dissociation of product species and to other causes of incomplete oxidation. The effects arising from differing diffusivities for heat transfer and reactant-species mass transfer, and from varying the equivalence ratio of the premixture, are considered. Algebraic expressions and a simple quadrature are derived which suffice to describe the evolution of the spherical flame speed to the asymptotic planar-flame value, as the magnitude of the flame radius increases from values modestly in excess of the diffusive scale to values which are large multiples of the diffusive scale, for a flame with a two-zone (convective-diffusive, diffusive-reactive) structure. Limited published data on the variation of flamefront-speed-versus-time behavior with equivalence ratio for simple-hydrocarbon/air mixtures are examined in view of the results.

1.0 INTRODUCTION

The propagation of flames through combustible mixtures depends in significant ways on several characterizing properties of the constituents and on the geometry of the configuration. This paper stems from an interest in the multiparameter dependence of the flame speed of a spherical flame on its radius, on the transport properties of the reactants, and on the stoichiometry of the combustible mixture (Strehlow 1984). Because of this multiparameter dependence it is very advantageous to so construct the analysis that ease of interpretation of the results is optimized. To that end, we have presented an analysis (Carrier et al. 1990) of a planar (one-dimensional) flame, to which the spherical flame evolves as it propagates to larger and larger radius -- we exclude from our examination near-limit flames that do not continue to propagate. The approximations adopted in these analyses are designed to clarify the roles of the several parameters of interest and to facilitate comparisons of related configurations. In particular, however, we provide an accurate and analytical treatment of these phenomena for flames of small radius as is consistent with the basic, well-established but approximate problem formulation that we adopt.

As is the case with most combustion problems, it is very advantageous to conduct the analysis in terms of dimensionless variables and parameters.

Our choices and notation were introduced in the companion, planar study (Carrier et al. 1990), and, for brevity, are not repeated here.

2.0 THE SPHERICAL FLAME

2.1 Formulation and Solution

We want to find a description of the combustion phenomenon that ensues when, at time t_i, a flame is ignited at $r = R_{min}$ in an initially homogeneous, combustible mixture. [The spherical radial coordinate r^* is nondimensionalized against a diffusive scale, so $r = r^*/\ell$, $\ell = \kappa_u/u_{ref}$, κ_u is the thermal diffusivity of the cold mixture, and u_{ref} is the planar-flame propagation speed for a stoichiometric mixture.] We want the description to be valid in $r > R_{min}$, $t > t_i$, and we require that, in $r > R_{min}$, there be no artifacts of the ignition process. That is, in $t > t_i$, the evolution of the phenomenon stems only from the initially present, homogeneously distributed supply of heat and reactants.

Consistent with the foregoing, there is no propagation phenomenon in which the flame radius $R(t)$ has a constant speed [$\dot{R}(t) = \text{const.}$] and/or has an invariant structure $\theta(r,t) = \Theta(x)$, where (in this section only) $x = r - R(t)$. However, we do anticipate that the temperature will be most conveniently described by

$$\theta(r,t) = \Theta[x,R(t)], \tag{2.1}$$

and that its evaluation will be quasisteady. That is, we expect that

$$\Theta_t \doteq -\dot{R}\,\Theta_x, \tag{2.2}$$

a statement which implies that we expect

$$\Theta_R(x,R) \ll |\Theta_x(x,R)|. \tag{2.3}$$

We also expect, of course, that the thickness of the reaction zone, within which diffusion and reaction are the significant mechanisms, is small compared with either the radius R or the thickness of the preheat region within which diffusion and convection are the dominant mechanisms.

The conservation laws are the time-dependent, three-dimensional, spherically symmetric counterparts of those used in the planar-flame analysis [RR is defined below in (2.11), and we take $k(\theta) = 1$, i.e., the thermal conductivity is held constant]:

$$L(\theta) = \rho\,\theta_t + \rho\,u\,\theta_r - \frac{1}{r^2}\left(r^2\,\theta_r\right)_r = \theta^{\alpha-2}\,RR, \tag{2.4}$$

$$\rho\,Y_t + \rho\,u\,Y_r - \frac{\sigma_F}{r^2}\left(r^2\,Y_r\right)_r = \theta^{\alpha-2}\,RR, \tag{2.5}$$

$$\rho\,X_t + \rho\,u\,X_r - \frac{\sigma_O}{r^2}\left(r^2\,X_r\right)_r = \theta^{\alpha-2}\,RR; \tag{2.6}$$

continuity requires that

$$r^2\,\rho_t + \left(r^2\,u\,\rho\right)_r = 0. \tag{2.7}$$

It is advantageous, both in the development of the analysis and in the verification of the quasisteady hypothesis, to treat first those mixtures for which $\sigma_F = \sigma_O = 1$. For such mixtures,

$$L(\theta + Y) = L(\theta + X) = 0. \tag{2.8}$$

Under the initial conditions $\theta(r,0) = \theta_u = 1$, $X(r,0) = X_u = b$, and $Y(r,0) = Y_u = a$(< b, for the fuel-lean case), equation (2.8) implies

$$\theta(r,t) + Y(r,t) = 1 + a, \tag{2.9}$$

$$\theta(r,t) + X(r,t) = 1 + b, \tag{2.10}$$

and (2.4) becomes [J^* is a known factor that varies with the cold-mixture properties -- see (2.46) in Carrier et al. (1990)]

$$L(\theta) = \theta^{\alpha-2}\,\frac{J^*}{u_{ref}^2}\,(1 + a - \theta)(1 + b - \theta)\,\exp[-E/(\theta - 1)] = \theta^{\alpha-2}\,RR. \tag{2.11}$$

Using (2.1), and also using the hypothesis that the length and time scales of θ <u>in the reaction zone</u> are such that only diffusion and reaction are important mechanisms, we have, as in the planar-flame counterpart,

$$\theta_{xx} = -\,\theta^{\alpha-2}\,RR\ . \tag{2.12}$$

In short, at the outer edge of the reaction zone,

$$\theta(0,R) = 1 + a, \tag{2.13}$$

$$\theta_x(0,R) = -\,\beta, \tag{2.14}$$

where [see (2.15) and (2.5) in Carrier et al. (1990), and recall that $k(\theta) = 1$]

$$\beta^2 = 2(1 + a)^{\alpha-2}\,\frac{J^*}{u_{ref}^2}\,G(a,b - a,E,1,1), \tag{2.15a}$$

$$G(a,b-a,E,\sigma_0,\sigma_F) = \int_1^{1+a} \left[\frac{(b-a)(1+a-T)}{\sigma_F} + \frac{(1+a-T)^2}{\sigma_0\,\sigma_F}\right] \exp\left[-\frac{E}{T-1}\right] dT\,. \qquad (2.15b)$$

In the preheat zone, $x > 0$, the reaction rate is negligible, and (2.4) and (2.7) can be combined to give

$$\left(r^2\,\rho\,\theta\right)_t + \left(r^2\,\rho\,u\,\theta\right)_r - \left(r^2\,\theta_r\right)_r = 0. \qquad (2.16)$$

We have confined our attention to isobaric configurations whose implication for the equation of state in the present approximations, $\rho\,\theta = 1$, assures that (2.16) reduces to

$$r^2\left(u - \theta_r\right) = f(t), \qquad (2.17)$$

where the function of integration is identified as follows. We anticipate [see Carrier et al. (1990), Section 4] that the burnt gas in $r < R(t)$ [where $R(t)$ is recalled to be the flame position] will be virtually motionless, so by (2.17) we have

$$u(r,t) = \theta_r(r,t) - \frac{R^2}{r^2}\,\theta_r[R(t),t]. \qquad (2.18)$$

Equations (2.4), (2.13), (2.14), and (2.18) imply that, for the preheat zone,

$$\rho\,\dot{R}\,\theta_R - \rho\left[\dot{R} - \theta_x(x,R) - \beta\,\frac{R^2}{r^2}\right]\theta_x - \frac{1}{r^2}\left(r^2\,\theta_x\right)_x = 0, \qquad (2.19)$$

with

$$\theta(0,R) = 1 + a,\ \theta_x(0,R) = -\beta,\ \theta(\infty,r) = 1. \qquad (2.20)$$

At this point, we explore the possibility that (2.19) can be modelled (i.e., replaced) by a much simpler equation whose analysis would be more elementary and whose interpretation and implementation would be extremely advantageous. While (2.2) and (2.3) furnish some of the tentative anticipations, it is easiest just to present the replacement equation and list its attributes than it is to construct the manner in which we "found" it. The replacement equation is

$$\left(r^2\,\theta_x\right)_x + \frac{\dot{R}}{1+a}\,r^2\,\theta_x = 0, \qquad (2.21)$$

and, again, it is to be solved under the conditions given in (2.20). A series expansion of $\theta(x,R)$ in powers of x, using (2.19), is precisely the same as that obtained using (2.21), through terms of order x^3. Furthermore, whichever of

these equations is used, θ_R and its slope θ_{Rx} are each zero at $x = 0$. It is clear that the macroscopic features of the structure of $\theta(x,R)$ as defined by (2.19) will be preserved by the $\theta(x,R)$ associated with (2.21). Accordingly, we shall adopt (2.21), as a suitable approximation to (2.19), but, when (2.21) is solved, we shall analyze critically the accuracy of its solution.

The solution of (2.21) is

$$\theta = 1 + \int_x^\infty \beta \frac{R^2}{r^2} \exp\left[-\frac{\dot{R}x_1}{1+a}\right] dx_1 = 1 + I(x;\beta,a,R,\dot{R}), \tag{2.22}$$

constrained by

$$I(0;\beta,a,R,\dot{R}) = a. \tag{2.23}$$

The constraint may be rewritten as

$$\frac{\beta R^2 \dot{R}}{1+a}\left\{\exp\left[\dot{R}R/(1+a)\right]\right\} \int_{\dot{R}R/(1+a)}^\infty \frac{\exp(-z)}{z^2} dz = a. \tag{2.24}$$

Under the definition of the exponential integral (e.g., Gautschi and Cahill 1967)

$$E_n(z) = \int_1^\infty \frac{\exp(-zt)}{t^n} dt \quad [n = 0, 1, 2, \ldots ; \text{Real}(z) > 0], \tag{2.25}$$

(2.24) may be rewritten as

$$\lambda[\exp(q)]\, E_2(q) = 1, \tag{2.26}$$

where λ, the ratio of the flame radius to the e-folding thickness of the diffusive-convective zone of the one-dimensional flame, is given by

$$\lambda = \beta R/a, \tag{2.27}$$

and q/λ, the ratio of the spherical flame speed (relative to the burnt gases) to the one-dimensional flame speed (relative to the burnt gases), is given by

$$q/\lambda = \frac{\dot{R}}{\beta(1+a)/a}. \tag{2.28}$$

[These characterizations with respect to the one-dimensional flame are evident from remarks in Carrier et al. (1990): see above (2.1) and (2.15), (2.19), and (2.20) in that text.] The quantity q/λ is plotted as a function of λ in Figure 1. This figure indicates that $(q/\lambda) \to 0$ as $\lambda \to 1$; i.e., quasisteady spherical flame propagation appears to lead to a self-contradiction for $\lambda < 1$, so, for $R < (a/\beta)$, an inherently transient ignition process seems involved. As $\lambda \to \infty$,

$q/\lambda \to 1 - (2/\lambda)$, or $\dot{R}/[(\beta/a)(1 + a)] = 1 - 2/(\beta R/a)$; for Lewis-Semenov number unity, Frankel and Sivashinsky (1983), who present results for the $R \to \infty$ limit only, give, in present notation, $\dot{R}/[(\beta/a)(1 + a)] = 1 - 2([\ell n(1 + a)]/a)/(\beta R/a)$. The two expressions agree only in the weakly exothermic limit $a \to 0$. For future reference, we also present $q/\lambda = F(q) = q[\exp(q)]E_2(q)$ vs. q in Figure 2.

For $\phi = 1$, $\beta = a$. Substitution of the approximate solution, (2.22) and (2.23), to the boundary-value problem (2.19)-(2.20) yields residuals [from (2.19)] as a function of x,R. If the absolute value of the residual is normalized by the magnitude of the diffusional term evaluated at $x = 0$ and R, then, for the typical value $a = 6$, the normalized residual is equal to 2.8×10^{-5} at $x = 0.01$ and rises to a maximum of about 0.38 at $x = 5$, for $R = 1.5$; is equal to 2.9×10^{-5} at $x = 0.01$ and rises to a maximum of 0.092 at $x = 1.5$, for $R = 3$; and is equal to 8×10^{-6} at $x = 0.01$ and rises to a maximum of about 0.075 at $x = 2$, for $R = 10$. As a check on (2.3), this approximate solution gives the magnitude of θ_x to be at least ten times the magnitude of θ_R for all values of x from zero to about 0.75, for $R = 1.5$; to about 1.75, for $R = 3$; to 3.0, for $R = 5$; and to infinity, for $R = 10$.

When one or both of σ_F and σ_O differ(s) from unity, another difficulty arises. If one proceeds as though θ, Y, and X, each evaluated on the hot side of the reaction zone, took on the values $(1 + a)$, 0, and $(b - a)$, respectively, the foregoing procedures applied to each of $\theta(x,R)$, $Y(x,R)$, $X(x,R)$ would lead to a mathematical system for which no solution exists. Physically, the imbalance that underlies that obstacle is as follows. The temperature distribution to which our procedures would lead is given schematically in Figure 3, but the Y distribution that satisfies its boundary condition at $x = 0$ cannot satisfy $Y(\infty,R) = a$ because the determination of $\dot{R}(R)$ has already been co-opted in the analysis leading to $\theta(x,R)$. However, there is a temperature, $1 + a + g(R)$, that can be assigned to $\theta(0,R)$, such that, with $Y(0,R) = 0$ (the reaction zone is defined to be the region in which the reaction is brought to completion), $Y(\infty,R)$ can have the value a. Analogously,

$$X(0,R) = b - a + h(R). \tag{2.29}$$

Since g and h change with time, it is clear that the temperature in the burnt-gas region is not uniform. It is also apparent that the slow and weak variation of θ in that region would diffuse innocuously with no impact on the continuing phenomenology at larger values of r.

Accordingly, in the reaction zone,

$$\sigma_F\, Y + \theta = 1 + a + g(R), \tag{2.30}$$

$$\sigma_0\, X + \theta = 1 + a + g(R) + \sigma_0[b - a + h(R)]. \tag{2.31}$$

When $\sigma_F = 1$, $g = 0$; when $\sigma_0 = 1$, $g = -h$; when $\sigma_F = \sigma_0 = 1$, $g = h = 0$; when $\sigma_0 = \sigma_F$, $h = 0$.

The integration corresponding to (2.14) and (2.15) implies

$$\theta_x^2(0,R) = 2[1 + a + g(R)]^{\alpha-2} \frac{J^*}{u_{ref}^2} G\left[a + g(R), b - a + h, E, \sigma_0, \sigma_F\right] \tag{2.32}$$

$$= (\beta')^2. \tag{2.33}$$

Also, by (2.30) and (2.31),

$$\theta_x^2(0,R) = \sigma_F^2\, Y_x^2(0,R) = \sigma_0^2\, X_x^2(0,R). \tag{2.34}$$

The conservation equations in the preheat zone are $\left[\theta_x(0,R) = -\beta'\right]$

$$\rho\, \dot{R}\, \theta_R^{(j)} - \rho\, \dot{R}\, \theta_x^{(j)} + \rho\left[\theta_x^{(j)}(x,R) + \beta' \frac{R^2}{r^2}\right]\theta_x^{(j)} - \frac{\sigma^{(j)}}{r^2}\left[r^2\, \theta_x^{(j)}\right]_x = 0, \tag{2.35}$$

where

$$\theta^{(j)} \text{ is } \theta, Y, \text{ or } X, \text{ and correspondingly } \sigma^{(j)} \text{ is } 1, \sigma_F, \text{ or } \sigma_0. \tag{2.36}$$

The arguments used to justify (2.21) are unchanged, so that (2.29) and (2.30) are replaced by [$a' = a + g(R)$]

$$\left[r^2\, \theta_x\right]_x + \frac{\dot{R}}{1 + a}\left[r^2\, \theta_x\right] = 0, \tag{2.37}$$

$$\sigma_F\left[r^2\, Y_x\right]_x + \frac{\dot{R}}{1 + a}\left[r^2\, Y_x\right] = 0, \tag{2.38}$$

$$\sigma_0\left[r^2\, X_x\right]_x + \frac{\dot{R}}{1 + a}\left[r^2\, X_x\right] = 0. \tag{2.39}$$

Each of θ, Y, and X can now be subjected to the procedures used to obtain θ for the $\sigma_F = \sigma_0 = 1$ case. One gets

$$\theta = 1 + \int_x^\infty \beta' \left[\frac{R^2}{r^2}\right] \exp\left[-\frac{\dot{R}x_1}{1 + a'}\right] dx_1, \tag{2.40}$$

$$Y = a - \int_x^\infty \frac{\beta'}{\sigma_F} \left[\frac{R^2}{r^2}\right] \exp\left[-\frac{\dot{R}x_1}{\sigma_F(1 + a')}\right] dx_1, \tag{2.41}$$

$$X = b - \int_x^\infty \frac{\beta'}{\sigma_0} \left[\frac{R^2}{r^2}\right] \exp\left[-\frac{\dot{R}x_1}{\sigma_0(1 + a')}\right] dx_1. \tag{2.42}$$

The boundary conditions at $x = 0$ then imply

$$\frac{\beta'(1 + a')}{\dot{R}} F\left[\frac{R\dot{R}}{1 + a'}\right] = a + g, \tag{2.43}$$

$$\frac{\beta'(1 + a')}{\dot{R}} F\left[\frac{R\dot{R}}{\sigma_F(1 + a')}\right] = a, \tag{2.44}$$

$$\frac{\beta'(1 + a')}{\dot{R}} F\left[\frac{R\dot{R}}{\sigma_0(1 + a')}\right] = a - h, \tag{2.45}$$

where [see (2.25) and Figure 2]

$$F(z) = z^2 [\exp(z)] \int_z^\infty \frac{\exp(-s)}{s^2} ds \tag{2.46a}$$

$$= z [\exp(z)] E_2(z). \tag{2.46b}$$

For any premixture characterized by given values of the parameters E, σ_0, σ_F, a, and b, the calculation of $\dot{R}$, recalled to be the spherical flame speed (relative to the burnt gases), as a function of R, recalled to be the flame radius, can proceed as follows. [It may be useful also to recall that this section has been developed under the fuel-lean (or stoichiometric) scenario $a \leq b$; for the fuel-rich scenario $a > b$, the symbols a and b should be interchanged, and the symbols σ_0 and σ_F should be interchanged.] For each of a sequence of real positive values assigned to the quantity q, where now [in correspondence with the definition given in (2.28)]

$$q = \frac{R\dot{R}}{1 + a'}, \tag{2.47}$$

one finds the value of the function F [defined in (2.46)] for each of the quantities q, (q/σ_0), and (q/σ_F). By dividing (2.43) by (2.44), one obtains the quantity g; by dividing (2.45) by (2.44), one obtains the quantity h. From (2.15), (2.21), (2.32), and (2.33), one now can obtain β'. From the definition given just above (2.37), one obtains a' (if $\phi \leq 1$, b' if $\phi > 1$). From (2.43), one obtains $\dot{R}$; from (2.47), one obtains R. Hence the sequence of values assigned to q yields $\dot{R}$ as a function of R, and thence, by one more quadrature, R is obtained as a function of time (elapsed since t_{ref}, when $R = R_{ref}$, the smallest R obtained from the sequence of values of q). The range of R reasonably examined is limited only by the occurrence of a singularity incurred in computation, or by the violation of a condition under which the above solution is derived. From examination of the asymptotic behavior of (2.43)-(2.47), we find that $\dot{R} \to 0$ at $R = (a/\beta')\sigma_F$ for $\phi < 1$, and at $R = (b/\beta')\sigma_0$ for $\phi > 1$, as generalizations of results previously found for $\sigma_F = \sigma_0 = 1$. It is reiterated that these results establish the scale smaller than which an explicitly unsteady initiation process is inherently involved in spherical propagation of a laminar flame. As $R \to \infty$, for $\phi < 1$, g and h vanish asymptotically, and $\dot{R}$ goes to the burned-gas speed of the planar flame:

$$\dot{R} \to \frac{\beta}{a}(1 + a), \quad \frac{g}{a} \sim -\frac{2\left[\sigma_F - 1\right]}{(\beta/a)R}, \quad \frac{h}{a} \sim -\frac{2\left[\sigma_F - \sigma_0\right]}{(\beta/a)R}; \tag{2.48}$$

for $\phi > 1$, the same formulas hold provided $a \to b$, $\sigma_F \to \sigma_0$, and $\sigma_0 \to \sigma_F$.

2.2 Discussion of Experimental Data

Experimental data are presented by Strehlow (1984) for the spherical-flame-front speed $\dot{R}$ as a function of spherical-flame-front position R, for nine stoichiometries distributed over the range $0.78 \leq \phi \leq 1.68$, for spark-ignited, atmospheric-pressure mixtures of propane and air; three of the values of the equivalence ratio are mislabeled, the proper labeling being given by Law (1989, p. 1394). The data are reproduced as Figure 4. There is the possibility of residual artifacts of the ignition event in the data. Frankel and Sivashinsky (1983), in work cited above [just after (2.28)], carried out an analysis valid <u>for large R only</u>, and found for $\phi < 1$, in the present terminology,

$$\frac{\dot{R}}{(\beta/a)(1 + a)} = 1 + \left[\frac{-\ell n(1 + a)}{a/(1 + a)} + \frac{\alpha I(a)}{2(1 + a)}\right] \frac{2}{(1 + a)(\beta/a)R}, \tag{2.49}$$

where

$$I(a) = \int_0^a \frac{\ell n(1 + z)}{z}\, dz, \quad \alpha = \frac{E}{1 + a}\left[\frac{\sigma_F - 1}{\sigma_F}\right] . \tag{2.50}$$

For $\phi > 1$, $a \to b$ and $\sigma_F \to \sigma_0$, in (2.49) and (2.50). According to (2.49) and (2.50), for $\sigma_F > \sigma_{Fc}$, where σ_{Fc} permits the expression in square brackets in (2.49) to vanish, $\dot{R}$ approaches its asymptotic value from above, as $R \to \infty$; for $\sigma_F < \sigma_{Fc}$, $\dot{R}$ approaches its asymptotic value from below. For $\phi > 1$, similar statements concerning the asymptotic approach of $\dot{R}$ can be made for $\sigma_0 > \sigma_{0c}$ and $\sigma_0 < \sigma_{0c}$. For the propane-air system, oxygen is the more rapidly diffusing reactant, and, indeed, in Strehlow's data $\dot{R}$ does approach its asymptotic value from above for <u>sufficiently</u> rich mixtures, whereas $\dot{R}$ approaches its asymptotic value from below for other stoichiometries. On this basis, without numerical comparison with Strehlow's data (which is reproduced in their paper with the typographical errors), Frankel and Sivashinsky (1983, p. 134) state that their "theoretical estimates yield both qualitative and quantitative agreement with experiment". Among the reasons for reservations are the following: (1) the transition in whether $\dot{R}$ decreases or increases to its limiting value occurs in the range $1.3 < \phi < 1.43$ in the data, whereas it occurs at $\phi = 1$ in the theory; (2) the theory is derived on the basis that α, defined in (2.50), is constant, but, since especially a and even σ vary significantly with ϕ, necessarily the dimensionless activation temperature E must vary with ϕ, a rather academic formulation; (3) the treatment in the theory of σ as constant is unsuitable (as an example) for hydrogen/air mixtures but no restrictions on the theory are stated; and (4) stoichiometric conditions are not treated by the theory.

Frankel and Sivashinsky (1983) adopt stoichiometrically invariant values (for the pertinent diffusivities) that they ascribe to Pelce and Clavin (1982), who in turn state that the values are from Fristrom and Westenberg (1965); we ourselves were unable to locate the cited values in that reference. Our calculations for the Lewis-Semenov numbers yield different values for these numbers (Figure 5); accordingly, our computations, based on the formulae derived in Section 2, give the firefront speed to be a monotonically increasing function of radius for all flammable propane/air mixtures (Figure 6). The range of flamefront radii examined in Figure 6 is far less than that in Figure 4, and we shall return to this matter. In fact, if we substitute the values that we believe to be appropriate for the transport properties of atmospheric-pressure propane/air mixtures of various equivalence ratios, we find that the behavior of the flamefront speed

as a function of the flamefront radius obtained from the expressions of Frankel and Sivashinsky (1983) is about the same as that obtained from the present results, and the behavior is quite at odds with that observed by Palm-Leis and Strehlow (1969) (Figures 7 and 8).

If indeed it were pertinent to compare the results of a theory addressing effects associated with the interplay of equivalence ratio, differing diffusivities, and curvature, then it may be useful to consider other data taken in the same apparatus by the same investigators (Palm-Leis 1966; Palm-Leis and Strehlow 1969, p. 118, Figure 5) for atmospheric-pressure methane-air flames (reproduced here as Figure 9). If the role of a stoichiometrically deficient, relatively quickly diffusing reactant is the explanation for an approach to asymptotic outward-spherical-flamefront-propagation speeds from higher values (that otherwise would be from smaller values -- since the preheating demands seem geometrically more challenging at smaller radii), then one might expect such decreasing-firefront-speed behavior in methane/air mixtures to arise at some fuel-lean stoichiometries. Although the precise equivalence ratios tested were not ascertained, the experimentalists do present results for the firefront speed as a function of firefront radius for five mixtures that are stated to span a wide range of equivalence ratios (from a near-lean-flammability-limit mixture to a stoichiometric mixture to a near-rich-flammability-limit mixture). In all cases, the flamefront speed clearly increases monotonically with flamefront radius, over the entire range of radii examined (0.5 cm to 7.5 cm). For completeness, our theoretical results for spherical methane/air flames are given in Figure 10.

However, important issues arise in connection with the very attempt to use the Strehlow data (Figure 4) to validate any model discussing the effect of differing diffusivities on outwardly propagating spherical flames. The effect of differing diffusivities on planar-flame propagation has been examined separately (see, for example, Carrier et al. 1990). Any additional effects owing to significant flame curvature are probably absent from the Strehlow data for the following reason. The spatial scale characterizing the thickness of a laminar flame is the diffusive scale $\ell = \kappa_u/u_{ref}$; for the cold hydrocarbon-air mixture, $\kappa_u = O(0.1\ cm^2/s)$ and $u_{ref} = O(40\ cm/s)$, so ℓ is a few hundredths of a millimeter. Even if we use burned-gas conditions, the estimated thickness but doubles, or so, since κ/κ_u varies as $(T/T_u)^{3/2}$, and u/u_{ref} varies as T/T_u, so ℓ/ℓ_u varies as $(T/T_u)^{1/2}$, a factor equal to no more than about two or three for physically interesting conditions. The Strehlow data are for flamefront radii of one-to-eight centimeters or so (there are a very few isolated readings for fuel-lean

stoichiometries at one-half-centimeter radius). Thus, the data describe phenomena occurring at flamefront radii of about one-hundred flame thicknesses or more, and thus describe effectively planar conditions. What is disconcerting about the data is that, even at flamefront radii of six-to-eight centimeters, many of the tests have not obtained asymptotic conditions -- it may be argued that some tests show no clear sign of approaching an asymptote. However, we may assign asymptotic values for each test by fitting each curve with the form $\dot{R}^* = c_1 + (c_2/R^*)$ -- a procedure that appears to be reasonable in practice, although we offer no reason why the adopted form is pertinent. (Actually, we obtain effectively the same estimate for the asymptotic value for $\dot{R}^*$ if we simply adopt the firefront speed at the largest value of R^* for which data are given.) We then take u_u^*, the experimentally measured planar-flame speeds for the propane-air mixtures over a wide range of equivalence ratios (Yu et al. 1986), and calculate appropriate burned-gas values (for comparison with the Strehlow data):

$$\dot{R}^* = \left[\frac{\rho_u^*}{\rho_f^*}\right] u_u^* = \frac{T_f}{T_u} \frac{(m_{ave})_u}{(m_{ave})_f} u_u^* \, , \quad \frac{1}{m_{ave}} = \sum_{i=1}^{N_t} \frac{Y_i}{m_i} \, , \tag{2.51}$$

where it is recalled that subscript u refers to the cold mixture and subscript f, to the burned gas. The quantity m_i is the molecular weight of species i of the N_t species present; the mass fractions for the burned gas are incidental information obtained from the equilibrium-mixture-composition computer codes (e.g., Gordon and McBride 1976) in the course of calculating the burned-gas temperature T_f. The molecular-weight factor was omitted from the previous approximate statement of the equation of state for the isobaric phenomena of interest, but here we seek to be a little more meticulous. We find (Figure 11) that the asymptotic $\dot{R}^*$ values ascribed to the Strehlow data are only roughly comparable to the $\dot{R}^*$ values inferred from planar-flame data -- and the Strehlow-data values particularly undershoot the planar-flame-derived values for the richest mixtures studied (i.e., for the largest equivalence ratios examined). We might ascribe this undershoot to radiational heat loss from the burned gas in the spherical flame propagation; we note that such radiational loss may arise in connection with large-molecular-weight hydrocarbons and other gaseous species, and need not involve necessarily the occurrence of carbonaceous particulate. One might ascribe this undershoot the variation in sign of $d\dot{R}^*/dR^*$ with ϕ for propane-air mixtures, but not for methane-air mixtures, is attributable to the greater radiational loss from sufficiently fuel-rich gas in the propane-air case. The amount of radiational loss would be expected to increase with the volume of burned gas. However, the

flamefront speed may be approaching an asymptotic value as the firefront radius increases, but, if so, it seems unlikely that the burned-gas volume in the experiments is of sufficient size that the burned gas is becoming opaque. Thus the reason for the change in sign of $d\dot{R}^*/dR^*$ with ϕ seems unresolved. The asymptotic results for spherical methane-air flames (that are analogous to the large-flamefront-radius results for propane-air flames) are given in Figure 12, together with more recent data.

The just-mentioned more recent data (Ronney and Wachman 1985, p. 115, Figure 4) for initially-atmospheric-pressure, methane-air mixtures (over the range of equivalence ratios from stoichiometry to the lean limit) present results for flamefront radius of 3 cm or greater. Hence, the same comments presented in connection with the Strehlow data again are pertinent. Over the range of flamefront radius of 3 cm to 6 cm, for which an isobaric approximation is appropriate (P. Ronney, private communication), $\dot{R}^*$ is constant for all equivalence ratios examined, except for those mixtures in the immediate vicinity of the lean-flammability limit. (The inferred values for the planar-flame speed are about 25% below those measured by other techniques, but the discrepancy concerns issues not pertinent to the present discussion.) In contrast to the data of Ronney and Wachman for methane/air mixtures, the data of Palm-Leis and Strehlow for methane/air mixtures does not report $\dot{R}^*$ to be constant over approximately the same range of flamefront-radius values. The explanation for nonconstant values of $\dot{R}^*$ in this flamefront-radius range for methane/air mixtures remains unidentified (as does the reason for the nonconstant values of $\dot{R}^*$ in this range for propane/air mixtures).

3.0 CONCLUDING REMARKS

We suggest that a need remains for careful experiments on isobaric spherical flame propagation, for a variety of simple-hydrocarbon/air mixtures over a wide range of equivalence ratios, with emphasis on (1) minimal, transient, localized energy deposition for ignition; (2) data collection at small flamefront radii, for purposes of elucidating curvature effects in the presence of differing diffusivities; and (3) observation whether flamefront speeds consistent with planar-flame speeds are achieved at appropriate firefront positions. In the absence of such data, especially for the flamefront speed as a function of flamefront radius, the clarification of key issues in the theoretical investigation of spherical flame propagation seems to be stymied.

ACKNOWLEDGMENT

The authors are pleased to acknowledge that this research was sponsored by the Air Force Office of Scientific Research, Systems Command, USAF, under contract F49620-87-C-0081, monitored by Dr. Julian Tishkoff. The U.S. Government is authorized to reproduce and distribute reprints for Governmental purposes.

REFERENCES

Carrier, G., Fendell, F., Chen, K., and Pallia, C. (1990). Evaluating a simple model for laminar-flame-propagation rates. I. Planar geometry. Submitted for publication.

Frankel, M. L., and Sivashinsky, G. I. (1983). On effects due to thermal expansion and Lewis number in spherical flame propagation. Combustion Science and Technology 31, 131-138.

Fristrom, R. M., and Westenberg, A. A. (1965). Flame Structure. New York, NY: McGraw-Hill.

Gautschi, W., and Cahill, W. F. (1967). Exponential integral and related functions. Handbook of Mathematical Functions with Formulas, Graphs, and Mathematical Tables, edited by M. Abramowitz and I. A. Stegun, 227-251. Washington, DC: U.S. Government Printing Office.

Gordon, S., and McBride, B. J. (1976). Computer program for calculation of complex chemical equilibrium compositions, rocket performance, incident and reflected shocks, and Chapman-Jouguet detonations. NASA SP-273, interim revision. Washington, DC: National Aeronautics and Space Administration.

Law, C. K. (1989). Dynamics of stretched flames. Twenty-Second Symposium (International) on Combustion, 1381-1402. Pittsburgh, PA: Combustion Institute.

Palm-Leis, A. (1966) Transient behavior of free flames in laminar and turbulent media. Ph.D. thesis. Urbana, IL: Department of Aeronautical and Astronautical Engineering, University of Illinois.

Palm-Leis, A., and Strehlow, R. A. (1969). On the propagation of turbulent flames. Combustion and Flame 13, 111-129.

Pelce, P., and Clavin, P. (1982). Influence of hydrodynamics and diffusion upon the stability limits of laminar premixed flames. Journal of Fluid Mechanics 124, 219-237.

Ronney, P. D., and Wachman, H. Y. (1985). Effect of gravity on laminar premixed gas combustion. I: flammability limits and burning velocities. Combustion and Flame 62, 107-119.

Strehlow, R. A. (1984). Combustion Fundamentals. New York, NY: McGraw-Hill.

Yu, G., Law, C. K., and Wu, C. K. (1986). Laminar flame speeds of hydrocarbon plus air mixtures with hydrogen addition. Combustion and Flame 63, 339-347.

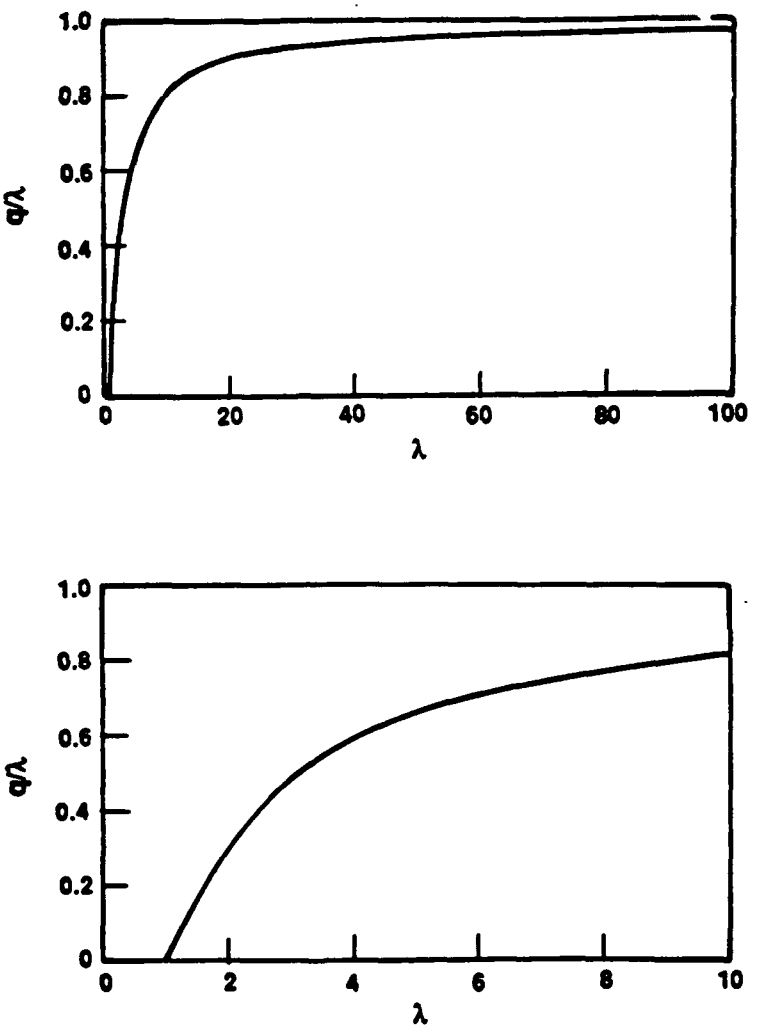

Figure 1. A plot of q/λ vs. λ, where $\lambda[\exp(q)]\ E_2(q) = 1$, and $E_2(q)$ is an exponential integral.

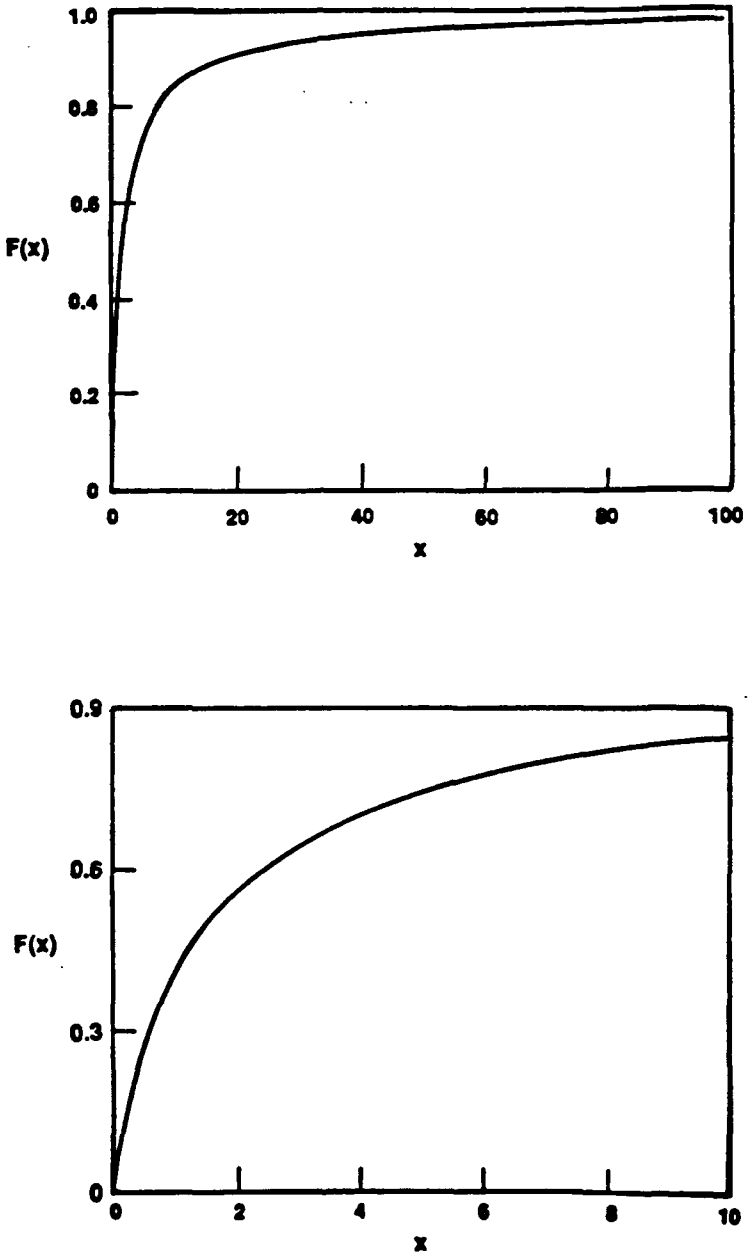

Figure 2. A plot of F(x) vs. x, where $F(x) = x[\exp(x)]E_2(x)$, and $E_2(x)$ is an exponential integral.

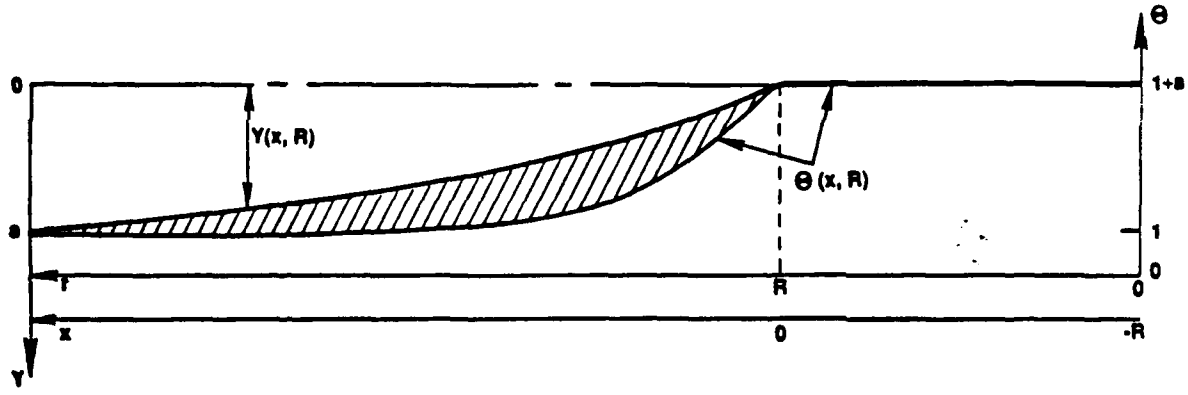

Figure 3. A schematic for discussion of the outward propagation of a fuel-lean spherical flame, where $\theta(x,R)$ is the (nondimensionalized) temperature, $Y(x,R)$ is the energetically adjusted mass fraction (with value a in the cold mixture), $x = r - R(t)$, and $r = R(t)$ is the (nondimensionalized) radial position of the flame front at time t. Hence, burned gas lies in $R(t) > r > 0$ and unburned gas in $\infty > r > R(t)$.

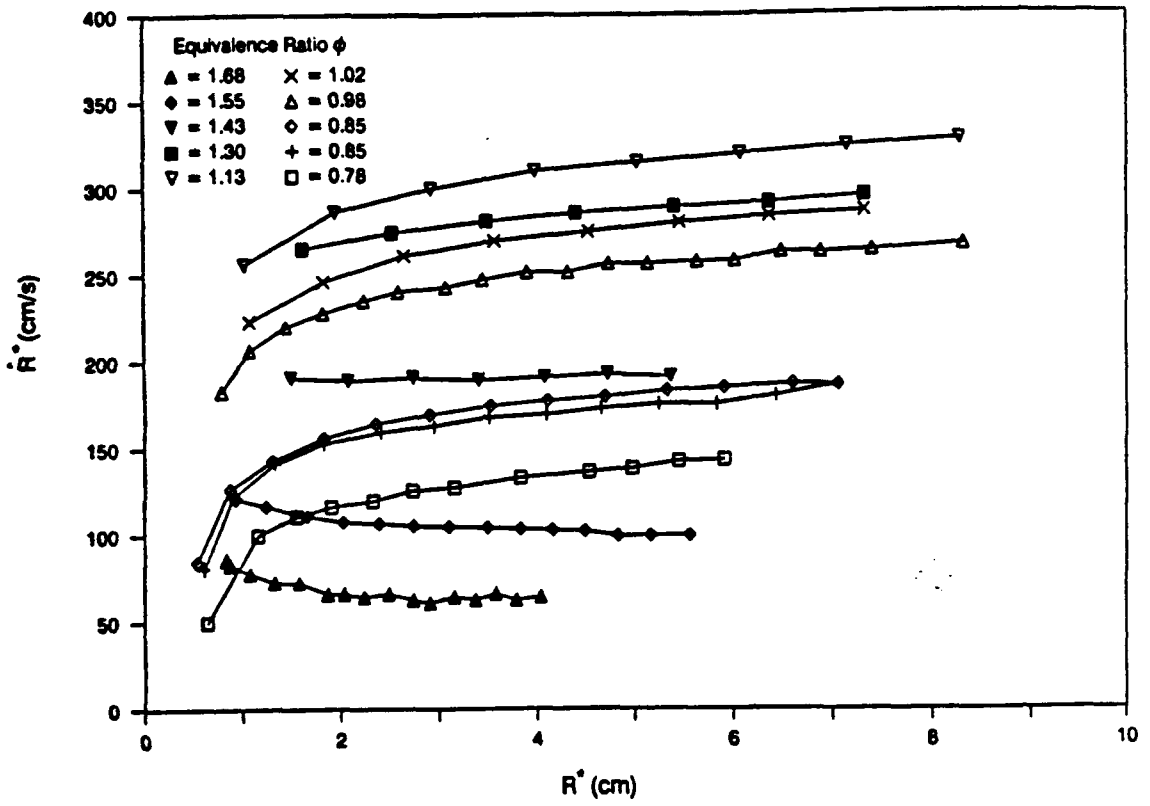

Figure 4. Experimental results reported for atmospheric-pressure propane/air mixtures, for the spherical-flamefront speed $\dot{R}^*$ as a function of spherical-flamefront radius R^*, for several values of the equivalence ratio ϕ (Palm-Leis 1966; Palm-Leis and Strehlow 1969; Strehlow 1984; Law 1989).

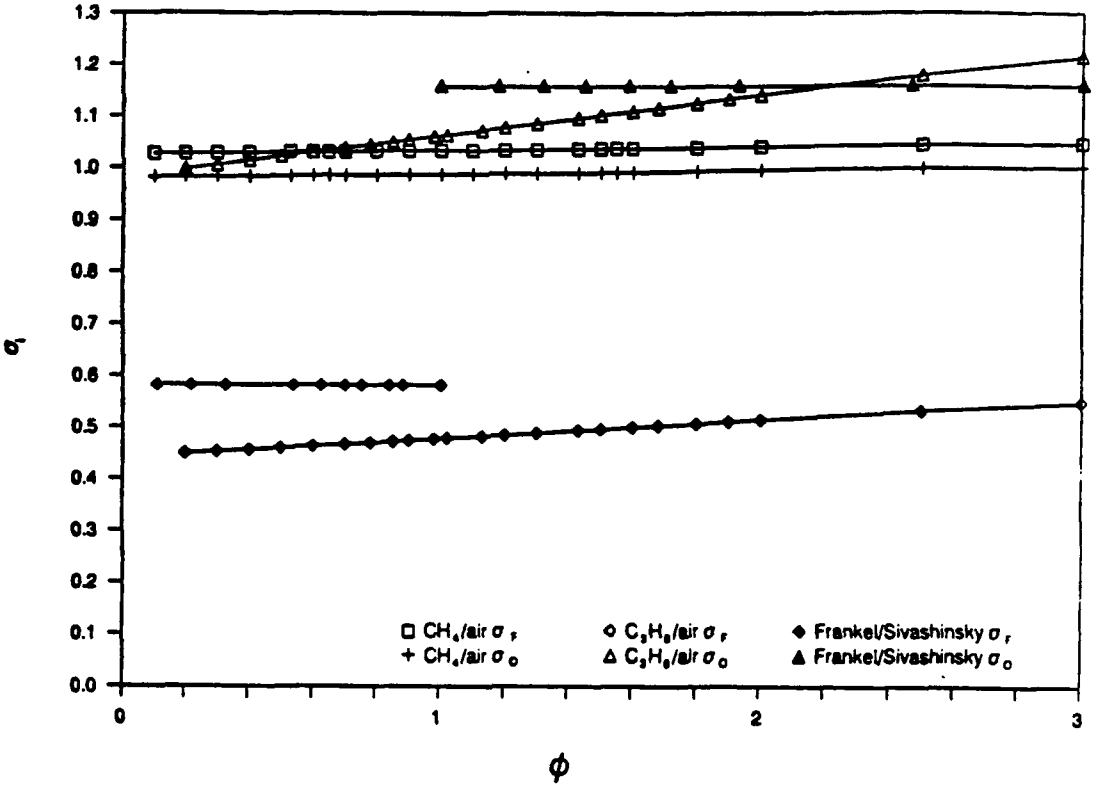

Figure 5. The Lewis-Semenov number for the fuel species σ_F and for oxygen σ_O, as a function of the equivalence ratio ϕ. The solid symbols denote the stoichiometrically invariant values adopted by Frankel and Sivashinsky (1983) for propane/air mixtures; only the σ_i of the stoichiometrically deficient species enters their model. The open symbols denote the values adopted here for propane/air and methane/-air mixtures; variability with ϕ arises from the variability of the thermal diffusivity. Mixtures are at atmospheric pressure.

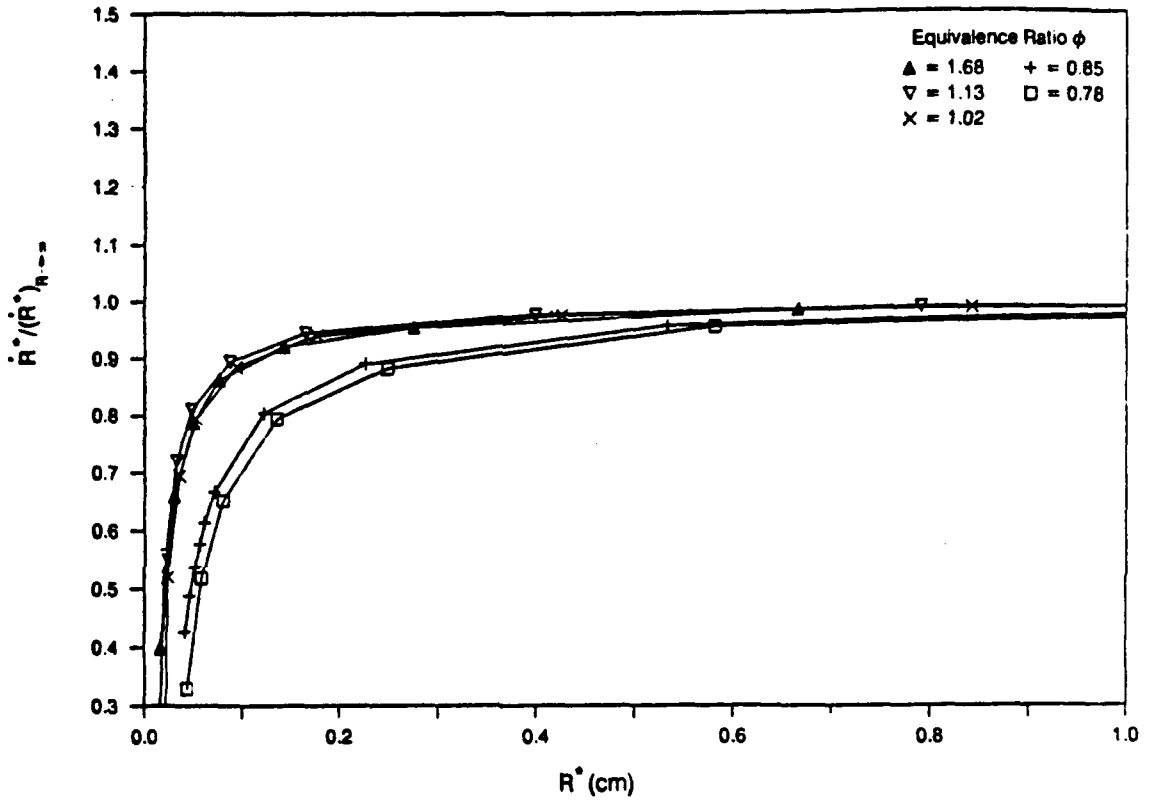

Figure 6. Variation of the normalized spherical-flamefront speed $\dot{R}^*$ with spherical-flamefront radius R^*, for atmospheric-pressure propane/air mixtures of various equivalence ratios ϕ, according to the present theory. We adopt $E = 25$, $D_{Fu} = 0.099\ cm^2/s$, $D_{Ou} = 0.22\ cm^2/s$.

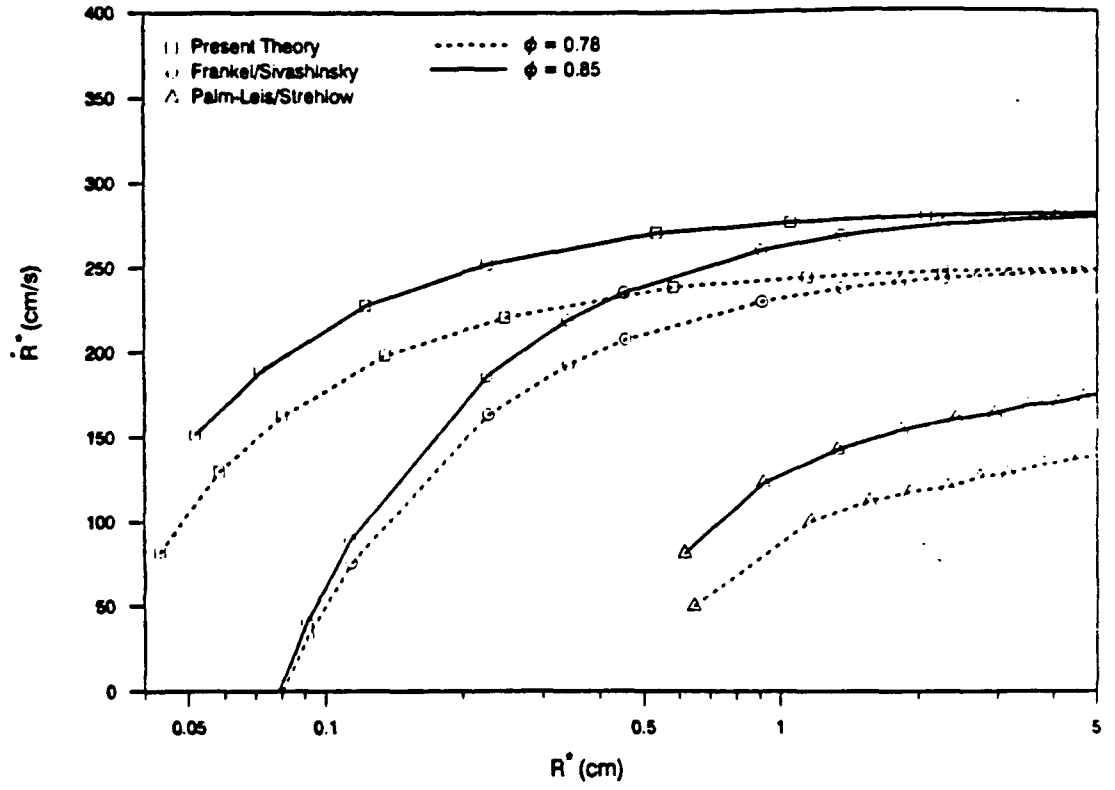

Figure 7. The spherical-flamefront speed $\dot{R}^*$ as a function of spherical-flamefront radius R^*, for fuel-lean equivalence ratios ϕ, for atmospheric-pressure propane/air mixtures. The observations of Palm-Leis and Strehlow (1969) are compared with the results of the present theory, and with the results obtained from the formulae of Frankel and Sivashinsky (1983) by substituting the same parameter values that we adopt.

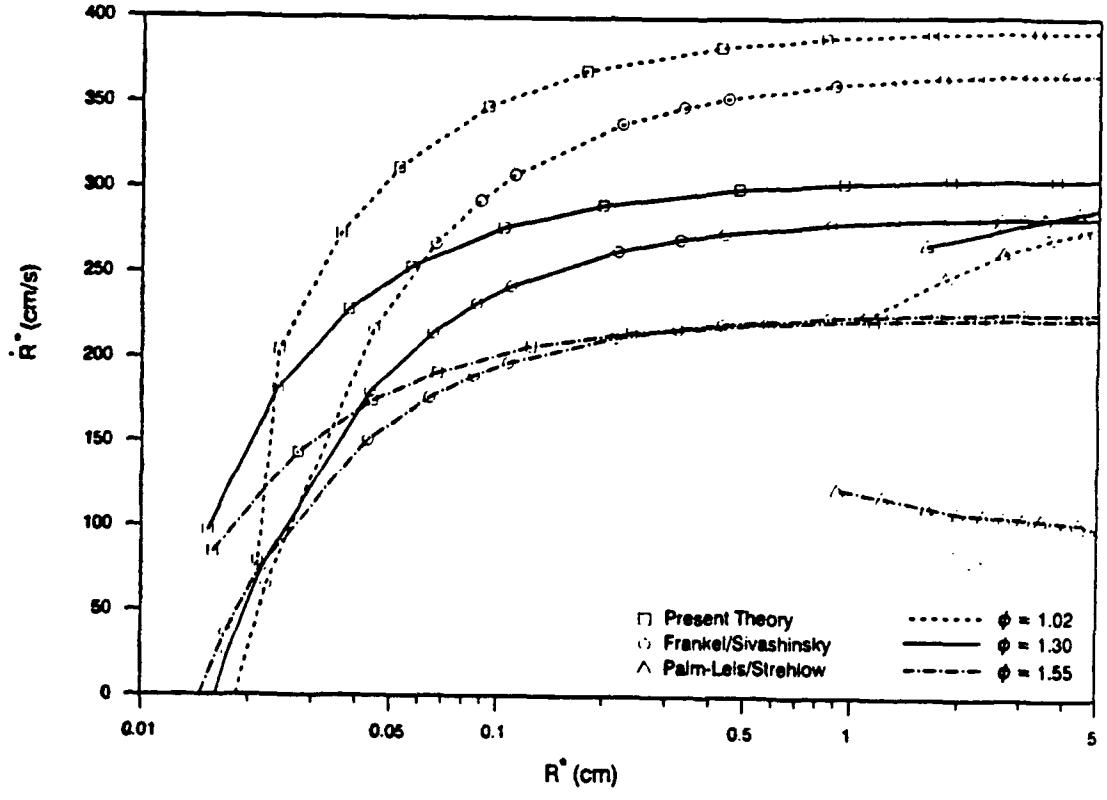

Figure 8. The same presentation as in Figure 7, but here for fuel-rich equivalence ratios.

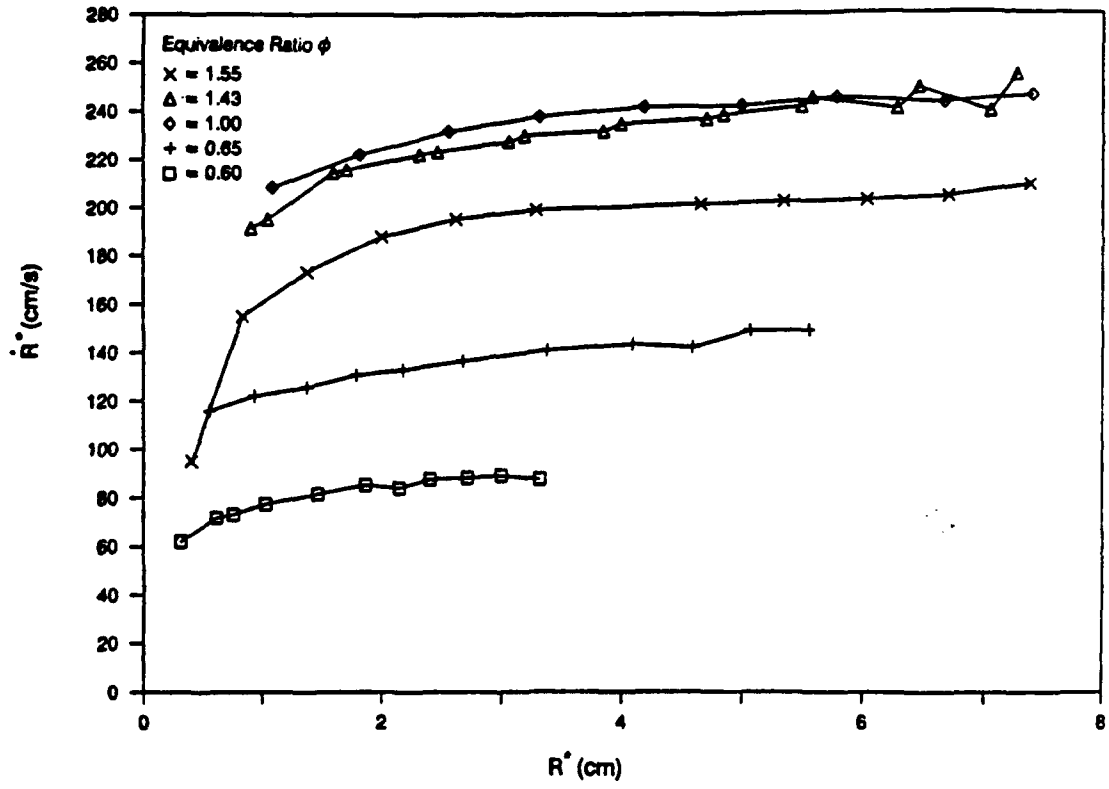

Figure 9. Experimental results reported for atmospheric-pressure methane/air mixtures, for the spherical-flamefront speed $\dot{R}^*$ as a function of spherical-flamefront radius R^*, for several estimated values of the equivalence ratio ϕ (Palm-Leis 1966; Palm-Leis and Strehlow 1969).

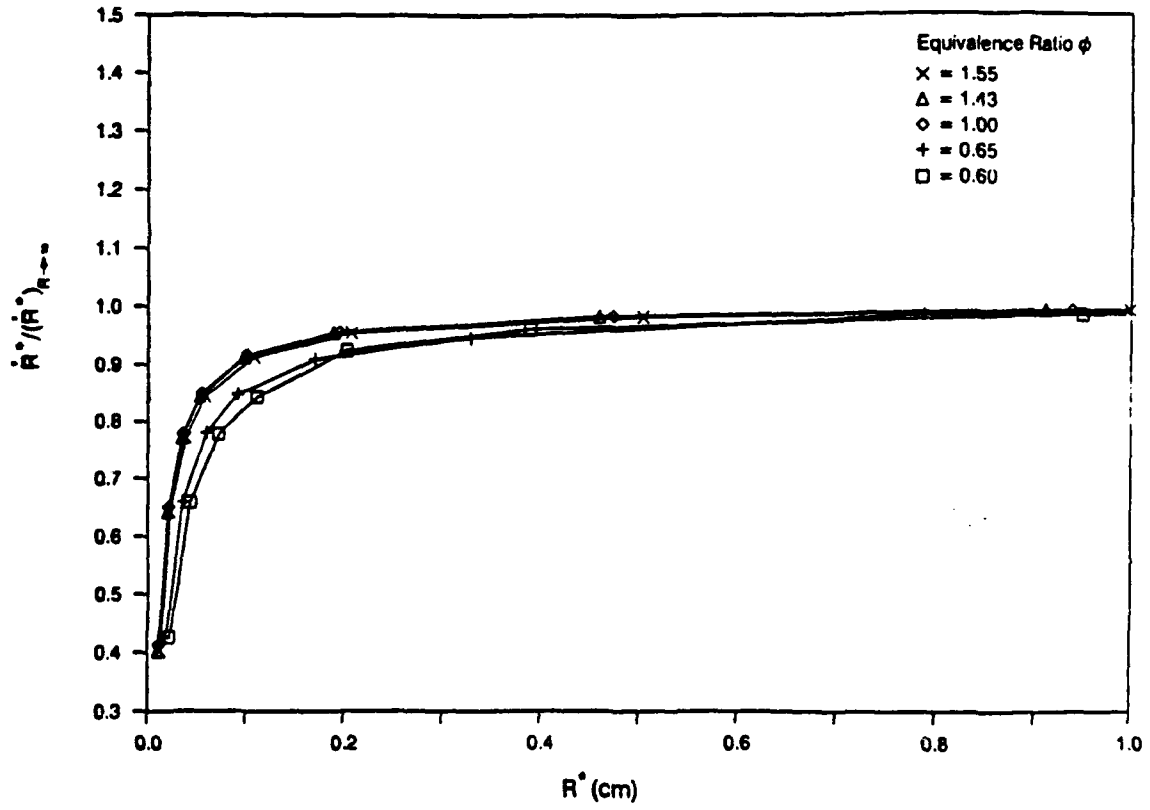

Figure 10. Variation of the normalized spherical-flamefront speed $\dot{R}^*$ with spherical-flamefront radius R^*, for atmospheric-pressure methane/air mixtures of various equivalence ratios ϕ, according to the present theory. We adopt $E = 25$, $D_{Fu} = 0.23\ cm^2/s$, $D_{Ou} = 0.22\ cm^2/s$.

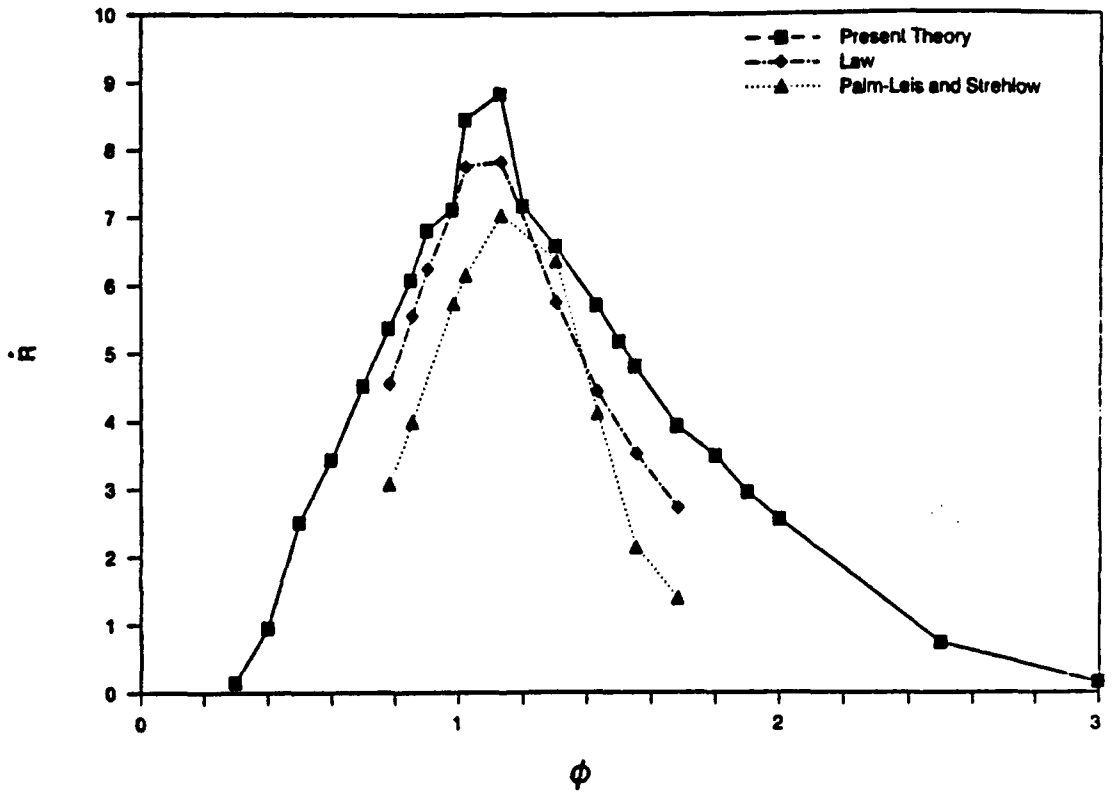

Figure 11. For atmospheric-pressure propane/air mixtures, the dimensionless spherical-flamefront speed $\dot{R}$ holding at large spherical-flamefront radius, as a function of the equivalence ratio ϕ. The spherical-flame data of Palm-Leis and Strehlow (1969), and the planar-flame data of Yu, Law, and Wu (1986) -- adjusted with the burned-gas-temperature/cold-mixture-temperature ratio (Gordon and McBride 1976), appear with results of the present theory.

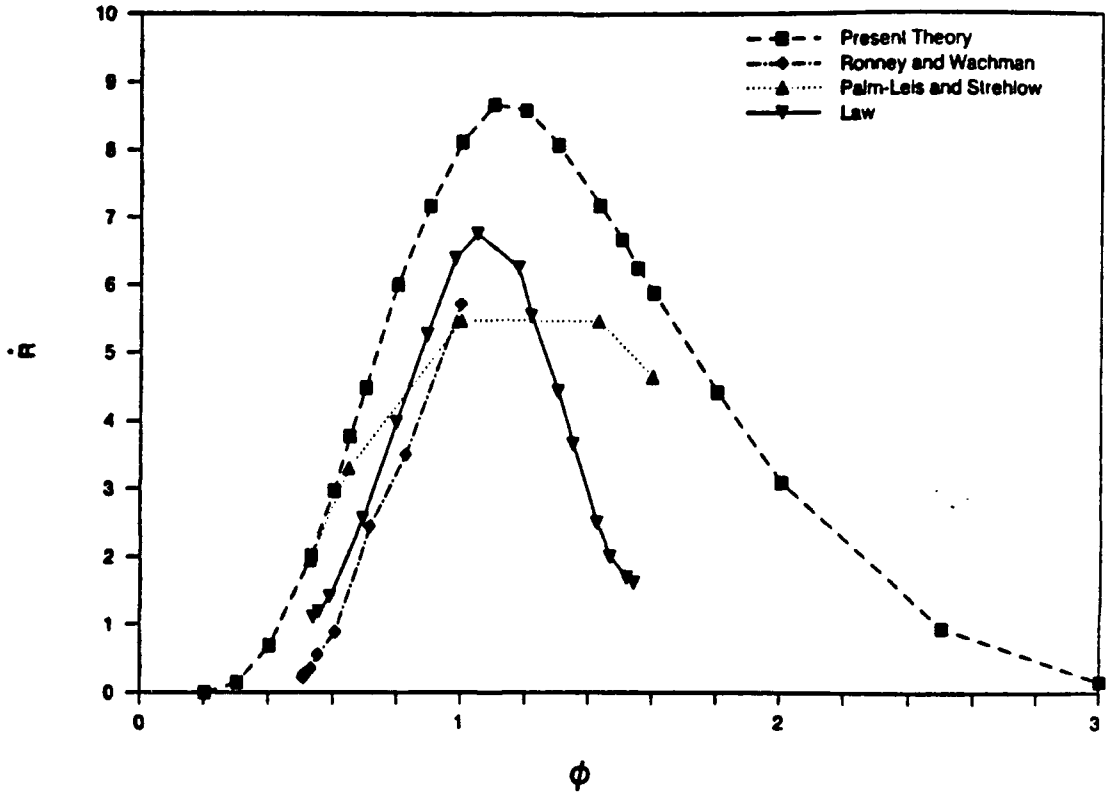

Figure 12. Same as Figure 11, but for methane/air mixtures. The spherical-flame data of Ronney and Wachman (1985) [obtained for fuel-lean mixtures only] also are presented. See the caption of Figure 9 concerning the data of Palm-Leis and Strehlow.

APPENDIX III.

Laser-Initiated Oblique Detonation Wave For Supersonic Combustion

G. Carrier, F. Fendell, D. McGregor, S. Cook, and M. Vazirani

TRW Space and Technology Group
Redondo Beach, CA 90278

AIAA Paper 91-0578
29th Aerospace Sciences Meeting
January 7-10, 1991 - Reno, NV

(Submitted to the Journal of Propulsion and Power)

LASER-INITIATED CONICAL DETONATION WAVE FOR SUPERSONIC COMBUSTION

G. Carrier*, F. Fendell**, D. McGregor†, S. Cook‡, M. Vazirani‡

TRW Space and Technology Group

Redondo Beach, CA 90278

Abstract

Preliminary theoretical studies are undertaken of the feasibility of an air-breathing supersonic combustor based on a stabilized, conically configured oblique detonation wave. The conical wave is the resultant of the interaction of a train of spherical detonation waves, each directly initiated by a very rapidly repeatedly pulsed laser, which is tightly focused on a fixed site (taken to be the origin of coordinates) in a steady uniform supersonic stream of combustible gaseous mixture. Downwind of the Chapman-Jouguet detonation is a supersonic isentropic inviscid flow. This expansional flow is selfsimilar, and describable entirely in terms of the spherical polar angle θ (where $\theta = 0$ is the axis of symmetry downwind of

---

*Consultant, Center for Propulsion Technology and Fluid Mechanics.

**Staff Engineer, Center for Propulsion Technology and Fluid Mechanics. Associate Fellow AIAA.

†Senior Project Engineer, Center for Propulsion Technology and Fluid Mechanics. Member AIAA.

‡Technical Support, Center for Propulsion Technology and Fluid Mechanics.

the nonintrusive-energy-deposition site, and $\theta = \beta$, $(\pi/2) > \beta > 0$, identifies the locus of the conical detonation wave). The combustor is idealized as a circular-cross-section pipe upwind of the axial position at which the conical detonation wave interacts with the wall. Downwind of this axial position, the reacted-gas flow is no longer selfsimilar, and we seek to identify a not-impractically-long, small-drag-incurring, axisymmetric nozzle configuration such that the method-of-characteristics-computed pressure field at the nozzle-exit plane is nearly uniform at the ambient-atmosphere value.

1. Introduction

Most designs for an air-breathing supersonic combustor (i.e., a combustor in which the flow is everywhere, except in wall boundary layers, supersonic) are based on the mixing-controlled burning of diffusion flames[1]. Here, however, we examine the feasibility for propulsion of an alternative design based on an oblique detonation wave (ODW). Not only is the entropy increase for an oblique wave less than that for a normal wave in the same flow, so more of the combustion heat is available to do useful work, but also, since the postdetonation flow is supersonic for the oblique wave, downwind disturbances cannot propagate upwind to disturb the wave.

While ODW combustors have been discussed theoretically and experimentally for decades, virtually all are predicated on the stabilization of the ODW by means of a pointed impervious body that lies intrusively and symmetrically in the rapidly flowing combustible mixture[1-6]. Use of an intrusive body without a positive ignition device incurs frictional drag, and may incur the large entropy losses associated with a normal shock if the body becomes blunted or misaligned with respect

to the flow; more importantly, in the rarefied flow at high altitudes for which such a combustor is likely to be utilized, the pressure of the (weakly) shocked gas may be modest enough that chemical reaction rates are relatively slow, ignition-delay times are significant, and the conversion of reactants to products may occur undesirably far downwind of the oblique shock[4,7-10].

2. Laser-Initiated Oblique Detonation Waves

Because of constraints on combustor length in practical aircraft, we examine the replacement of the intruding body by a nonintrusive positive ignition device. Specifically, we consider the use of a rapidly repeatedly pulsed laser, tightly focused on a fixed site in the midst of the flowing combustible mixture, to effect the direct photochemical initiation of a train of spherical detonation waves (Figure 1). The combustible mixture may (or may not) need to be sensitized to the incident laser radiation by trace-level doping with a suitable additive species. As the time interval between successive laser pulses approaches zero, the interaction of the spherical detonations (Figure 2) produces virtually the same stabilized conically-configured detonation wave as would be produced by a tightly focused, continuous laser source; that such is the case follows from the fact that the same element of mixture can be converted from reactants to products but once, and the fact that the scalloped interface between reacted and nonreacted mixture (Figure 3) is smoothed as the interval between pulses is decreased. The entropy rise across reflected shocks that are part of the interacting-detonation phenomena is a major source of losses in the pulsed-detonation configuration; these losses decrease as the pulse spacing is shortened.

Another motivation for preferring a rapidly repeatedly pulsed laser arises from the desirability of depositing into the reactive mixture only the minimal energy and power (over the minimal volume) necessary to induce the direct initiation of detonation. An appreciably larger energy deposition, possibly into already-burned mixture, would be required to stabilize an ODW by a continuous optical source. Furthermore, continuous deposition might give rise to a locally strong (normal) detonation wave. Even if existing pulsed lasers do not possess sufficiently rapid repetition rate, candidate lasers may soon be developed, particularly if the motivation provided by a proof-of-principal study can be established at this time. We note that successful demonstration of the direct photochemical initiation of a detonation in appreciably-subatmospheric-pressure mixtures has been reported by Lee and coworkers[11], by use of xenon flash lamps.

Observationally, spherical detonation waves develop a cellular structure, so that the ODW may have finite thickness, possibly on the order of a centimeter.[12-14] However, while our treatment (below) of the ODW as a surface without structure may not be meticulously precise, this detail would not seem to be of critical importance to our examination of ODW-based propulsion. Nevertheless, we emphasize the desirability of laboratory experiments. Highest priority is experimentation to establish the pulse-initiated-detonation limits on deposition energy, time interval for deposition, seeding (if necessary), and deposition volume. Furthermore, the interaction of two spherical detonation waves set off in close spatial proximity, one just after the other, seems worthy of study to be sure that unforeseen transitions to stronger detonations with their attending larger

entropy rise do not occur. Finally, the interaction of a spherical detonation with a container wall ought to be examined to be certain that no unexpected noise, vibration, or structural consequences arise that can lead to stronger detonation. It seems unlikely that detonation will propagate upwind into the undisturbed flowing reactive mixture in the subsonic sublayer immediately contiguous to the combustor walls.

We remark that it is possible to conceive of the nonintrusive local deposition of reduced energy and power by a rapidly pulsed repeatedly laser such that a train of spherical deflagration waves, as opposed to spherical detonation waves, are induced (Appendix A). The lateral rate of spread of a spherical detonation wave tends to be comparable to the convective speed of a supersonic stream, so that a train of spherical detonation waves can span a combustible stream with flame within a relatively short streamwise distance downwind of the spatially fixed, periodic-energy-deposition site. In contrast, the highly subsonic rate of lateral spread of a spherical deflagration wave is so miniscule relative to a supersonic convective speed that the combustible stream would be spanned with flame only impractically far downwind. The only recourse is to deposit deflagration-inducing energy at many spanwise sites, but then the possibility of transition to a large-entropy-loss-incurring normal-detonation-wave structure arises. Finally, while deflagration-to-detonation transition is observed in many contexts[12,15], the residence-time and entropy-increase constraints in the present propulsive context makes such a design highly problematic.

3. Outline and Objectives of the Investigation

In a uniform channel flow at a speed that is several times the Chapman-Jouguet (CJ) detonation speed, the weak detonation (for which the

downstream flow is uniform and supersonic) implies an entropy rise across the detonation that is greatly in excess of the entropy rise across a CJ detonation in the same flow; the strong normal detonation (for which the downstream flow is uniform and subsonic) implies an entropy rise that is huge compared with that of the weak detonation.[12,15] [The term weak detonation is used here and elsewhere in this text in the sense defined (Ref. 15, p. 29) in connection with situations in which a uniform one-dimensional burning of the combustible mixture occurs. A weak normal detonation is much stronger than an oblique CJ detonation in the same flow.] We believe that we can select a channel of cross-section A(x) [with $A'(x) > 0$] so that the flow downstream of the quasi-conical-detonation region has very low losses and gives rise to a quasi-uniform exit flow whose averaged entropy weakly exceeds that emerging from the detonation itself.

For the conical detonation produced in the limit of very short pulse spacing, the flow configuration, upstream of the cross-section at which the detonation front intersects the channel wall, will be selfsimilar (Figure 4). [Background (included here as Appendix B for the reader's convenience) is furnished by the long-known selfsimilar property of the expansional flow behind a spherical detonation propagating radially outward in an unbounded expanse of initially stagnant mixture.[16-18]] We find this similarity solution for the present configuration, and then continue the supersonic-flow analysis downstream of that intersection. Upon analyzing a modest number of channel shapes, we expect to have a rather good estimate of the performance (thrust-to-drag ratio) to be expected from the type of configuration under study.

4. The Postdetonation Similarity Flow

Since the Rankine-Hugoniot statements (relating conditions upwind and immediately downwind of the oblique, conical, structureless detonation shown in Figure 4) are known, we proceed to quantify that portion of the shocked, chemically reacted, supersonic flow that may be treated as selfsimilar. This portion contains fluid elements to which information concerning the finite (cylindrical-) radial dimension of the container has not reached. For the steady compressible axisymmetric inviscid flow of an ideal gas, we adopt a spherical-polar-coordinate system (r^*,θ,ϕ) anchored at the laser-energy-deposition site; since dimensionless quantities are to be introduced, a super asterisk denotes a dimensional quantity (in Sections 4 and 5 and in Appendix C only); r^* is the spherical radial coordinate, θ is the polar angle (where $\theta = 0$ is directly downwind), and ϕ is the azimuthal angle (of which the description is independent). We shall have occasion (in treating the nozzle flow) to introduce a coanchored (alternative) cylindrical-polar-coordinate system (σ^*,x^*,ϕ), where σ^* is the cylindrical radial coordinate $[0 < \sigma^* < \sigma_w(x^*)$, with the container radius σ_w^* independent of x^* upwind of the circle demarking the detonation-pipe "intersection"] and x^* is the axial coordinate (positive downwind). In other sections and appendices, no dimensionless quantities are introduced, and the super asterisk is dispensed with.

We let subscript o refer to the known uniform conditions in the cold mixture, and subscript 1 refers to conditions immediately downwind of the detonation. If $\vec{v}^*$ is the velocity, p^* is the pressure, ρ^* is the density, and T^* is the temperature, then (Figure 4) for the ideal gas (if R^* is the gas constant and a_o^* is the speed of sound in the cold flow)

$$\vec{v}(\theta) = \frac{\vec{v}^*(\theta)}{a_o^*} = \frac{u^*(\theta)}{a_o^*}\,\hat{r} + \frac{w^*(\theta)}{a_o^*}\,\hat{\theta} = u(\theta)\,\hat{r} + w(\theta)\,\hat{\theta}\ ; \tag{1}$$

$$p(\theta) = \frac{p^*(\theta)}{p_o^*}\ ,\ \rho(\theta) = \frac{\rho^*(\theta)}{\rho_o^*}\ ,\ T(\theta) = \frac{T^*(\theta)}{p_o^*/(\rho_o^* R^*)} = \frac{p(\theta)}{\rho(\theta)}\ ; \tag{2}$$

$$a_o^* = \left[\gamma p_o^*/\rho_o^*\right]^{1/2}\ ,\ a_1^* = \left[\gamma p_1^*/\rho_1^*\right]^{1/2}\ ,\ p_1 = \frac{p_1^*}{p_o^*}\ ,\ \rho_1 = \frac{\rho_1^*}{\rho_o^*}\ ; \tag{3}$$

$$a_1^2 = \frac{a_1^{*2}}{a_o^{*2}} = \frac{p_1}{\rho_1}\ ,\ M_o = \frac{u_o^*}{a_o^*}\ ,\ M = \frac{u_o^* \sin\beta}{a_o^*} \text{ so } M = M_o \sin\beta, \tag{4}$$

where u_o^* is the (purely axial) cold-mixture velocity and M is the Chapman-Jouguet Mach number (the Mach number of the component of the cold-mixture speed that is normal to the oblique wave). For completeness, the Rankine-Hugoniot relations for the detonation[15] identify [$\gamma \equiv c_p^*/c_v^*$, $\alpha \equiv \gamma\, q^*/a_o^{*2}$, where q^* is the heat of reaction per mass of mixture, c_p^* is the (constant) heat capacity at constant pressure, and $c_p^* - c_v^* = R^*$]

$$p_1 = 1 + \alpha\,(\gamma - 1)\left\{1 + \left[1 + \frac{2\gamma}{\alpha(\gamma^2 - 1)}\right]^{1/2}\right\}, \tag{5}$$

$$\frac{1}{\rho_1} = 1 + \frac{\alpha\,(\gamma - 1)}{\gamma}\left\{1 + \left[1 + \frac{2\gamma}{\alpha(\gamma^2 - 1)}\right]^{1/2}\right\}, \tag{6}$$

$$M = \left[1 + \frac{\alpha\,(\gamma^2 - 1)}{2\gamma}\right]^{1/2} + \left[\alpha\,\frac{(\gamma^2 - 1)}{2\gamma}\right]^{1/2}. \tag{7}$$

Since (7) gives M in terms of input quantities, and M_o is given, (4) identifies the angle β.

The component (of the cold flow) that is parallel to the detonation and is unaltered across the wave is identified:

$$u_1 = \frac{u_1^*}{a_o^*} = \frac{u_o^*}{a_o^*} \cos \beta = M_o \cos \beta = \left[M_o^2 - M^2\right]^{1/2} , \tag{8}$$

by (4). The component of the just-detonated flow that is perpendicular to the wave is at the local sound speed (the Chapman-Jouguet condition):

$$w_1 = - a_1 = - \left[p_1/\rho_1\right]^{1/2} . \tag{9}$$

Thus, the streamlines are deflected away from the axis of symmetry upon crossing the oblique wave.

In the selfsimilar postdetonation flow, conservation of radial momentum gives (if subscript θ denotes ordinary derivative)

$$u_\theta = w, \tag{10}$$

a statement that the azimuthal component of vorticity vanishes, as do the radial and polar-angle components of vorticity. Continuity gives

$$\frac{(\rho\, w \sin \theta)_\theta}{\sin \theta} + 2\, \rho u = 0 \text{ so } \frac{\rho_\theta}{\rho} = - \frac{2u + w \cot \theta + w_\theta}{w} . \tag{11}$$

The Bernoulli equation gives

$$a_1^2 \left[\frac{\rho}{\rho_1}\right]^{\gamma-1} = I(u,w;a_1,\gamma,u_1,w_1) \equiv a_1^2 + \frac{\gamma - 1}{2} \left[u_1^2 - u^2 + w_1^2 - w^2\right] , \tag{12a}$$

with

$$p/p_1 = (\rho/\rho_1)^\gamma . \tag{12b}$$

Differentiating (12a) and substituting for (ρ_θ/ρ) in (11) gives

$$w_\theta = - \frac{2u + w \cot \theta + \left[w^2 u / I\left[u,w;a_1,\gamma,u_1,w_1\right]\right]}{1 - \left[w^2/I\left[u,w;a_1,\gamma,u_1,w_1\right]\right]} . \tag{13}$$

The coupled equations (10) and (13) may be integrated numerically from $\theta = \beta$ to $\theta = \theta_i$, $\beta > \theta_i > 0$, upon assignment of input values to the parameters

M_0, α, and γ; explicit dimensional results are obtained by specifying p_0^* to complement T_0^*, implicitly selected in assigning a value to M_0 and α. Near $\theta = \beta$ the equations are singular, so the following expansions may be used to "start" the solution:

$$u(\theta) = u_1 + a_1 (\beta - \theta) - (2/3)\epsilon (\beta - \theta)^{3/2} + \ldots, \tag{14}$$

$$w(\theta) = w_1 + \epsilon (\beta - \theta)^{1/2} + \ldots, \quad \epsilon = - \left[\frac{2a_1}{\gamma + 1}\left[u_1 - a_1 \cot \beta\right]\right]^{1/2}, \tag{15}$$

where physical considerations select the negative root for the quadratic for ϵ^2, and u_1 and w_1 are given by (8) and (9). The integration may be terminated at $\theta = \theta_i$, where

$$\tan \theta = - w(\theta)/u(\theta), \quad \theta_i > \theta > 0, \tag{16}$$

a (physically anticipated and mathematically confirmed) condition that states that the flow in $\theta_i > \theta > 0$ is entirely axial and constant, and has no finite velocity component in the cylindrical radial direction. In cylindrical polars,

$$\vec{v} = U \hat{x} + v \hat{\sigma}, \quad U = u \cos \theta - w \sin \theta, \quad v = w \cos \theta + u \sin \theta . \tag{17}$$

Under (16), $v = 0$, $U = u/\cos \theta$. But if $\rho_\theta = 0$, (11) and (16) give $u = -w_\theta$; this, with (10), implies that $w = -B \sin \theta$, B const.; hence, $u = B \cos \theta$, or $U = B$. Thus, a constant, purely axial flow in the core is consistent with a thermodynamically uniform core: in $\theta_i > \theta > 0$, $\rho(\theta) = \rho(\theta_i)$, $p(\theta) = p(\theta_i)$.

Further, since the core gas, having transversed the detonation further upwind of where the gas near the pipe wall crosses the detonation, has had an opportunity to expand, we expect the density, pressure, and temperature to increase monotonically as σ increases from σ_i to 1 at $x = L$. Here [if σ^* is recalled to be the cylindrical radial coordinate, with $0 < \sigma^* < \sigma_w^*(x^*)$, where σ_w^* is recalled to be the wall position]

$$\sigma \equiv \frac{\sigma^*}{r^*_{pipe}} , \quad L \equiv \frac{L^*}{r^*_{pipe}} = \frac{1}{\tan \beta} , \quad \sigma_i = L \tan \theta_i ; \tag{18}$$

$$x \equiv \frac{x^*}{r^*_{pipe}} , \quad \sigma_w(x) \equiv \frac{\sigma^*_w(x^*)}{r^*_{pipe}} ; \tag{19}$$

r^*_{pipe} is radius of the pipe; as previously noted, $\sigma_w = 1$ for $0 < x < L$. Thus L, the dimensionless axial length from the energy-deposition site to the detonation-wall interaction, is known since β is known. It is convenient to introduce a translated axial coordinate ($x' \equiv x'^*/r^*_{pipe}$)

$$x' = x - L , \tag{20}$$

so $x' = 0$ is the axial plane containing the detonation-wall interaction.

We present some results for the similarity flow in terms of θ (Figure 5), but other results are presented (for engineering insight) in terms of the dimensional cylindrical radial coordinate σ^* (Figures 6 and 7) where at $x'^* = 0$

$$\sigma^* = r^*_{pipe} \sigma = r^*_{pipe} L \tan \theta = r^*_{pipe} (\tan \theta / \tan \beta) . \tag{21}$$

This form is convenient for initiating the nozzle calculation at $x^* = L^*$, i.e., at $x'^* = 0$; of course, it is necessary to specify a value for the pipe radius. These figures indicate that β and θ_i decrease as γ decreases (with α,M_0 fixed), as α decreases (with γ,M_0 fixed), and as M_0 increases (with α,γ fixed). For fixed γ, M_0, and α, both u and w algebraically increase (but p, ρ, and T decrease) as θ decreases from the conical locus of the detonation ($\theta = \beta$) to the conical locus of constant-property-core edge ($\theta = \theta_i$). We below compute nozzle results for the conditions based on

$p_o^* = 7$ kPa, $T_o^* \simeq 201.7$ K, but such near-tropopause conditions are probably not of primary practical interest.

5. Nozzle Design

Downwind of the similarity flow, we undertake an optimization problem of inverse type: rather than seeking the implications for the (axially-decreasing) pressure field of given container shape, we seek to identify a boundary configuration that gives a nozzle-exit-plane pressure field that is virtually constant (with the cylindrical radial coordinate σ) at the ambient value p_o^*.

An informative illustrative calculation for the nozzle wall (Figure 8) is the "streamline wall"--the downwind continuation of the similarity-flow streamsurface that passes through the detonation-pipe intersection, $r^* = r^*_{pipe}/\sin\beta$, $\theta = \beta$ (or $\sigma = 1$, $x' = 0$). If $r \equiv r^*/r^*_{pipe}$ and the streamfunction $\psi \equiv \psi^*/(\rho_o^* a_o^* r^*_{pipe})$, then, if subscripts r and θ denote partial differentiation,

$$d\psi(r,\theta) = \psi_r\, dr + \left[\frac{1}{r}\psi_\theta\right] r\, d\theta = 0,\ \rho(\theta)\vec{v}(\theta) = \text{curl}\left[\frac{\psi(r,\theta)}{r\sin\theta}\hat{\phi}\right] ; \tag{21}$$

$$\frac{dr}{r\, d\theta} = \frac{-\frac{1}{r}\psi_\theta}{\psi_r} = \frac{-\rho\, u \sin\theta}{-\rho\, w \sin\theta} = \frac{u(\theta)}{w(\theta)} . \tag{22}$$

If $r_{sw}(\theta)$ denotes the nozzle configuration just defined as the streamline wall,

$$r_{sw}(\theta) = \begin{cases} \dfrac{1}{\sin\beta}\exp\left[\displaystyle\int_\beta^\theta \frac{u(\theta_1)}{w(\theta_1)}\, d\theta_1\right] , & \theta_i < \theta < \beta \\ r_{sw}(\theta_i)\dfrac{\sin\theta_i}{\sin\theta} , & 0 < \theta < \theta_i \end{cases} ; \tag{23}$$

in cylindrical-polar coordinates, the equivalent parametric prescription for $\sigma_w(x')$ is

$$\sigma_w(\theta) = \sin\theta \left[r_{sw}(\theta)\right] , \quad x'(\theta) = \cos\theta \left[r_{sw}(\theta)\right] - L . \tag{24}$$

Since $U > 0$, $w < 0$, $0 < \theta_i < \beta$, the streamline wall expands out radially, then becomes a pipe (of circular cross-section) of (cylindrical) radius $[\sin\theta_i]\,[r_{sw}(\theta_i)]$ at $x' = x'_i \equiv [\cos\theta_i]\,[r_{sw}(\theta_i)] - L$. While the pressure at $x' > x'_i$ remains uniform in σ, the value in general is far above the ambient value p_o^*.

Thus, a reasonable family of nozzle configurations to investigate (by numerical integration of the conservation equations for steady isentropic inviscid axisymmetric supersonic flow within an impervious container, with initial conditions at $x' = 0$ given as a function of σ by the results of Section 4) are those that follow the "streamline-wall" shape to some distance $x'(> 0)$ at which $d\sigma_w/dx'$ equals a preselected value; thenceforth, i.e., for all larger x', $\sigma_w(x')$ is taken to be a cone with angle equal to the $d\sigma_w/dx'$ value selected. The suitable nozzle wall terminates at $x' = x'_e$, where $p(x'_e) \simeq 1$ [i.e., $p^*(x'^*_e) \simeq p_o^*$, the ambient pressure]. "Tracking" the streamline wall initiates the uniformization of the postdetonation pressure field; "tracking" the conical extension aids the pressure-reduction process. Rough estimation of pertinent values for x'_e is given in Appendix C.

The thrust T^* is given by, if $\sigma_w^*(0)$ denotes σ_w^* evaluated at $x'^* = 0$,

$$T^* = 2\pi \int_0^{\sigma_w^*(0)} (p^* + \rho^* u^{*2})_{x'^*=0}\, \sigma^*\, d\sigma^*$$

$$- 2\pi \int_0^{\sigma_w^*(x'^*_e)} (p^* + \rho^* u^{*2})_{x'^*=x'^*_e}\, \sigma^*\, d\sigma^* \tag{25a}$$

$$= 2\pi \int_0^{x'^*_e} [\sigma^*_w(x'^*)]\{p^*[\sigma_w(x'^*), x'^*]\} \frac{d\sigma^*_w(x'^*)}{dx'^*} dx'^* \ . \qquad (25b)$$

In the Newtonian approximation (that molecules encountering a surface impact and slide along it without rebounding, so that their momentum normal to the surface is reduced to zero) appropriate for hypersonic flow, the wave drag D* owing to the flow past the container is given by

$$D^* = 2\pi \rho^*_o u^{*2}_o \int_0^{x'^*_e} \frac{[\sigma^*_w(x'^*)]\ [d\sigma^*_w(x'^*)/dx'^*]^3}{1 + [d\sigma^*_w(x'^*)/dx'^*]^2} dx'^* \ . \qquad (26)$$

For a conical nozzle of (constant) angle θ,

$$D^* \to \pi \rho^*_o u^{*2}_o \sin^2\theta \{[\sigma^*_w(x'^*_e)]^2 - [\sigma^*_w(0)]^2\} \ . \qquad (27)$$

We seek a nozzle configuration such that the ratio T^*/D^* sufficiently exceeds unity so, even with accounting for the (relatively small) frictional drag, the combustor would be practical for propulsion. Actually, (27) suggests that a roughly conical sheath emanating from $x^* = 0$ might usefully envelop the pipe-nozzle configuration, in that the sheath might flare near $x^* = 0$ (so that $\sin^2\theta$ is large where σ^{*2} is small), and evolve to a pipe at larger x^* (so that $\sin^2\theta$ is small where σ^{*2}_w is large).

The nozzle flows here are calculated by a modified method-of-characteristics (MoC) procedure. Whereas conventionally compatibility relations for the two families of characteristics are introduced, here use is made of a computational mesh of streamlines and the right-running family of characteristics. This formulation permits convenient treatment of nonuniform values of the molecular weight and nonuniform values of the ratios of the specific heats; however, in the present approximation this capability was not utilized. The calculations reported here typically

involved a mesh of 70 streamlines and 250-to-300 characteristics; 70 of the characteristics emanated from points along the "starting line" (i.e., emanated from values of σ^* at $x'^* = 0$), and the remainder emanated from points along the nozzle wall [i.e., emanated from values of $\sigma_w^*(x'^*)$]. The execution time was typically 15 minutes on a personal computer with the performance of an IBM AT. Several cases were checked by computing essentially identical results with the VNAP2 computer program, which adopts the unsplit MacCormack scheme[19]; however, in other cases, extensive "tuning" was required before VNAP2 yielded mathematically and/or physically plausible results, so eventually the MoC procedure was used exclusively.

The MoC calculations indicate that, for the conditions at $x'^* = 0$ given by the solid lines in Figures 7 and 8, a nozzle contour that adopts the streamline wall to a distance $x'^* = 12.67$ cm, and then smoothly is continued as a 5° right-circular cone, results in a pressure of 6.94 kPa very nearly uniformly at all radial positions $0 < \sigma^* < \sigma_w^*(x_e'^*)$, where $x_e'^* = 3.0$ m and $\sigma_w^* \simeq 47.5$ cm at this axial distance. Meticulously, the pressure at the axis of symmetry does slightly exceed the cited pressure, computed to hold at the wall. As an indication of the sensitivity of the calculations, we present results (Figures 9, 10, and 11) for a nozzle contour that follows the streamline wall to $x'^* = 10$ cm, then smoothly is continued as a 5.93° cone to a distance $x_e'^* \simeq 2.5$ m; actually, at axial distance 2.5 m, for which the nozzle-wall radius is 46.2 cm, the pressure at the wall has expanded past 7 kPa to 6.48 kPa.

6. Concluding Comments: Effect of a Nonuniform Mixture

Since achieving intimate mixing of fuel injected into high-speed air is a major topic of current high-speed-propulsion research (and of high-

energy-chemical-laser research), in practice the cold stream is expected to consist of imperfectly mixed fuel and air. We discuss here briefly a throughput flow consisting of a fraction composed of well-mixed fuel and air, through which is interspersed imperfectly mixed blobs with fuel and air in stoichiometric proportion. We do not delve here into the creation of such a mixture, and the scale of the blobs is to be determined by further research; nevertheless, a millimeter scale may be plausible. The well-mixed fraction of the throughput is converted to product gases across the weak detonation (Figure 12).

The "lumpy" blobs are compressed during passage through the detonation, but these blobs remain unreacted over the centimeter-or-so scale of the (cellular) oblique wave. They do, however, react in the hot flow downstream of the front, as an isolated diffusion-controlled reaction occurs in each blob. If the blobs are of dimension $\underline{a}$, their burn-up time is about a^2/D, where D is the Fickian diffusion coefficient of the lighter reactant. In fact, if one takes the liberty of introducing the concept of an equivalent deflagration, the "lumpy" blobs have a relatively slow flame speed. The fact that unreacted pockets of reactive mixture occur behind a real detonation front is well appreciated in a solid detonable mixture.[20] However, this phenomenon in solid explosives is a consequence of uncontrollable departure from ideal behavior. The distinction here is that we raise the possibility of intentionally tailoring a gaseous mixture to control the nature of the departure from perfect mixing. For example, if the total heat release per unit mass of mixture is denoted Γ, and if the heat release per unit mass of mixture across the weak detonation is α, then we seek to extract the heat $(\Gamma - \alpha)$ without incurring any shocks, or at

most minimal shocks. While the entropy at the downwind plane at which the mixture is fully converted to product must be higher than the entropy just after the weak detonation, we seek to achieve the lowest possible entropy state in the fully-burned gas (given the upwind thermodynamic state and flow speed, and given a quasi-one-dimensional flow at the downwind exit plane with cross-sectional area about the same as that for the upwind cold flow). Thus, research into whether attempting to tailor imperfect mixing offers a possibility for enhancing performance may be worthwhile.

Appendix A. Energy Deposition for the Initiation of Detonation and Deflagration

Consider a gaseous mixture with composition such that the mixture lies within the limits of detonation and deflagration. In order to initiate a deflagration wave with a nonintrusive local deposition of energy to the combustible mixture, one must supply an appropriate amount of energy to the blob of mixture, irradiated during a time interval that is small compared with the time required for the loss of much of that heat by diffusion to the contiguous medium. These requirements, and their counterparts for the initiation of a detonation, may be only loosely quantifiable, but the effort is a good place to start.

Let the radius of the blob to receive the deposited energy be denoted by b, so that the mass of the (say, roughly spherical) blob is $(4/3)\pi\rho_0 b^3$, where ρ_0 is the density of the ambient (unreacted) premixture, and b refers to the unheated state. While the minimum energy deposition required to initiate a continuing deflagration cannot be found trivially, it is sufficient to deposit an amount of energy, E, equal to the amount of heat

that complete combustion of that mass of premixture would provide; i.e., $E = (4/3)\pi\rho_0 b^3 q$, where q is the heat of reaction per mass of mixture. Diffusion to contiguous material would occur on a time scale $T_D \simeq b^2/\kappa$, where κ characterizes the thermal diffusivity of the ambient medium; thus, the deposition time T should obey $T \ll b^2/\kappa$.

A detonation will be directly initiated if, in addition to the foregoing, the deposition time T is so brief that the acoustic transit time across the blob (or half of it) is large compared to T. That is, if a_0 is the ambient speed of sound, the energy deposition may initiate a deflagration (but not a detonation) if $(a_0 T/b) \gg 1$; but a detonation may be initiated if the deposition time T (and also the time required for local reaction) obeys $T \ll b/a_0$.

Thus, if (as an example) $\kappa = 0.1$ cm^2/s, b = 0.1 cm, and $a_0 = 3 \cdot 10^4$ cm/s, for a deflagration (with T in seconds) $3 \cdot 10^5\ T \gg 1 \gg 10^{-1}\ T$. Thus $T = 10^{-2}$ s and $E = (4/3)\kappa\rho_0 b^3 q$ would imply initiation of a deflagration with very little chance of either failure to ignite or initiation of detonation. For the same illustrative parameters, one could expect with confidence to initiate a detonation if the deposition of E units of energy occurred in 10^{-7} s. Experiments are needed to obtain a more accurate criteria for the initiation of either a deflagration or detonation. It is easily possible that the minimum time for energy deposition for initiation of a detonation could be only 10^{-6} s and that the minimum energy could be as small as $(4/3)\pi\rho_0 b^3 q/10$. The point is that somewhere between deposition times of 10^{-2} s and 10^{-7} s the situation gets "delicate" and the need of study is evident.

The minimum (normalized) amount of deposited energy required to achieve direct initiation of a detonation plausibly varies with the (normalized) time of deposition as sketched in Figure 13. That is, $E/[(4/3)\pi\rho_o b^3 q]$ increases with relatively large values of $(a_o T/b)$, simply because some of the earlier-deposited energy is carried away from the blob prior to the achievement of detonation onset by later-deposited energy; for smaller values of $(a_o T/b)$, no such dispersing of deposited energy occurs, and the minimum energy requirement for direct initiation suffices. There is experimental evidence (albeit presented in the dimensional form of critical initiation energy vs. time of deposition) that is fully consistent with this discussion [Ref. 12, p. 407, Figure 13-7(a)].

For initiation of detonation, the heated gas will be confined to approximately its original volume, so that its early temperature rise $(\Delta T)_i = q/c_v$, where c_v is the specific heat at constant volume of the gas. Specifically, for a spherical detonation wave, the heated gases are strongly confined by the dynamics of the propagation mechanism, so that, just behind the wave front, the temperature has a maximum whose order of magnitude is $(\Delta T)_i$, and the pressure near the wave front is of order p_i, where

$$p_i = \rho_o R[(\Delta T)_i + T_o],$$

and R is the gas constant and T_o is the ambient temperature. These estimates are based on the above-noted possibility (confirmed in some cases involving deflagrations) that the total energy absorbed from the laser beam into the sample need be but a small fraction of the heat of combustion. In contrast, in a deflagration the time of deposition is long enough that the burnt gases will have expanded during the burning to a new volume at which

the pressure is virtually the same as the ambient pressure (in the unburnt gas). For a deflagration, the rather uniform temperature rise in the burnt domain is approximately q/c_p.

Appendix B. Selfsimilar Treatment of the Shocked and Reacted Gas in a Spherical Detonation

The state of the shocked and reacted gas just downstream of a spherical Chapman-Jouguet detonation (Ref. 17, p. 195, Figure 43) is characterized by pressure p_f, density ρ_f, sound speed a_f, and particle speed u_f, such that u_f relative to the speed of the detonation wave is sonic, i.e., is equal to $a_f [= (\gamma p_f/\rho_f)^{1/2}$, for the perfect-gas model adopted here]. If R(t) is the radial position of the outwardly propagating spherical wave, then in $0 < r < R(t)$, for time $t > 0$, the pertinent equations are ($\gamma = c_p/c_v$)

$$r^2\rho_t + (\rho r^2 u)_r = 0 , \tag{B.1}$$

$$\rho u_t + \rho u u_r + p_r = 0 , \tag{B.2}$$

$$p/p_f = (\rho/\rho_f)^{\gamma} . \tag{B.3}$$

The position $R(t) = \dot{R}t$, where $\dot{R}$ is a constant, specifically, the speed of a Chapman-Jouguet detonation. That is, we focus on constraints that would be the result of an extrapolation back in time of a selfsimilar solution[16-18] of the above conservation laws subject to the thermodynamic properties of the shocked and reacted gas. Hence, at $r = R(t)$,

$$\rho = \rho_f, \; p = p_f, \; u_f = \dot{R} - a_f . \tag{B.4}$$

The selfsimilar variable is necessarily of the form $\eta = r/(kt)$, where k is a parameter of the problem that has the dimensions of velocity.

Without loss of generality, we adopt $k = a_f$. We define

$$\rho(r,t) = \rho_f\, G(\eta),\ p(r,t) = p_f\, H(\eta),\ u(r,t) = a_f\, F(\eta)\ . \tag{B.5}$$

Under (B.5), the statements (B.1) - (B.4) become, since $H = G^\gamma$, two coupled quasilinear ordinary differential equations:

$$\eta\left[(F - \eta)^2 - G^{\gamma-1}\right]G_\eta = -2\, F(F - \eta)G, \tag{B.6}$$

$$\eta\left[(F - \eta)^2 - G^{\gamma-1}\right]F_\eta = 2\, FG^{\gamma-1}\ , \tag{B.7}$$

over $0 < \eta < \lambda$, $\lambda = \dot{R}/a_f$, where

$$G(\lambda) = 1,\ F(\lambda) = \lambda - 1\ . \tag{B.8}$$

This system may be reduced to a single autonomous equation by judicious substitution[16] but that reformulation does not appear to aid present purposes of extracting quantitative profiles. The system (B.6) - (B.8) is singular at $\eta = \lambda$, and it helps to deduce that, near $\eta = \lambda$,

$$F \simeq \lambda - 1 - \tau(\lambda - \eta)^{1/2}\ ,\ G \simeq 1 - \tau(\lambda - \eta)^{1/2}\ , \tag{B.9}$$

$$\tau = 2\{(\lambda - 1)/[(\gamma + 1)\lambda]\}^{1/2}\ . \tag{B.10}$$

With the aid of (B.9) and (B.10), numerical integration of (B.6) - (B.8) from $\eta = \lambda$ toward smaller η may proceed; the integration proceeds to $\eta = \eta_i (< \lambda)$, where $F(\eta_i) = 0$ -- in fact, $F(\eta) = 0$, $0 \le \eta \le \eta_i$, so $G(\eta) = G(\eta_i)$ in $0 \le \eta \le \eta_i$. Some numerical results are graphed by Sedov[17], but these seem not to be easily accessible, so some results are presented here (Figure 14). Barenblatt[21] has dwelled upon the not-entirely-smooth behavior earlier noted by Zeldovich to hold at $\eta = \eta_i$; for our purposes, this behavior is very familiar in hyperbolic systems and violates no criteria with significant physical implications.[18]

Appendix C. A Crude Estimate of Nozzle Length

Adopting the definitions and relations of (1)-(9), we introduce the stagnation speed of sound for the ambient flow, a^*_{so}, and for the state just downwind of the oblique detonation, a^*_{s1}:

$$a^{*\,2}_{so} = a^{*2}_{o} + [(\gamma - 1)/2]\, u^{*2}_{o} \quad , \quad a^{*\,2}_{s1} = a^{*\,2}_{so} + (\gamma - 1)\, q^{*} \quad . \tag{C.1}$$

The speed of the flow just behind the detonation, $|\vec{v}^*_1|$, is known from (4) and (7), since

$$|\vec{v}^*_1|^2 = a^{*2}_{1} + u^{*2}_{o} \cos^2\beta \quad . \tag{C.2}$$

Since subscript e denotes conditions holding at the exit plane, by definition or deduction it follows that

$$|\vec{v}^*_e|^2 = U^{*2}_{e} + v^{*2}_{e} \quad , \quad p^*_e = p^*_o \quad , \quad a^{*\,2}_{se} = a^{*\,2}_{s1} \quad , \quad p^*_{se} = p^*_{s1} \quad , \tag{C.3}$$

since the exit plane flow is an isentropic expansion of the flow just downwind of the detonation; p^*_{si} is defined to be the stagnation pressure at state i.

From Bernoulli's equation and (C.3), p^*_{se} is obtained:

$$\frac{p^*_{se}}{p^*_1} = \frac{p^*_{s1}}{p^*_1} = \left[1 - \frac{\gamma - 1}{2} \frac{|\vec{v}^*_1|^2}{a^{*\,2}_{s1}}\right]^{-\gamma/(\gamma-1)} \quad . \tag{C.4}$$

Also from Bernoulli's equation and (C.3),

$$\frac{p^*_o}{p^*_{se}} = \left[1 - \frac{\gamma - 1}{2} \frac{|\vec{v}^*_e|^2}{a^{*\,2}_{s1}}\right]^{\gamma/(\gamma-1)} \quad ; \tag{C.5a}$$

by rearranging, we obtain $|\vec{v}^*_e|$:

$$\frac{|\vec{v}_e^*|}{a_{s1}^*} = \left\{\frac{2}{\gamma - 1}\left[1 - \left[\frac{p_o^*}{p_{se}^*}\right]^{(\gamma-1)/\gamma}\right]\right\}^{1/2} . \qquad (C.5b)$$

Since

$$\rho_{se}^* = \frac{\gamma\, p_{se}^*}{a_{se}^{*\,2}} , \qquad (C.6)$$

from (C.5a) we obtain ρ_e^*:

$$\frac{\rho_e^*}{\rho_{se}^*} = \left[1 - \frac{\gamma - 1}{2}\frac{|\vec{v}_e^*|^2}{a_{s1}^{*\,2}}\right]^{1/(\gamma-1)} . \qquad (C.7)$$

If the flow is nearly one-dimensional with cross-sectional area A^*, we obtain a crude estimate of the cylindrical radius of the nozzle at the exit plane $\sigma_e^*[\equiv \sigma_w^*(x_e'^*)]$:

$$\rho_e^*\,|\vec{v}_e^*|\,A_e^* = \rho_o^*\,u_o^*\,A_o^* \text{ so } \frac{A_e^*}{A_o^*} = \frac{\sigma_e^{*2}}{r_{pipe}^{*\,2}} = \frac{\rho_o^*\,u_o^*}{\rho_e^*\,|\vec{v}_e^*|} . \qquad (C.8)$$

Whereas (C.8) results in general in an implicit equation for $x_e'^*$, for a conically shaped nozzle (of selected angle θ) joining the pipe radius r_{pipe}^* to the exit radius σ_e^*, the nozzle length $x_e'^*$ is roughly estimated to be

$$x_e'^* = (\sigma_e^* - r_{pipe}^*)/\tan\theta . \qquad (C.9)$$

ACKNOWLEDGEMENT

This work was sponsored by the Air Force Office of Scientific Research, Air Force Systems Command, USAF, under contract F49620-87-C-0081; the technical monitor was Julian Tishkoff. The authors are grateful to

Wilhelm Behrens, James Kliegel, Peter Lohn, and Barry Pearce of TRW, whose cooperation facilitated the carrying out of the work reported here. The authors also thank Kathy Van Slyke for typing the manuscript and Victor Swayne for preparation of the figures.

References

[1]Waltrup, P.J., "Hypersonic Airbreathing Propulsion: Evolution and Opportunities," Conference Proceedings, Aerodynamics of Hypersonic Lifting Vehicles, Advisory Group for Aerospace Research and Development, Neuilly sur Seine, France, April 1987, pp. 12-1--12-29.

[2]Gross, R.A., "A Study of Combustion in Supersonic Flow," Research, Vol. 12, Oct.-Nov. 1959, pp. 381-389.

[3]Gross, R.A., and Chinitz, W., "A Study of Supersonic Combustion," Journal of the Aero/Space Sciences, Vol. 27, July 1960, pp. 517-524, 534.

[4]Rubins, P.M., and Rhodes, R.P., "Shock-Induced Combustion with Oblique Shocks: Comparison of Experiment and Kinetic Calculations," AIAA Journal, Vol. 1, Dec. 1963, pp. 2778-2784.

[5]O'Brien, C.J., and Kobayashi, A.C., "Advanced Earth-to-Orbit Propulsion Concepts," AIAA Paper 86-1386, AIAA, Washington, DC, June 1986.

[6]Pratt, D.T., Humphrey, J.W., and Glenn, D.E., "Morphology of a Standing Oblique Detonation Wave," AIAA Paper 87-1785, AIAA, Washington, DC, June 1987.

[7]Fujiwara, T., Matsuo, A., and Nomoto, H., "A Two-Dimensional Detonation Supported by a Blunt Body or a Wedge," AIAA Paper 88-0098, AIAA, Washington, DC, Jan. 1988.

[8]Wang, Y.Y., Fujiwara, T., Aoki, T., Arakawa, H., and Ishiguro, T., "Three-Dimensional Standing Oblique Detonation Wave in a Hypersonic Flow," AIAA Paper 88-0478, AIAA, Washington, DC, Jan. 1988.

[9]Cambier, J.-L., Adelman, H., and Menees, G.P., "Numerical Simulations of Oblique Detonation in Supersonic Combustors," Journal of Propulsion and Power, Vol. 5, July-August 1989, pp. 482-491.

[10]Cambier, J.-L., Adelman, H., and Menees, G.P., "Numerical Simulations of an Oblique Detonation Wave Engine," Journal of Propulsion and Power, Vol. 6, May-June 1990, pp. 315-323.

[11]Lee, J.H., Knystautas, R., and Yoshikawa, N., "Photochemical Initiation of Gaseous Detonations," Acta Astronautica, Vol. 5, Nov.-Dec. 1978, pp. 971-982.

[12]Strehlow, R.A., Combustion Fundamentals, 2nd ed., McGraw-Hill, New York, NY, 1984, pp. 407-409.

[13]Lee, J.H.S., "Initiation of Gaseous Detonations," Annual Review of Physical Chemistry, Vol. 28, 1977, pp. 75-104.

[14]Lee, J.H.S., "Dynamic Parameters of Gaseous Detonations," Annual Review of Fluid Mechanics, Vol. 16, 1984, pp. 311-336.

[15]Williams, F.A., Combustion Theory, 2nd ed., Benjamin/Cummings, Reading, MA, 1985, pp. 24-33.

[16]Zeldovich, I.B., and Kompaneets, A.S., Theory of Detonation, 1st ed., Academic, New York, NY, 1960, pp. 279-284.

[17]Sedov, L.I., Similarity and Dimensional Methods in Mechanics, Academic, New York, NY, 1959, pp. 193-200.

[18]Landau, L.D., and Lifshitz, E.M., Fluid Mechanics, 1st ed., Pergamon, New York, NY, 1959, pp. 486-491.

[19]Cline, M.C., "VNAP2: a Computer Program for Computation of Two-Dimensional, Time-Dependent, Compressible, Turbulent Flow," Report LA-8872, Los Alamos National Laboratory, Los Alamos, NM, August 1981.

[20]Davis, W.C., "The Detonation of Explosives," Scientific American, Vol. 256, May 1987, pp. 106-112.

[21]Barenblatt, G.I., Similarity, Self-Similarity, and Intermediate Asymptotics, Consultants Bureau, New York, NY, 1979, pp. 63-74.

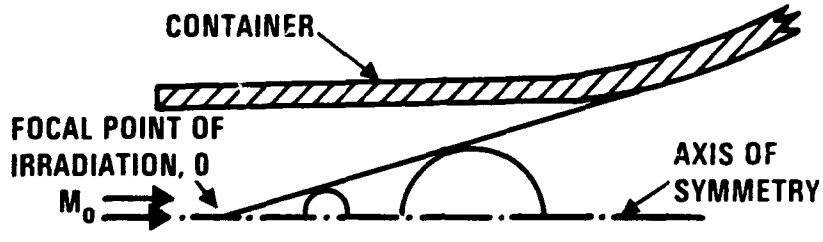

Figure 1. Each of the periodic pulses nonintrusively deposits sufficient energy [in a uniform supersonic stream (Mach number M_0) of combustible mixture, flowing in an axisymmetric container] to initiate directly a CJ detonation, which expands radially as it is convected downwind. The envelope of detonation-front positions is indicated.

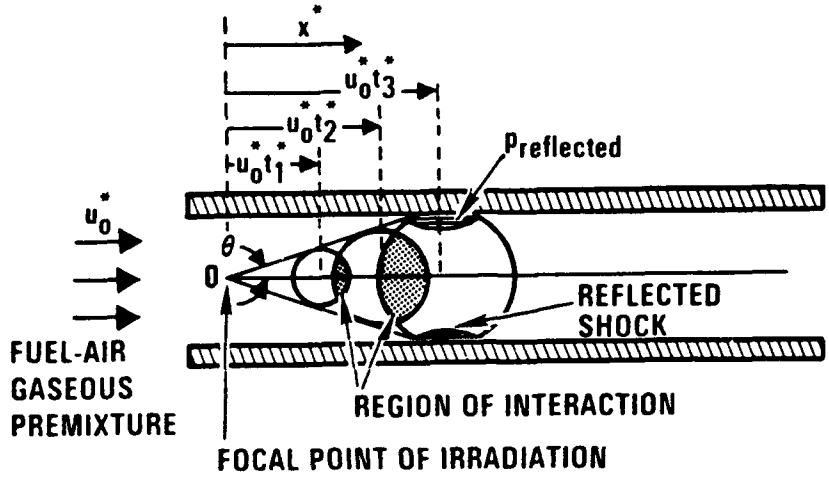

Figure 2. A simplified schematic showing three detonation fronts initiated in a premixed supersonic stream which is travelling faster than the detonation fronts (which travel at speed u_0^* sin β). The downwindmost front has interacted with the nonflared wall, and a resulting shock travels through already-reacted gas. Time $t_3^* > t_2^* > t_1^*$, such that $(t_3^* - t_2^*) = (t_2^* - t_1^*)$.

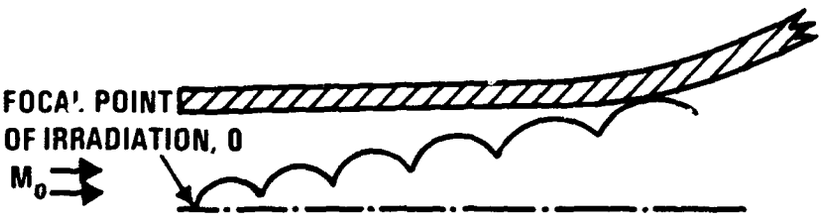

Figure 3. The "scalloped" front constituted by portions (actually, zonal strips) of the interacting spherical CJ detonation waves initiated by pulsing at a fixed finite frequency.

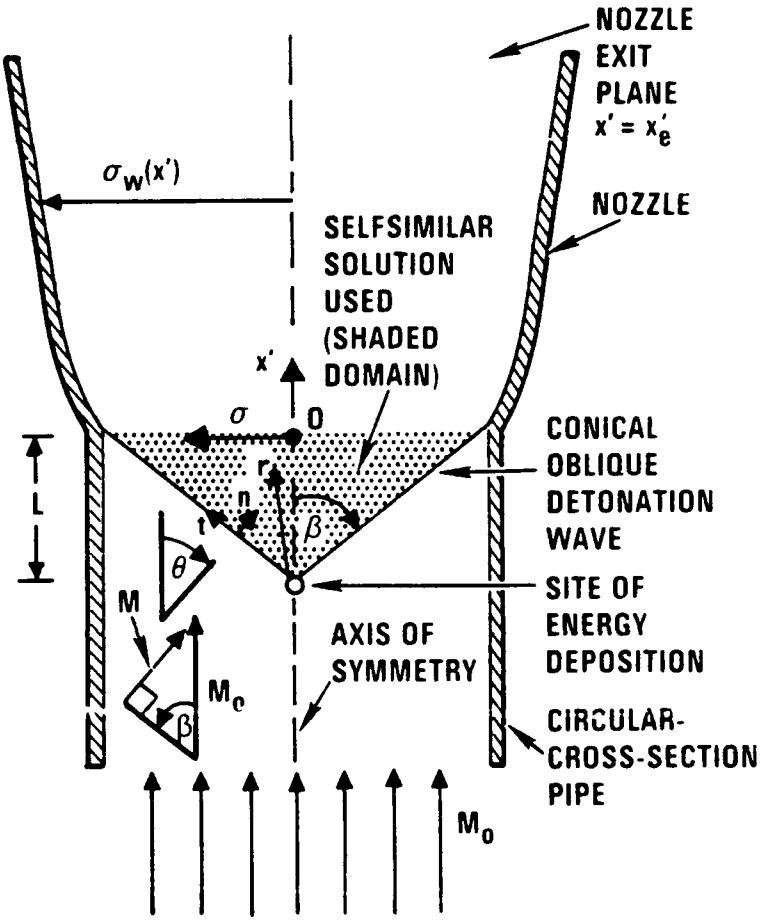

Figure 4. Schematic (not to scale) of a supersonic combustor ($x = x' + L$; n, t are normal, tangential coordinates). The selfsimilar solution actually holds for $x' > 0$ near the axis, as determined by the "inward-running" characteristic from the nozzle-pipe joining.

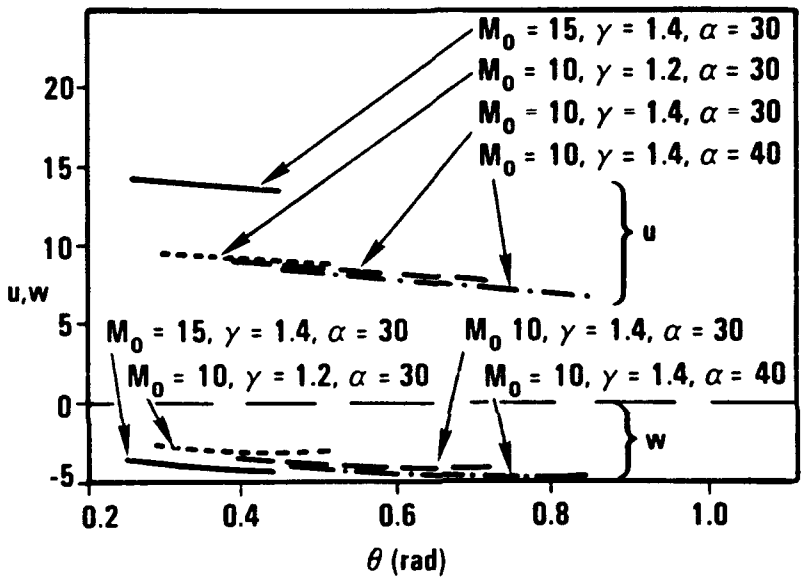

Figure 5. Dimensionless (spherical-)radial velocity component u and polar-angle velocity component w, as functions of the polar angle θ, for various values of the ambient Mach number M_0, heat-capacity ratio γ, and chemical-heat-to-static-enthalpy ratio α. The range depicted is $\theta_1 < \theta < \beta$, i.e., from the uniform-core-edge cone to the detonation-wave cone.

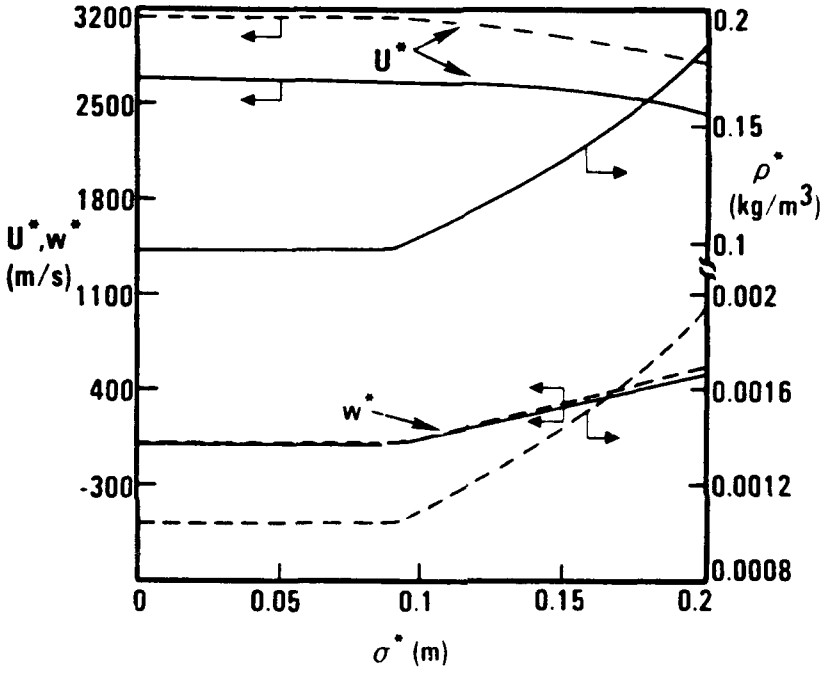

Figure 6. Axial velocity component U^*, (cylindrical-)radial velocity component v^*, and density ρ^*, computed from the similarity solution and presented as functions of the (cylindrical-)radial coordinate σ^*. Here, $M_o = 10$, $\alpha = 30$, $\gamma = 1.4$, $r^*_{pipe} = 0.2$ m, $\beta \simeq 49°$. For the solid curves, $p^*_o = 7$ kPa, $T^*_o \simeq 201$ K; for the dashed curves, $p^*_o = 0.1$ kPa, $T^*_o = 271$ K.

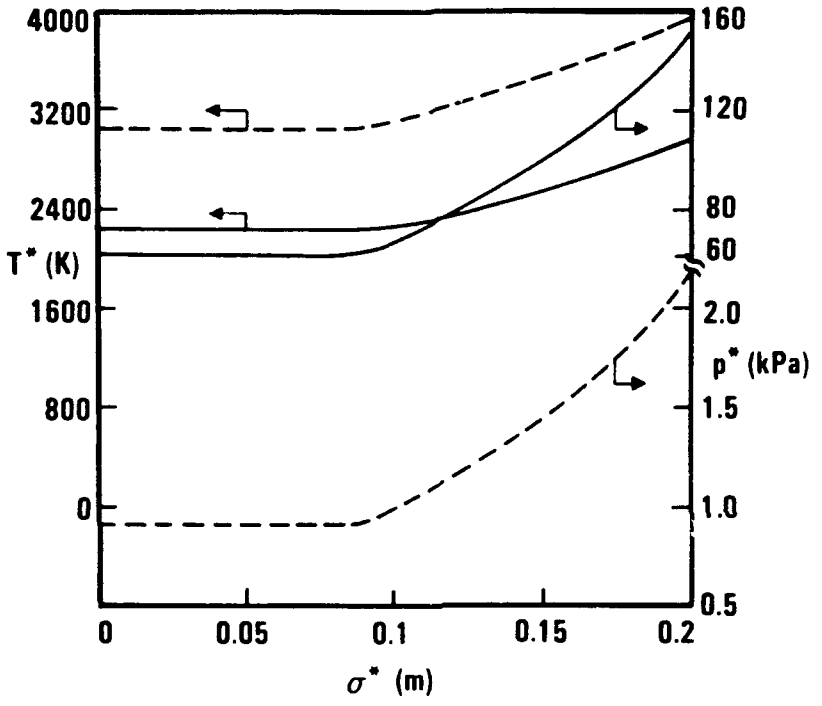

Figure 7. Temperature T^* and pressure p^*, computed from the similarity solution and expressed as functions of the (cylindrical-)radial coordinate σ^*, for the conditions of Figure 6.

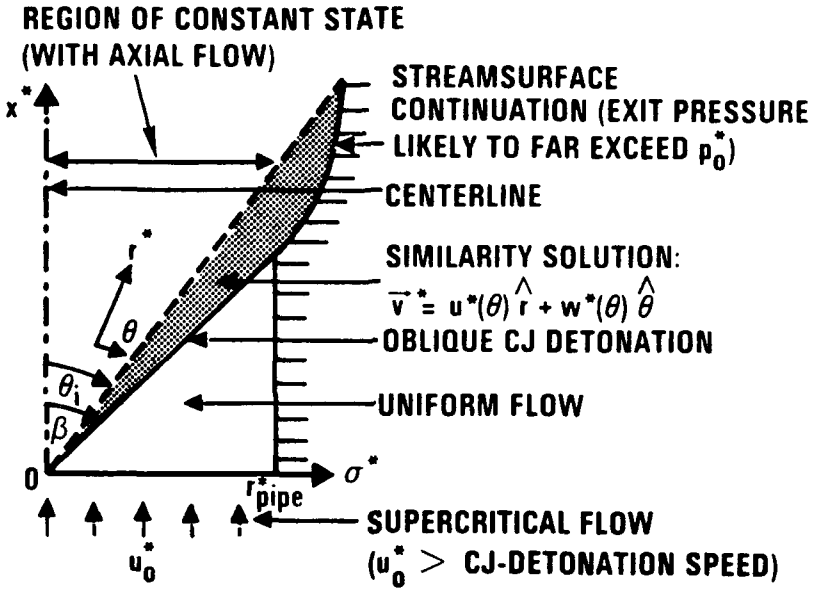

Figure 8. Downwind continuation of the streamsurface through the detonation-wall intersection is sketched as the nozzle configuration. At the downwind site at which the nonuniform (shaded) region of the reacted flow no longer persists, the pressure is uniform, but typically far exceeds ambient. Adjoining a small-angle cone to expand to ambient pressure incurs impractical nozzle length.

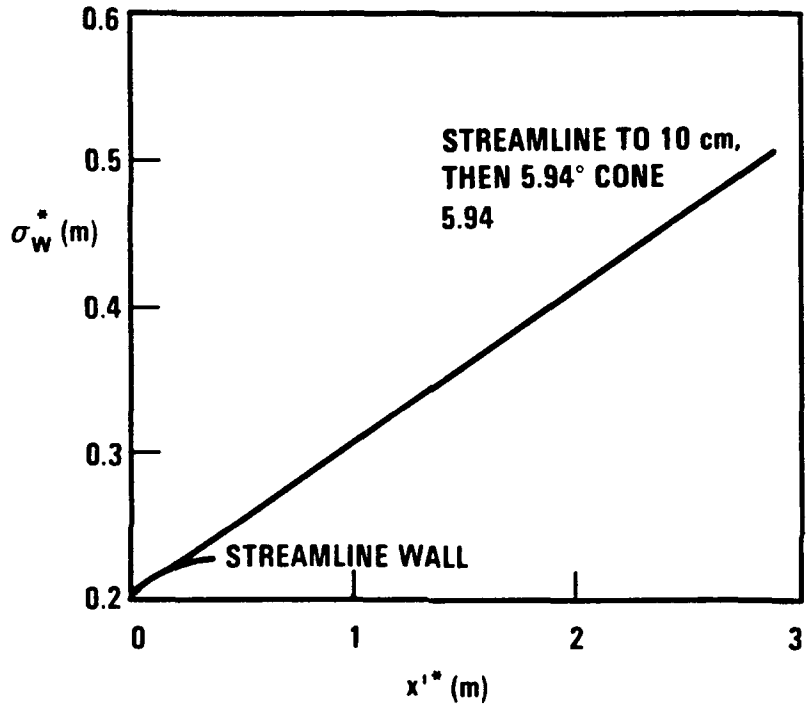

Figure 9. The nozzle-wall geometry for the so-called streamline wall (drawn to the axial distance at which the pressure is uniformized radially), and also for the wall shape (examined in Figures 10 and 11) of 10-cm span along the streamline wall followed smoothly by a 5.94° cone. The conditions are those in Figure 6 (solid curves).

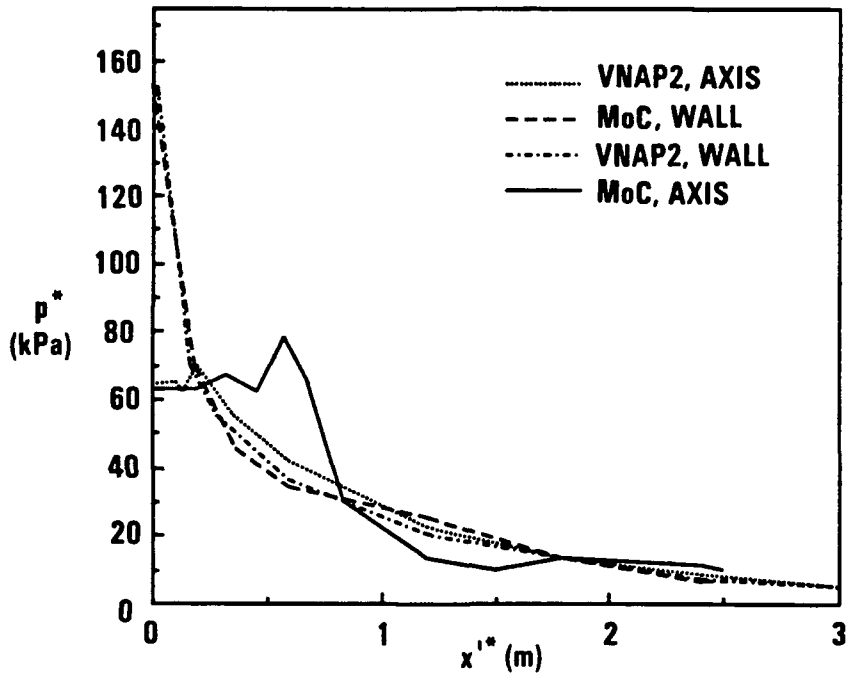

Figure 10. Pressure p^* at the axis of symmetry $\sigma^* = 0$ and at the nozzle wall $\sigma^* = \sigma^*_w$, as a function of the axial distance x'^*. For the geometry, see the "cone" in Figure 9; for the starting conditions at $x'^* = 0$, see the solid curves in Figures 6 and 7. Results are from a method-of-characteristics (MoC) code and from the VNAP2 code[19].

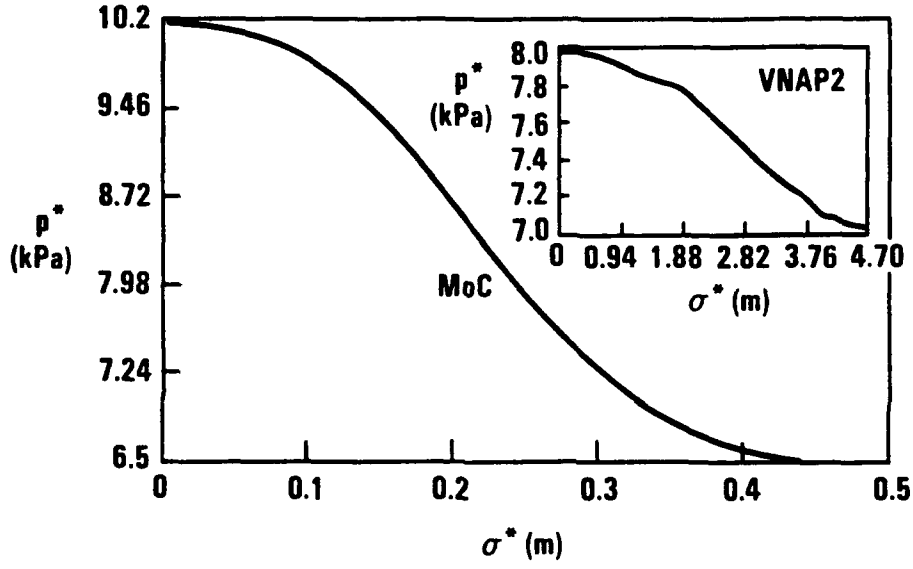

Figure 11. Pressure p^* as a function of radial coordinate σ^* at the exit plane, for the case discussed in Figure 10. The exit plane $x_e'^* = 2.47$ m for VNAP2 results, = 2.5 m for MoC results.

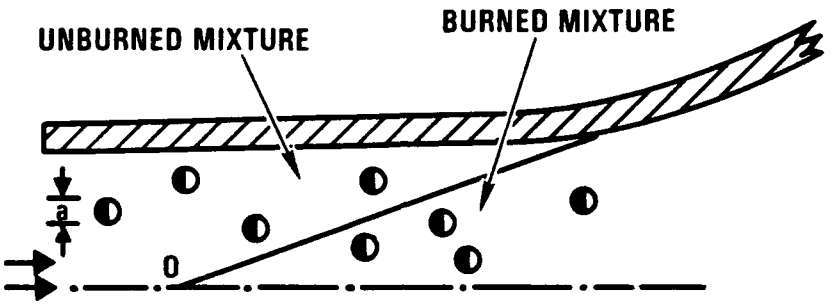

Figure 12. The half-shaded spheroids of scale a denote the (I-N)% of the mixture constituted by biobs consisting of fuel (shaded) and air (unshaded) in stoichiometric proportion. The well-mixed N% is converted to product gas in the oblique detonation.

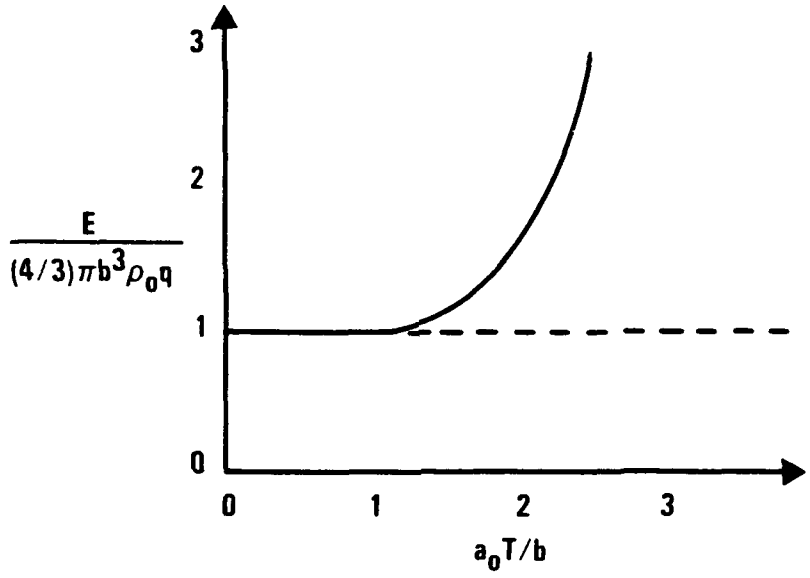

Figure 13. A rough sketch of how the minimum deposited energy required for the direct onset of detonation, E, normalized against the chemical heat of reaction available in the irradiated blob (taken for specificity, to be a sphere initially of radius b, of density ρ_0, and of exothermicity per mass q), is anticipated to vary with the deposition interval T, normalized against (b/a_0), where a_0 is the speed of sound in the ambient detonable gaseous mixture.

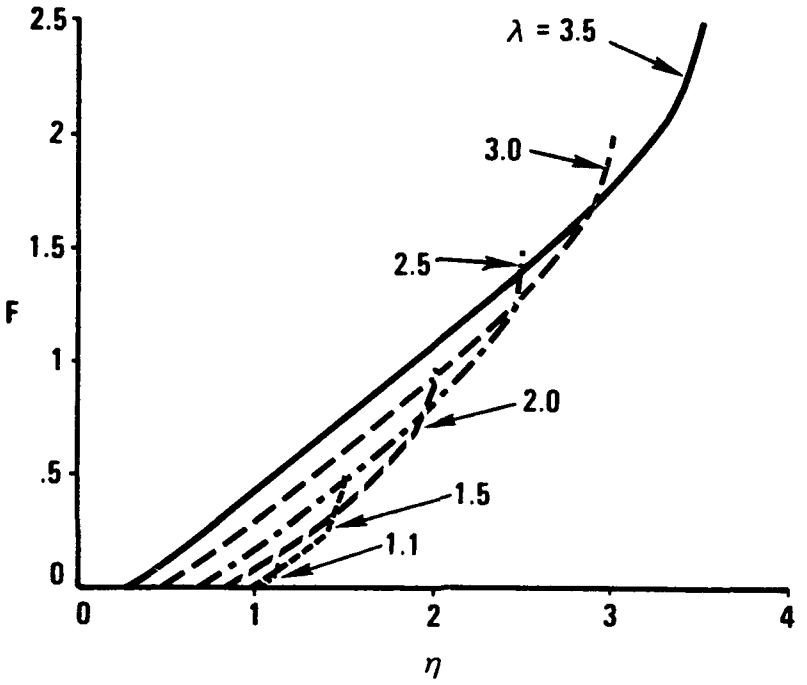

Figure 14. For a spherical detonation, the dimensionless flow speed F of the shocked and reacted gas, as a function of the similarity variable η defined below (A.4), for the ratio of specific heats γ = 1.4, for several values of the ratio λ of the CJ-wave speed to the just-detonated-gas sound speed.

APPENDIX IV.

Ignition of $H_2/O_2/NH_3$, $H_2/Air/NH_3$ and $CH_4/O_2/NH_3$ Premixed Flows By Excimer Laser Photolysis of NH_3

Mau-Song Chou and Tmitri J. Zukowski

TRW Space and Technology Group
Redondo Beach, CA 90278

(Submitted to Combustion Science and Technology)

Abstract

We have achieved volumetric ignition of H_2/O_2, H_2/air and CH_4/O_2 mixtures in an open flow system initially at 1 atm and room temperature via an ArF excimer laser (193 nm) photolysis of a small amount of NH_3 doped in the flow mixtures. The ignition appears to be homogenous since the ignition delay times measured at several locations are close in value. The minimum ignition energy density is measured to be 137 ± 8, 190 ± 20 and 300 ± 30 mJ/cm^3 for stoichiometric mixtures of $H_2/O_2/NH_3$, H_2/air/NH_3 and $CH_4/O_2/NH_3$ flows, respectively, and appears to be insensitive to the fuel equivalence ratio between 0.35 and 3.0. The ignition delay time depends strongly on the initial NH_3 concentration and the laser energy deposition density, however is also nearly invariant to the equivalence ratio. The required minimum ignition energy density appears to be substantially lower than that expected for thermal ignition. Preliminary kinetic modeling calculations suggest that the hot H atoms and/or electronically excited $NH_2(A)$ from the photolysis of NH_3 may play an important role in enhancing the ignition.

I. Introduction

Photochemical ignition of combustion provides an opportunity to study details of the associated chemical processes, since energy can be directed homogeneously and within a short duration into a specific mode of a reactant, to prepare a well-defined initial condition. Earlier experiments by Farkas et al. [1] have shown that H_2/O_2 mixtures with a small amount of NH_3 become explosive at a moderate temperature (~420°C) under ultraviolet radiation. The reaction appears to proceed much more rapidly via NH_3 photolysis, rather than by other means of photogeneration of H atoms, such

as via photosensitized mercury atoms that dissociate H_2 into 2H [2]. It has been speculated that NH_2 may play an important role in the ignition chemistry; however, the detailed reaction mechanism remains poorly understood [3].

Recent advances in high-energy ultraviolet lasers have renewed interest in photochemical ignition, since these lasers can generate sufficient radicals by photolysis to initiate combustion in an exceptionally controlled way. Laser-spark has been used to ignite fuel-oxidizer mixtures, either by gaseous breakdown [4,5] or multiphoton processes [6,7], within a tightly focused spot. Absorption of laser photons which produce reactive radical species in the absence of spark formation has also been used to initiate combustion. For example, Lavid et al. [8] have used a F_2 laser at 157 nm to dissociate O_2 to ignite H_2/O_2 mixtures, and Lucas et al. [9] have used a KrF laser at 248 nm to dissociate O_3 to ignite H_2/O_2-, CH_4/O_2-, and C_3H_8/O_2 mixtures. We are primarily interested in the latter kind of photochemical ignition. The related subjects of ignition by the addition of radicals have been studied theoretically by Guirguis and Oppenheim [10], Sloane [11-13], and Sloane and Schoene [14].

In this paper, we describe a study of ignition initiated by photolysis of NH_3 by the use of an ArF laser at 193 nm in mixtures of $H_2/O_2/NH_3$ and H_2/air/NH_3 and $CH_4/O_2/NH_3$. We have also performed kinetic modeling simulation on the ignition of H_2/O_2 by radical addition. Our kinetic modeling calculations suggest that the highly energetic photo-fragments, such as hot H atoms and electronically excited $NH_2(\tilde{A})$, may play an important role in the initiation of combustion.

II. Review of Relevant Photochemistry

Light of 193 nm wavelength excites NH_3 into $\nu_2' = 6$ of the $\tilde{A}^1A_2'' \leftarrow \tilde{X}^1A_1'$ transition [15,16], and the excited NH_3 dissociates into NH_2 and H with nearly unit quantum efficiency [17,18]. The molar extinction coefficient for NH_3 at 193 nm is measured to be 3250 liter/mole-cm [19], which is much higher than that of O_2 [20]. The absorption by O_2 is estimated to be less than about one percent of that by NH_3 under our experimental conditions. The bond dissociation energy for NH_3, $D_0(H\text{-}NH_2)$, is ~446.4 kJ/mole [21,22]; hence there is about 171.5 kJ/mole residual energy left from the 193 nm photons. Based on the distribution of the translational energy of the H atom photofragments from the photolysis of NH_3, Biesner et al. [23] conclude that about 21 percent of the residual energy is in the form translational excitation and the rest is in the excitation of NH_2. These investigators also derive a branching ratio of 0.33 for the yield of $NH_2(A)$ to $NH_2(X)$. However, a lower branching ratio (0.025) was reported earlier by Donnelley et al. [24] based on the NH_2 emission following the 193 nm photolysis of NH_3.

At higher laser intensity, NH(A) can also be produced by a sequential two-photon absorption process via an internally excited intermediate state of $NH_2(\tilde{X})$ [25,26]. The molar extinction coefficient for the absorption of the intermediate $NH_2(\tilde{X})$ at 193 nm is measured to be ~10.4 ℓ $mole^{-1}$ cm^{-1} by Hofzumahaus et al. [27].

Quenching of the internally excited photolysis products of $NH_2(\tilde{X})$ by O_2 and H_2 appear to be relatively slow [25]. This implies that chemical reactions with the two collision partners are not an important channel for

the decay of $NH_2(\tilde{X})$. The photolysis products of $NH_2(\tilde{A})$ appear to have two components: ~85% in a short-lived component and ~15% in a long-lived component [28]. The former is postulated to be pure $NH_2(\tilde{A})$, while the latter to be a mixed state of $NH_2(\tilde{A})$ and $NH_2(\tilde{X})$. The long-lived component is not very reactive with O_2 [25]. However, the reactivity of the short-lived component with O_2 has not been reported in the literature.

The reaction of NH_2 and O_2 has been recently reviewed by Hanson et al. [29]. Fujii et al. [30] proposed that the reaction proceed as follows,

$$NH_2 + O_2 \rightarrow HNO + OH. \qquad (1)$$

The rate constant is determined to be $10^{12.25}$ exp(-15,000/RT) with an activation energy of ~63 kJ/mole. The $NH_2(\tilde{A})$ state has an excitation energy of 122 kJ/mole above the $NH_2(\tilde{X})$ ground state. It is possible that the short lived component of the $NH_2(\tilde{A})$ from the photolysis of NH_3 may enhance the rate of Reaction 1. However, quenching cross sections for the short-lived component are generally quite high with collisional partners, including NH_3, H_2, Ar and H_e [25,31], the loss of the short-lived component is likely to be dominated by collisional quenching rather than by the reaction with O_2.

The hot H atoms from the photolysis of NH_3 may enhance the rate of reaction with O_2 [32-36]:

$$H + O_2 \rightarrow OH + O. \qquad (2)$$

According to a theoretical study by Miller [32], the reaction cross section has a threshold energy of about 52 kJ/mole and rises gradually to a broad maximum of ~0.4 $\mathring{A}^2$ for translation energies between 105 and 209 kJ/mole. The distribution of H atom kinetic energy from the photolysis of

NH_3 has been measured by Biesner [22,23]. From this one estimates that ~20 percent of the H atoms should have a kinetic energy above the threshold. Using the measured H atom distribution profile and the calculated reaction cross section [32], one derives an effective rate constant (k_2) of ~9.4 x 10^{12} cm^3/mole-s for those H atoms with translational energy above the threshold. A major competing reaction for the H atoms is Reaction 3, which may be considered as a chain-breaking reaction, since HO_2 is not very reactive:

$$H + O_2 + M \rightarrow HO_2 + M. \qquad (3)$$

The product of the rate constant of k_3 [37] and the gas density (M) is calculated to be about 3.6 x 10^{12} cm^3/mole-s at one atmosphere. This indicates that ~20 percent of the H atoms produced from NH_3 photolysis may react with O_2 favorably via Reaction 2.

III. Experimental Procedure

The experimental arrangement is shown in Figure 1. A Lambda Physik Excimer Laser (150 EST), which provides ArF laser radiation at 193 nm, is used as the photolysis source. This excimer laser system consists of two laser units. The output from an unstable resonator of the first unit is amplified through the second unit to achieve a high energy output with a low beam divergence. A UV grade MgF_2 lens with a 50 cm focal length is used to deliver the beam with a rectangular profile of about 2.1 mm wide x 7.1 mm high at the leading edge and 1.2 mm wide x 3.3 mm high at the trailing edge of a 6-cm diameter flat flame burner (McKenna Products). The focus of the laser beam is far past the burner to avoid any gaseous breakdown in the mixtures. The laser beam size is determined by burn spots on Polariod films.

The incident as well as the transmitted laser energies are monitored by the use of quartz flat beam splitters and laser energy ratiometer probes (Laser Precision Model 7200). A typical incident laser energy is in the range of 100-290 mJ per pulse. The OH emission is monitored at three locations along the beam path: 2.2 cm, 3.0 cm and 3.8 cm from the leading edge of the burner. The center location (3 cm) is observed with a monochromator and photomultiplier tube, whereas the other two locations are monitored with a band-pass filter (at 310 nm with 10 nm bandwidth) and photomultiplier.

The premixed gas mixtures which are prepared in a stainless steel manifold are flowed through the flat flame burner. Coaxial N_2 shroud gas is used to minimize any mixing of the combustible flow mixtures with the surrounding air. Matheson anhydrous grade ammonia (99.99%), hydrogen (99.995%) and O_2 (99.5%) are used. The total gas flow is 3.75 ℓ/min for $H_2/O_2/NH_3$ and $CH_4/O_2/NH_3$, and 8.75 ℓ/min for H_2/air/NH_3 mixtures. These correspond to cold gas linear velocities of 1.3 and 3.0 mm/min, respectively. Ignition experiments are conducted on the premixed gases in an open system at ~1 mm immediately above the flat flame burner. All the data are collected at 1 atm and at room temperature.

Majority of the experiments are carried out under conditions that the incident excimer laser energy is sufficiently high to bleach out the NH_3 absorption along the irradiated pathlength, but is not too high to cause any significant multiphoton effects. This should yield a relatively uniform laser energy deposition density and a well defined production of initial radical density from the photolysis in spite of any non-uniformity or hot spots in the laser beam profile.

We have made numerous observations with an optical multichannel analyzer (OMA). The emission during ArF laser irradiation is found to be mainly composed of the NH band at 336 nm, NH_2 at 500-800 nm and OH bands at 308 nm and 283 nm. No atomic or ionic emission lines indicative of plasma formation are observed. This precluse ignition caused by any laser induced gaseous breakdown.

IV. Results and Discussion

$H_2/O_2/NH_3$ Mixtures

The results for the ignition of $H_2/O_2/NH_3$ mixtures by photolysis of NH_3 are summarized in Figures 2-7. Figures 2a-2c show typical OH emission temporal profiles in three different time scales to illustrate various events. Shown in Figure 2a is a prompt OH emission with a rapid rise and fall which is nearly coincident with the excimer laser pulse (which also has two maxima). The prompt OH emission is present independently of whether the mixture is ignited or not. Figure 2b shows that the OH emission decreases nearly to the background level after the prompt OH emission, and then increases rapidly after a certain delay time. Figure 2c shows that the delayed OH emission reaches a maximum and then decreases to a relatively low steady-state value. The peak intensity of the prompt OH is in this case about 5 times of that of the delayed OH emission which in turn is about an order of magnitude higher than the steady state value at the late time.

The presence of the strong prompt OH emission implies that the initial photolysis products may be converted rapidly into O and OH, since the OH emission is formed mainly via a three body recombination of H + O + M or an energy transfer from some excited species to the ground OH molecules. It

is known that thermal H atoms and $NH_2(X)$ are not reactive with O_2 at a relatively low temperature, this suggests that the hot H atoms and possibly $NH_2(A)$ from the photolysis of NH_3 may indeed react with O_2 rapidly to convert into the more reactive species of O and OH as discussed in Section II.

The delayed OH emission as shown in Figure 2b is indicative of combustion since it occurs only if the mixture is ignited. An ignition delay time may therefore be assigned based on the delayed emission by extrapolating the linear portion of the OH emission rise to the zero intensity base line. Figures 3-5 summarize the measured ignition delay times as function of incident laser energy monitored at three different locations for various initial NH_3 mole fractions. Several noticeable features are summarized below: (1) The ignition delay times at the three locations appear in general to be relatively close in value for the incident excimer laser energy above that required to bleach out the NH_3 absorption as shown for all the data in Figures 3 and 4 and part of the data with incident laser energy above the bleaching threshold (~155 mJ) in Figure 5. The variation in the ignition delay times among the three locations under bleaching conditions are not enough to be accounted for by flame propagation from a particular ignition site. This suggests that the ignition sites are probably well distributed in the entire irradiated volume. The variation may only reflect some statistical instability of the local ignition events. (2) The ignition delay time is in general relatively insensitive to the incident laser energies for those above the bleaching threshold as shown in Figures 4 and 5. This is probably expected since the laser energy deposition should remain constant under bleaching

conditions irrespective of increases in the incident laser energy. However this independency on the incident laser energy appears to break down more noticeably for a lower NH_3 mole fraction as shown in Figure 3. Here the ignition delay time decreases more substantially with increasing incident laser energy. The cause for this may be attributed to the fact that as the NH_3 concentration is reduced to that near a critical value needed for ignition, the ignition becomes more sensitive to any multiphoton processes. One of the important multiphoton processes is a sequential two-photon absorption which dissociates NH_3 into NH(A) and 2 H as discussed in Section II. The quantum yield for this process is estimated to be $\sim 1.8 \times 10^{-3}$ at 140 mJ and $\sim 3.5 \times 10^{-3}$ at 260 mJ of the incident laser energy. Although these values are only moderate as compared to the nearly unity for the single photon process, it is conceivable that any mildly increase in the radical concentration may drastically enhance the ignition process for those with low NH_3 mole fraction near that required for ignition.

Figure 6 shows the ignition delay time as function of initial NH_3 mole fraction for several fuel equivalence ratios. Also shown in the abscisa is the laser energy deposition density which is derived experimentally from the difference in the incident and transmitted laser energy divided by the total irradiated volume. The derived laser energy deposition density agrees well with that expected to bleach out the NH_3 initially in the mixtures. The ignition delay time plotted here is an average value for all the data with incident laser energies above a bleaching threshold. Some ambiguity may remain for those events with low initial NH_3 mole fraction by using the average value due to the observed variation with incident laser energy. This ambiguity however, appears to be relatively unimportant in

view of the steeper variation of the ignition delay time with the initial NH_3 mole fraction. The error bar given for the cases with the stoichiometric ratio (ϕ = 1.0) indicates one standard deviation in the spread of the measured data points. The ignition delay times which depends strongly with the initial NH_3 mole fraction, is however, nearly independent of the fuel equivalence ratio between 0.35 and 3.0 within the experimental uncertainty. Also shown in Figure 6 is an approximate threshold value of initial NH_3 mole fraction or laser energy deposition density needed for ignition. Below this threshold no ignition occurs. Figure 7 summarizes the derived minimum NH_3 mole fraction and the corresponding minimum laser energy deposition density needed for ignition for several equivalence ratios. It is noted that the required minimum laser energy deposition density is also insensitive to the fuel equivalence ratio between 0.35 and 3.0. We have also performed additional experiments using a larger laser beam with a nominal size of ~2.1 mm x 8.5 mm. The ignition delay time and the minimum laser energy deposition density for this condition are not significantly different from that shown above.

The observation that the minimum ignition energy density and ignition delay time are insensitive to the equivalence ratio is of interest. Lucas et al. [9] have also shown that the minimum laser energy deposition density is insensitive to the equivalence ratio between 0.7 and 3.3 by the photolysis of O_3, and Lavid et al. [8] have shown a minimum near 0.6 and increasing only moderately at 0.4, 1.0 and 1.6 by the photolysis of O_2. On the contrary, the minimum ignition energy increases very drastically on both sides of the equivalence ratios from that near the stoichiometric ratio for ignition induced by electric sparks [3], laser-sparks [4-5] and

multiphoton excitation processes [6-7]. One of the main differences here is that the radicals are produced at a relatively low temperature. In a theoretical study, Sloane [11] has predicted that the minimum ignition energy is nearly insensitive to the equivalence ratio between 0.4 and 1.2 for the ignition of CH_4/air by the addition of atomic oxygen. This suggests that a photochemical method or other suitable means of radical additions may be useful for ignition of extreme lean on rich fuel mixtures which may not be readily achieved by a conventional thermal or spark ignition.

Maas and Warnatz [38] have recently modeled the thermal ignition of H_2/O_2 premixtures and predicted that a minimum energy density of ~430 mJ/cm^3 needed for ignition of a stoichiometric mixture initially at 1 atm and room temperature. The observed threshold for ignition (137 ± 8 mJ/cm^3) by the NH_3 photolysis is significantly lower than that predicted for the thermal ignition. This suggests that the method of radical addition by photolysis may be more efficient in the initiation of combustion. The radical pair density of NH_2 + H needed for ignition by the photolysis of NH_3 is estimated to be ~ 1.3×10^{17} cm^{-3}. This value is very close to the atomic oxygen concentration needed for ignition based on the photolysis of O_3 reported by Lucas et al. [9]. This implies that the photolysis products of NH_2 and H are as effective as the reactive O atoms in initiating combustion. Our kinetic modeling calculations, to be described later, indicate that if the NH_2 and H were thermalized before reaction, ignition should not have occurred. This suggests that the hot H atoms and $NH_2(\tilde{A})$ produced from the NH_3 photolysis may enhance the initiation of combustion.

H_2/air/NH_3 Mixtures

The air flow is simulated by the use of an appropriate ratio of O_2 and N_2 flows. The results for the ignition of H_2/air/NH_3 stoichiometric flow mixtures by NH_3 photolysis are summarized in Figure 8. The ignition delay time plotted here is an average value for all the data with incident laser energies above the bleaching threshold. The error bar indicates one standard deviation. The ignition delay time depends strongly on the initial NH_3 mole fraction or the laser energy deposition density. In comparing to the $H_2/O_2/NH_3$ mixtures, the minimum laser energy deposition density needed for ignition is higher, and the ignition delay time is longer for the same energy deposition density. This is probably expected due to the increase in the total heat capacity with excess N_2. However, the ignition threshold appears to increase only moderately from 137 ± 8 mJ/cm^3 for the $H_2/O_2/NH_3$ to ~190 ± 20 mJ/cm^3 for the H_2/air/NH_3 flow mixtures.

$CH_4/O_2/NH_3$ Mixtures

The results for the ignition of $CH_4/O_2/NH_3$ stoichiometric flow mixtures by NH_3 photolysis are summarized in Figure 9. The ignition delay time plotted here is an average value for all the data with incident laser energies above the bleaching threshold. The error bar indicates one standard deviation. The ignition delay depends strongly with the initial NH_3 mole fraction or the laser energy deposition density. The minimum NH_3 mole fraction needed for ignition is measured to be 1.2 ± 0.1% and the corresponding minimum laser energy deposition density is 300 ± 30 mJ/cm^3. These values are higher compared to that for the $H_2/O_2/NH_3$ mixtures.

Kinetic Modeling of $H_2/O_2/NH_3$ Ignition

Ignition of $H_2/O_2/NH_3$ mixtures by NH_3 photolysis is simulated by using the zero-dimensional version of the HCT code of Lund [39], and also the CHEMKIN code of Kee et al. [40]. The zero dimensional modeling which assumes no loss of energy and species out of the irradiated volume should yield an upper bound on the ignition delay time and the mixture ignitability. The H-O-N reactions and rate constants are adopted from those complied with the codes. Both codes yield similar results for all the conditions reported here.

The experimental results with an initial NH_3 mole fraction of 0.012 under bleaching conditions are considered for modeling comparison. Table 1 summarizes the results for four different input conditions. The gas temperature is estimated by assuming that all the available residual energy of the photon energy after breaking the N-H bond from the photolysis of NH_3 is utilized in heating the gas mixture initially at room temperature. This estimated gas temperature should be an upper bound value since some of the residual energies are known to retain in the photolysis products of hot H atoms and internally excited NH_2.

In case 1, if all the initial NH_3 molecules are assumed to be photolyzed into H and NH_2 and that the energetics in the photolysis products are quenched before reaction proceeds, one predicts no ignition within 1 second time span. This may be explained by the fact that thermal H atoms are likely to recombine with O_2 to form unreactive HO_2 and that NH_2 are not reactive with O_2 at a relatively low temperature. This calculation suggests that the energetics contained in the photolysis products should be considered to explain the experimental observation.

As discussed in Section II, 20% of the H atoms produced from the NH_3 photolysis [22-23] should have translational energy above the threshold for Reaction 2 [28]. In case 2, 20% of the H atoms are assumed to convert into OH and O. However no ignition is predicted within 1 second time span. Also discussed in Section II, the short-lived component of the $NH_2(A)$ from NH_3 photolysis is likely to be collisionally quenched rather than to react with O_2. Nevertheless, in case 3, 21% yield of NH_2 [23] are assumed to convert into HNO and OH via Reaction 1. This yields a predicted ignition delay time of 1.1 ms which is too long compared to the observed value of 27 ± 8 μs. In case 4, if all the H atoms from the NH_3 photolysis are assumed to convert into OH and O via Reaction 2, one calculates an ignition delay time of 130 μs which is still too long compared to the observed value. Although we have not been able to predict an ignition delay time in agreement with that observed even under a very optimistic condition, these calculations suggest that the energetics in the photolysis products, including hot H atoms and possibly $NH_2(A)$, may play an important role to enhance the initiation of the combustion.

In addition, we have investigated the dependence of the ignition-delay time on both the fuel-equivalence ratio and the initial radical concentration, by computer calculations. We again have used the Chemkin code for a batch-process (zero-spatial-dimension) model. The initial concentrations of O, OH, and NH_2 are taken to be identical. This choice implies that all of the H atoms from the photolysis of NH_3 are converted rapidly into O and OH. Although this may be an oversimplifying assumption, it serves the objective of predicting the variation of the ignition-delay time on the equivalence ratio and the initial radical concentration.

The calculated ignition-delay time (Fig. 10) for H_2/O_2 mixtures, initially at 1 atm and 369 K, depends quite sensitively on the initial radical concentration, as we have observed (Fig. 6). Furthermore, the calculated ignition-delay time appears to be relatively insensitive to the fuel-equivalence ratio, again as we have observed. Within the experimental uncertainty, we cannot resolve the slight variation predicted.

Since the ignition-delay time is relatively insensitive to the equivalence ratio, we expect that the minimum ignition-energy density also should be insensitive to the equivalence ratio. This is indeed what is observed (Fig. 7). For an electric spark, the minimum energy increases drastically for both fuel-lean and fuel-rich mixtures. A major reason for the very different ignition behavior for the two methods of ignition may concern the fact that the electric spark creates a small ignition kernel, which is strongly influenced by gas-transport phenomena, as now discussed.

According to Lewis and von Elbe [3], spark ignition occurs only if the energy added to the gas is sufficient to heat a volume of the gas of about the thickness of steadily propagating flame to the adiabatic flame temperature. By relating the flame thickness to the laminar burning velocity S_L, the minimum spark-ignition energy may be given approximately as [41, 42]

$$E_{min} \simeq (4/3)\ [k/(C_p \rho\ S_L)^3]\ \rho\ C_p\ (T_\infty - T_o),$$

where k is the thermal conductivity, C_p is the specific heat, ρ is the gas density, T_∞ is the adiabatic flame temperature, and T_o is the initial gas temperature. This equation indicates a strong dependence of the minimum ignition energy on the laminar burning velocity. For both H_2/O_2 and CH_4/O_2

mixtures, the laminar burning velocity is maximum near the stoichiometric mixture, and falls off rapidly away from that mixture. This observation qualitatively explains the sensitive dependence of spark-ignition energy on equivalence ratio. Recently Sloane [13] and Sloane and Schoene [14] have modeled the ignition of a small volume of thermally heated CH_4/air mixture, and have qualitatively explained spark-ignition behavior. Maas and Warnatz [38] also have predicted the minimum ignition-energy density for H_2/O_2 mixtures when thermal energy is added to a volume of about 1-mm radius within a relatively large volume of gas mixture. Their work shows that the spark-ignition energy is strongly influenced by gas-transport phenomena, and that the ignition energy becomes strongly dependent on equivalence ratio when the ignition-spot size is small. When the spot size is larger, the ignition is influenced strongly by chemistry, and the minimum ignition-energy density becomes insensitive to the equivalence ratio, independently of whether the initial energy is added in the form of heat or of radical dissociation.

V. Conclusion

We have achieved volumetric homogeneous ignition of $H_2/O_2/NH_3$, H_2/air/NH_3 and $CH_4/O_2/NH_3$ mixtures in an open flow system initially at 1 atm and room temperature via photolysis of NH_3. The emission spectrum monitored by an OMA shows no discernable atomic or ionic emission, precluding ignition caused by gaseous breakdown. The ignition delay times based on the 308 nm OH emission band at three locations appear to be close in value, suggesting the presence of well distributed ignition sites within the entire irradiated volume. The ignition delay time depends strongly on

the initial NH_3 mole fraction and nearly independent of the fuel equivalence ratio between 0.35 and 3.0 in $H_2/O_2/NH_3$ mixtures. The minimum ignition energy density is also insensitive to the equivalence ratio. Furthermore, the required minimum ignition energy density (137 ± 8 mJ/cm^3) appears to be substantially less than that by a thermal process (~ 430 mJ/cm^3) for a stoichiometric H_2/O_2 mixture.

Our kinetic modeling calculations show that if the hot H atoms and $NH_2(A)$ from the photolysis of NH_3 were collisionally quenched rapidly, ignition should not have occurred. This implies that the excitation energy contained in the initial photolysis products may play an important role in enhancing the ignition. However, the detailed mechanism leading to the enhanced ignition with low required ignition energy density and short ignition delay time remains not well understood.

We acknowledge E.Y. Wang (TRW) and J.Y. Chen (Sandia National Laboratories) for assistance in computer modeling calculations and T. Sloane (General Motors) for helpful discussions. This work was sponsored by the Air Force Office of Scientific Research, Air Force System Command, USAF, under Contract F49620-87-C-0081.

Table 1. Computer Modeling of H_2/O_2 Ignition by NH_3 Photolysis[a]

Case No.	Gas Composition (mole fraction)		Gas Temperature	Ignition-Delay Time	Remarks On Gas Composition
1	H_2 O_2 H NH_2	0.651 0.325 0.012 0.012	369	> 1 s	Energetics in the photolyzsis products of H and NH_2 were collisionally quenched.
2	H_2 O_2 H NH_2 O OH	0.651 0.324 0.0096 0.0012 0.0024 0.0024	369	> 1 s	20% of H reacted with O_2 to form OH + O.
3	H_2 O_2 H NH_2 O OH HNO	0.648 0.323 0.0096 0.0094 0.0024 0.0049 0.0025	369	1.1 ms	20% of H and 21% of NH_2 reacted with O_2 to form OH + O and HNO + O, respectively.
4	H_2 O_2 NH_2 O OH	0.643 0.321 0.012 0.012 0.012	369	130 μs	All H atoms reacted with O_2 to form OH + O.

(a) Assuming that the initial NH_3 mole fraction is 0.012 and all NH_3 molecules are photolyzed into H + NH_2 under bleaching condition.

REFERENCES

1. Farkas, H. L., Haber, F., and Harteck, P., Z. Elektrochem. 36:711 (1930).
2. Taylor, H. S., and Salley, D. J. Amer. Chem. Soc. J. 55:96 (1933).
3. Lewis, B., and von Elbe, G. Combustion, Flames and Explosions of Gases, 3rd edition. Academic, New York, 1987.
4. Weinberg, F. J., and Wilson, J. R. 1971. Proc. Roy. Soc., Lond. A321:41 (1971).
5. Syage, J. A., Fournier, E. W., Rianda, R., and Cohen, R. B. J. Appl. Phys. 64:1499 (1988).
6. Forch, B. E., and Miziolek, A. W. Combust. Sci. Tech. 52:151 (1987).
7. Forch, B. E., and Miziolek, A. W. Opt. Lett. 11:129 (1986).
8. Lavid, M., and Stevens, J. G. Combust. Flame 60:195 (1985).
9. Lucas, D., Dunn-Rankin, D., Hom, K., and Brown, N. J. Combust. Flame 69:171 (1987).
10. Guirguis, R. H., Oppenheim, A. K., Karasalo, I., and Creighton, J. R., Progress in Astronautics and Aeronautics, Washington, DC, American Institute of Aeronautics and Astronautics, 1981, Vol. 76, p. 134.
11. Sloane, T. M. Combust. Sci. Tech. 34:317 (1983).
12. Sloane, T. M. Combust. Sci. Tech. 42:131 (1985).
13. Sloane, T. Combust. Sci. Tech. 63:287 (1989).
14. Sloane, T., and Schoene, A. Y. 22nd Symposium (Int.) on Combust., 1988, p. 1669.
15. Vaida, V., McCarthy, M. I., Engelking, P. C., Rosmus, P., Werner, H. J., and Botschwina, J. Chem. Phys. 86:6669 (1987).

16. Rosmus, P., Botschwina, P. Werner, H. J., Vaida, V., Engelking, P. C., and McCarthy, M. I., J. Chem. Phys. 86:6677 (1987).

17. Okabe, H. Photochemistry of Small Molecules. John Wiley, New York, 1978.

18. McCarthy, M. I., Rosmus, P., Werner, H. J., Botschwina, P. and Vaida, V., J. Chem. Phys. 86:6693 (1987).

19. Kenner, R. D., Rohrer, F., and Stuhl, F. J. Chem. Phys. 86:2036 (1987).

20. Thompson, B. A., Harteck, P., and Reeves, R. R. J. Geophys. Res. 68:6431 (1963).

21. Gibson, S. T., Greene, J. P., and Berkowitz, J. J. Chem. Phys. 83:4319 (1985).

22. Biesner, J., Schnieder, L., Schmeer, J., Ahlers, G., Xie, X., Wedge, K. H., Ashfold, M. N. R., and Dixon, R. N. J. Chem. Phys. 88:3607 (1988).

23. Biesner, J. Schnieder, L., Ahlers, G., Xie, X., Wedge, K. H., Ashfold, M. N. R., and Dixon, R. N. J. Chem. Phys. 91:2901 (1989).

24. Donnelly, V. M., Baronavski, A. P., and McDonald, J. R. Chem. Phys. 43:271 (1979).

25. Kenner, R. D., Rohrer, F., Browarzik, R. K., Kaes, A., and Stuhl, F. Chem. Phys. 118:141 (1987).

26. Kenner, R. D., Browarzik, R. K., and Stuhl, F. Chem. Phys. 121:457 (1988).

27. Hofzumahaus, A. and Stuhl, F. J. Chem. Phys. 82:5519 (1985).

28. Donnelly, V. M., Baronavski, A. P., and McDonald, J. R. Chem. Phys. 43:283 (1979).

29. Hanson, R. K. and Saliman, S. Combustion Chemistry, Springer, New York, 1984, Chapter 6.

30. Fujii, N., Miyama, H., Koshi, M., and Asaba, T. 18th Symposium (Int.) on Combustion, 1981, p. 873.

31. Halpern, J. B., Hancock, G., Lenzi, M., and Welge, K. H. J. Chem. Phys. 63:4808 (1975).

32. Miller, J. A. J. Chem. Phys. 74:5120 (1981).

33. Kleinermans, K., and Wolfrum, J. J. Chem. Phys. 80:1446 (1984).

34. Kleinermans, K., and Linnebach, E. J. Chem. Phys. 82:5012 (1985).

35. Kleinermans, K., and Schinke, R. J. Chem. Phys. 80:1440 (1984).

36. Bronikowski, M. J., Zhang, R., Rakestraw, D. J. and Zare, R. N. Chem. Phys. Lett. 156:7 (1989).

37. Pitz, W. J., Westbrook, C. K., Proscia, W. M., and Dryer, F. L. 20th Symposium (Int.) on Combust., 1984, p. 831.

38. Maas, U., and Warnatz, J. Combust. Flame 74:53 (1988).

39. Lund, C. M. Report No. UCRL-52504. Lawrence Livermore National Laboratory, 1978.

40. Kee, R. J., Miller, J. A., and Jefferson, T. H. Report No. SAND 80-8003, Sandia National Laboratory, 1980.

41. Williams, F.A., Combustion Theory, 2nd ed., Benjamin-Cummings, 1985.

42. Ronney, P.R., "A review of flame ignition," Combustion Institute, Western States Section Spring Meeting, April 30-May 2, 1990, Banff, Alberta, Canada.

Figure Captions

1. Schematic of experimental arrangement for the ignition of premixed combustible flows by ArF excimer laser photolysis of NH_3, M: mirror, QF: quartz flat and PMT: photomultiplier tube.
2. Typical OH Emission profiles at three different time scales to show various events following ArF excimer laser irradiation: (a) prompt OH emission, (b) rise of delayed OH emission, and (c) rise and fall of the delayed OH emission.
3. Ignition delay time in stoichiometric $H_2/O_2/NH_3$ mixtures with 0.0065 mole fraction of NH_3 as function of incident laser energy based on the OH emission measurements at three locations: (∇) 2.2 cm, (0) 3.0 cm, and (Δ) 3.8 cm downstream of the burner leading edge.
4. Ignition delay time in $H_2/O_2/NH_3$ stoichiometric mixtures with 0.0086 mole fraction of NH_3 as function of incident laser energy based on the OH emission at three locations: (∇) 22 cm, (0) 3.0 cm and (Δ) 3.8 cm downstream of the burner leading edge.
5. Ignition delay time in $H_2/O_2/NH_3$ stoichiometric mixtures with 0.0135 mole fraction of NH_3 as function of incident laser energy based on OH emission at three locations: (∇) 2.2 cm, (0) 3.0 cm and (Δ) 3.8 cm downstream of the burner leading edge. The arrow indicates the minimum incident laser energy needed to bleach out the NH_3 absorption up to the 3.8 cm location.
6. Ignition delay time in $H_2/O_2/NH_3$ mixtures as function of initial NH_3 mole fraction and laser energy deposition density for several fuel equivalence ratios: (Δ) 0.35, (∇) 0.5, (0) 1.0, (•) 2.0, ( ) 3.0. The error bar given for the cases with fuel equivalence ratio of 1.0

indicates one standard deviation in the spread of the measured data points. The shaded area indicates the region of no ignition.

7. Minimum laser energy deposition density and minimum initial mole fraction of NH_3 needed for ignition of $H_2/O_2/NH_3$ mixtures at several fuel equivalence ratios.
8. Ignition delay time in H_2/air/NH_3 stoichiometric mixtures as function of initial NH_3 mole fraction and laser energy deposition density. The error bar indicates one standard deviation in the spread of the measured data points. The shaded area indicates the region of no ignition.
9. Ignition delay time in $CH_4/O_2/NH_3$ stoichiometric mixtures as function of initial NH_3 mole fraction and laser energy deposition density. The error bar indicates one standard deviation in the spread of measured data points. The shaded area indicates the region of no ignition.
10. Calculated dependence of the ignition-delay time for H_2/O_2 mixtures as a function of fuel-equivalence ratio, for an initial temperature of 369 K and an initial pressure of 1 atm. The initial concentrations of the radicals NH_2, O, and OH are taken to be equal, and to be equal to mole fraction 0.01, 0.012, and 0.014 in three calculated cases.

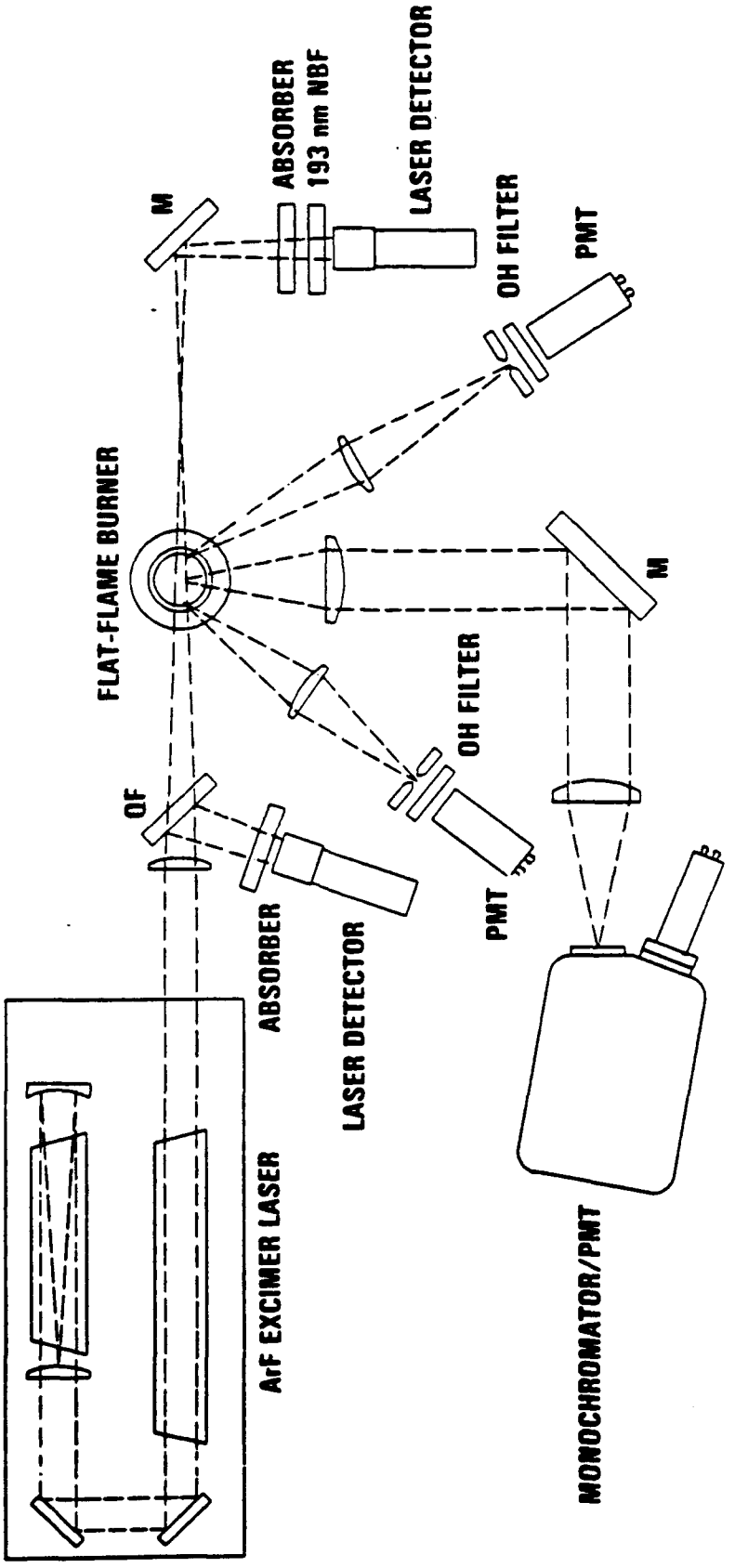
M
ABSORBER
193 nm NBF
LASER DETECTOR
OH FILTER
PMT
FLAT-FLAME BURNER
M
OH FILTER
OF
ABSORBER
LASER DETECTOR
PMT
ArF EXCIMER LASER
MONOCHROMATOR/PMT

FIGURE 1.

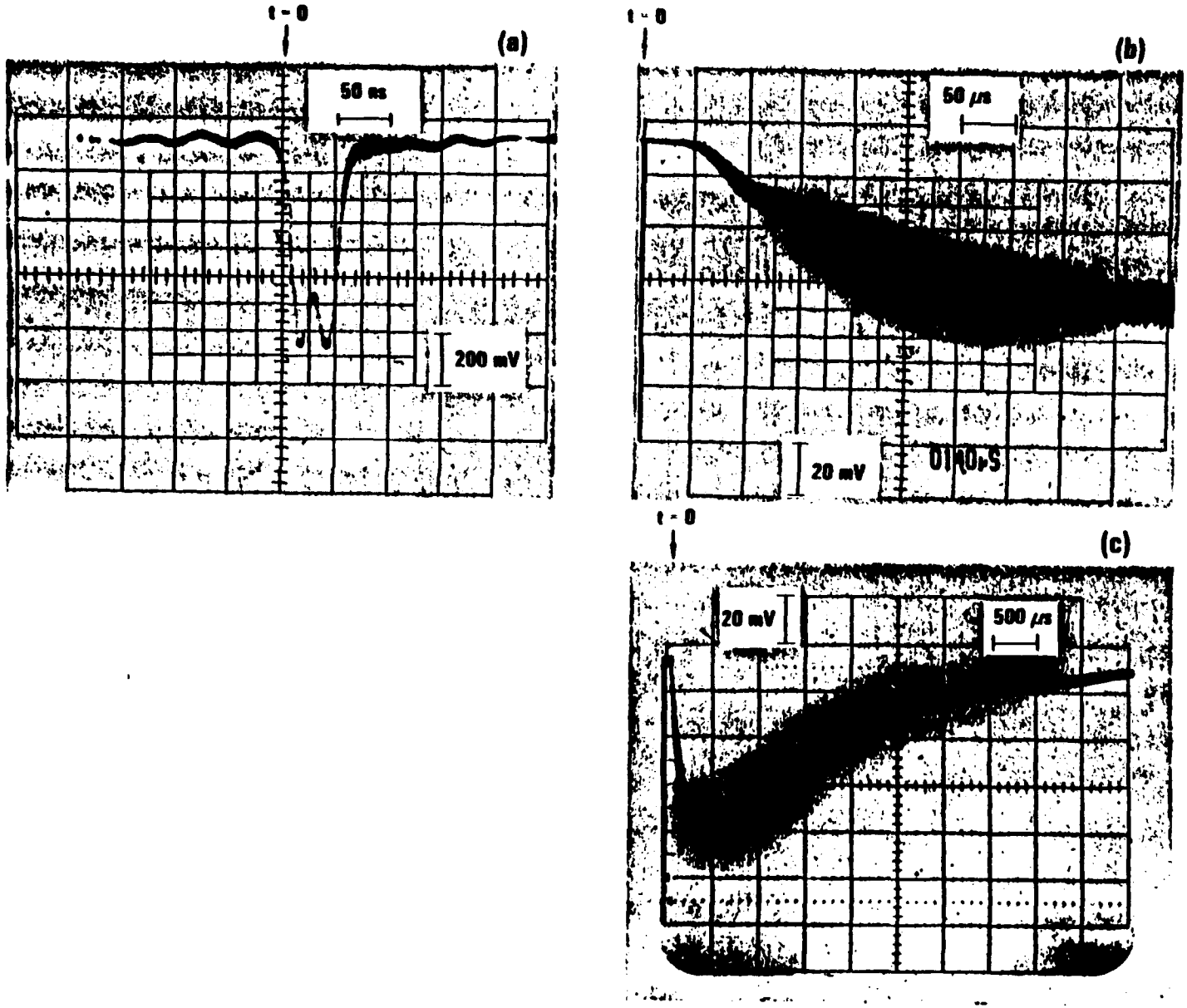

FIGURE 2.

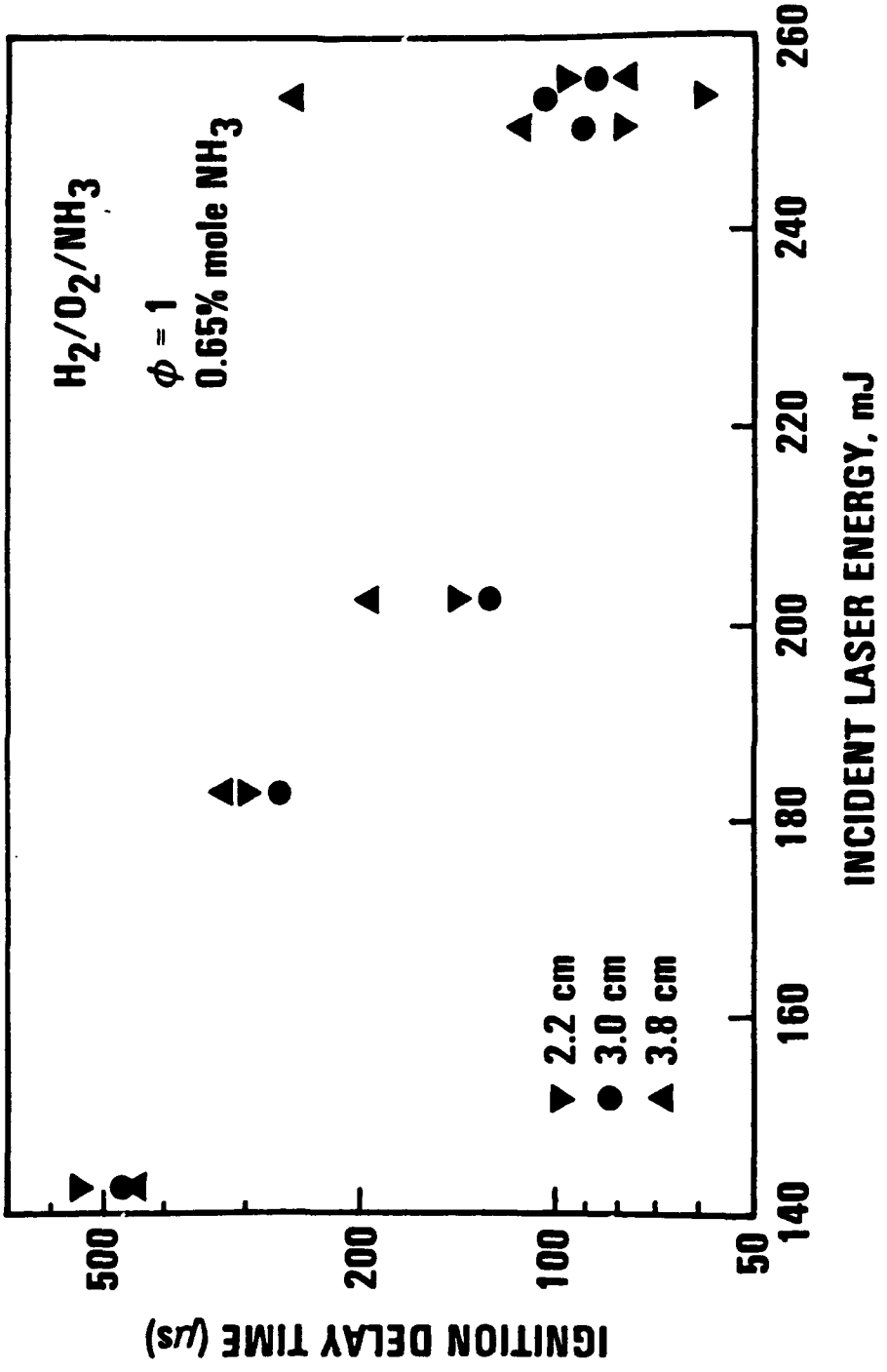
$H_2/O_2/NH_3$
$\phi = 1$
0.65% mole NH_3
▼ 2.2 cm
● 3.0 cm
▲ 3.8 cm
IGNITION DELAY TIME (μs)
500
200
100
50
140
160
180
200
220
240
260
INCIDENT LASER ENERGY, mJ

FIGURE 3.

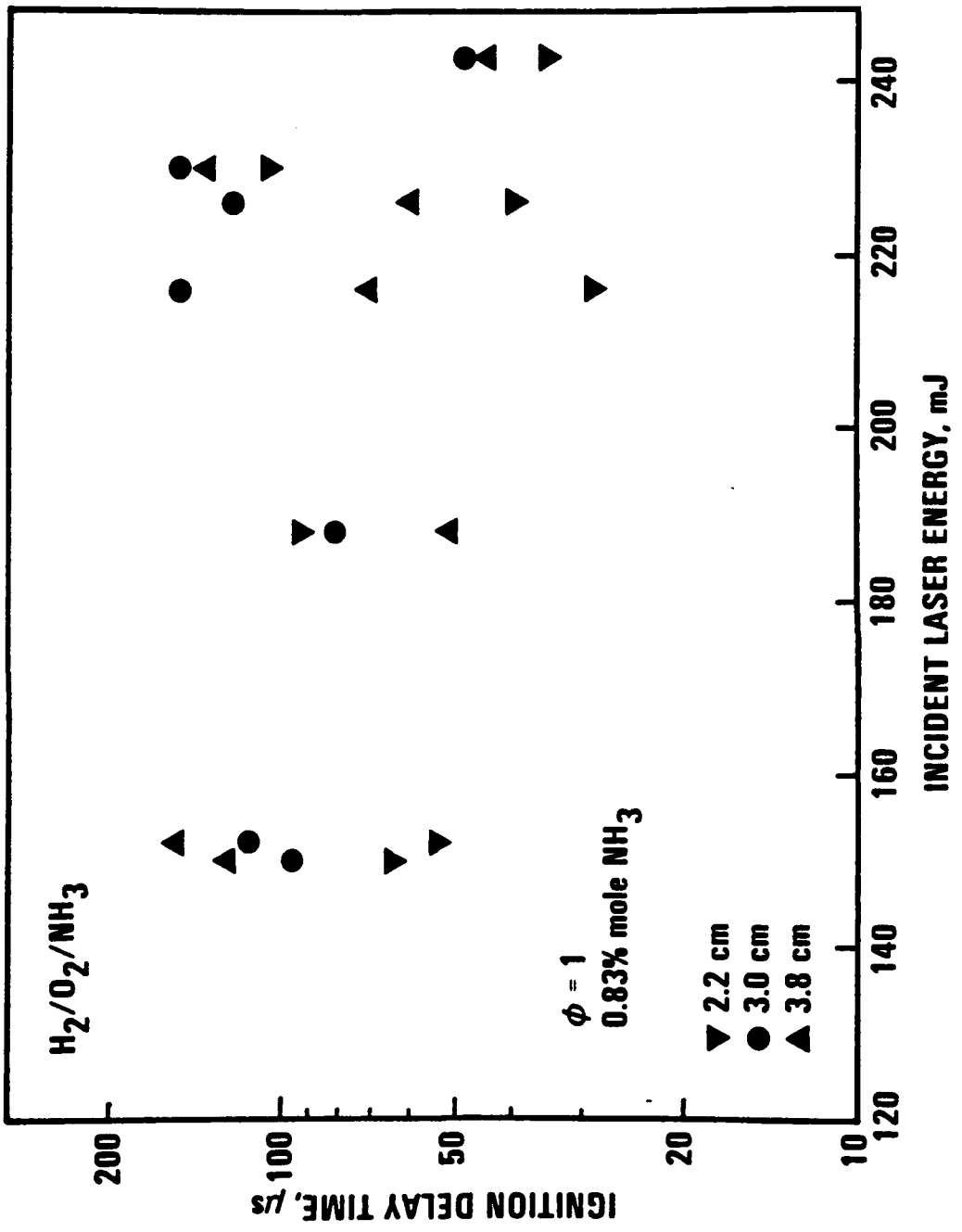
$H_2/O_2/NH_3$
$\phi = 1$
0.83% mole NH_3
▼ 2.2 cm
● 3.0 cm
▲ 3.8 cm
IGNITION DELAY TIME, μs
200
100
50
20
10
120
140
160
180
200
220
240
INCIDENT LASER ENERGY, mJ

FIGURE 4.

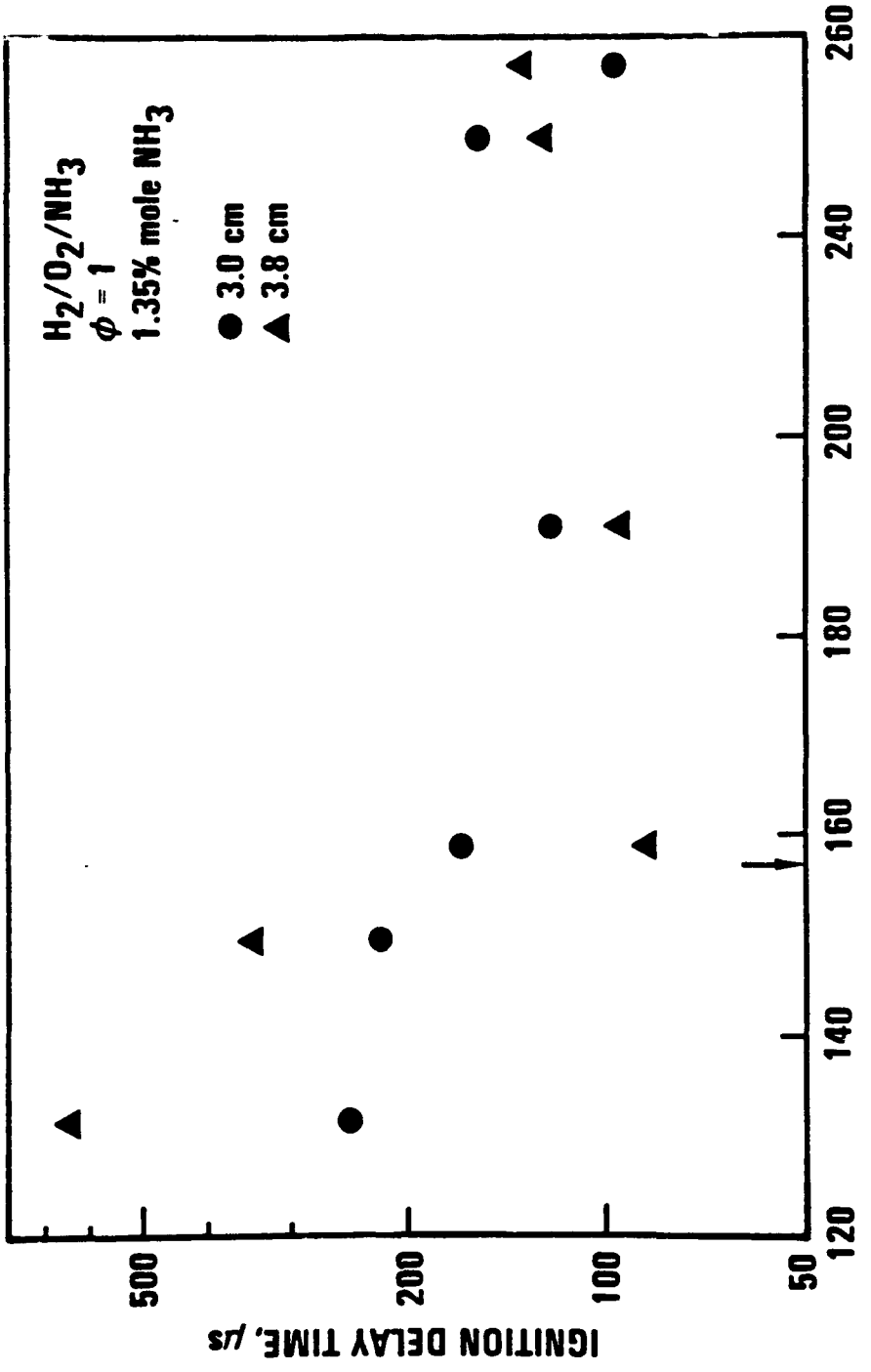
$H_2/O_2/NH_3$
$\phi = 1$
1.35% mole NH_3
● 3.0 cm
▲ 3.8 cm
IGNITION DELAY TIME, μs
500
200
100
50
120
140
160
180
200
240
260
INCIDENT LASER ENERGY, mJ

FIGURE 5.

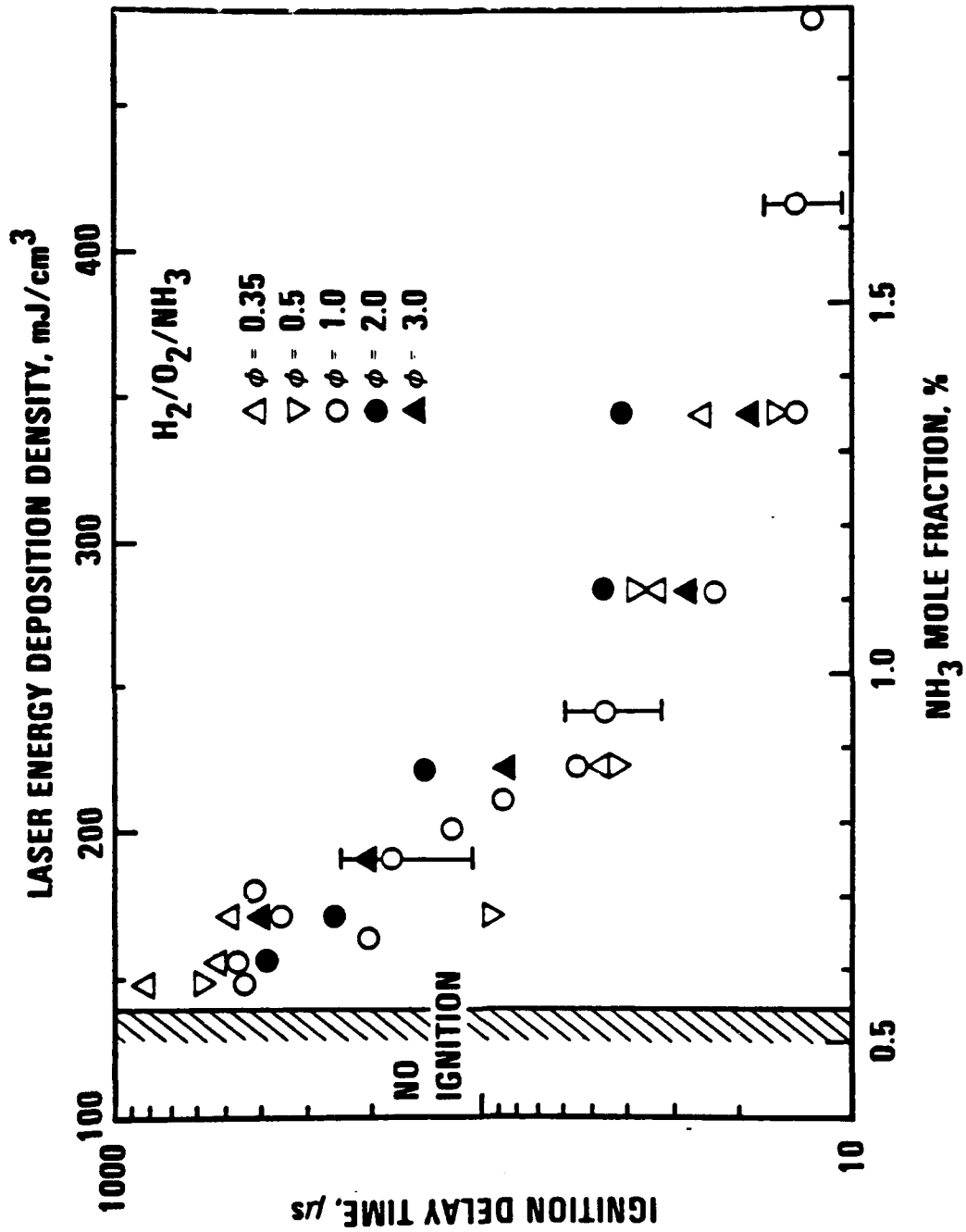
LASER ENERGY DEPOSITION DENSITY, mJ/cm3
400
300
200
100
H2/O2/NH3
Δ ϕ = 0.35
▽ ϕ = 0.5
○ ϕ = 1.0
● ϕ = 2.0
▲ ϕ = 3.0
NO IGNITION
1000
100
10
IGNITION DELAY TIME, μs
0.5
1.0
1.5
NH3 MOLE FRACTION, %

FIGURE 6.

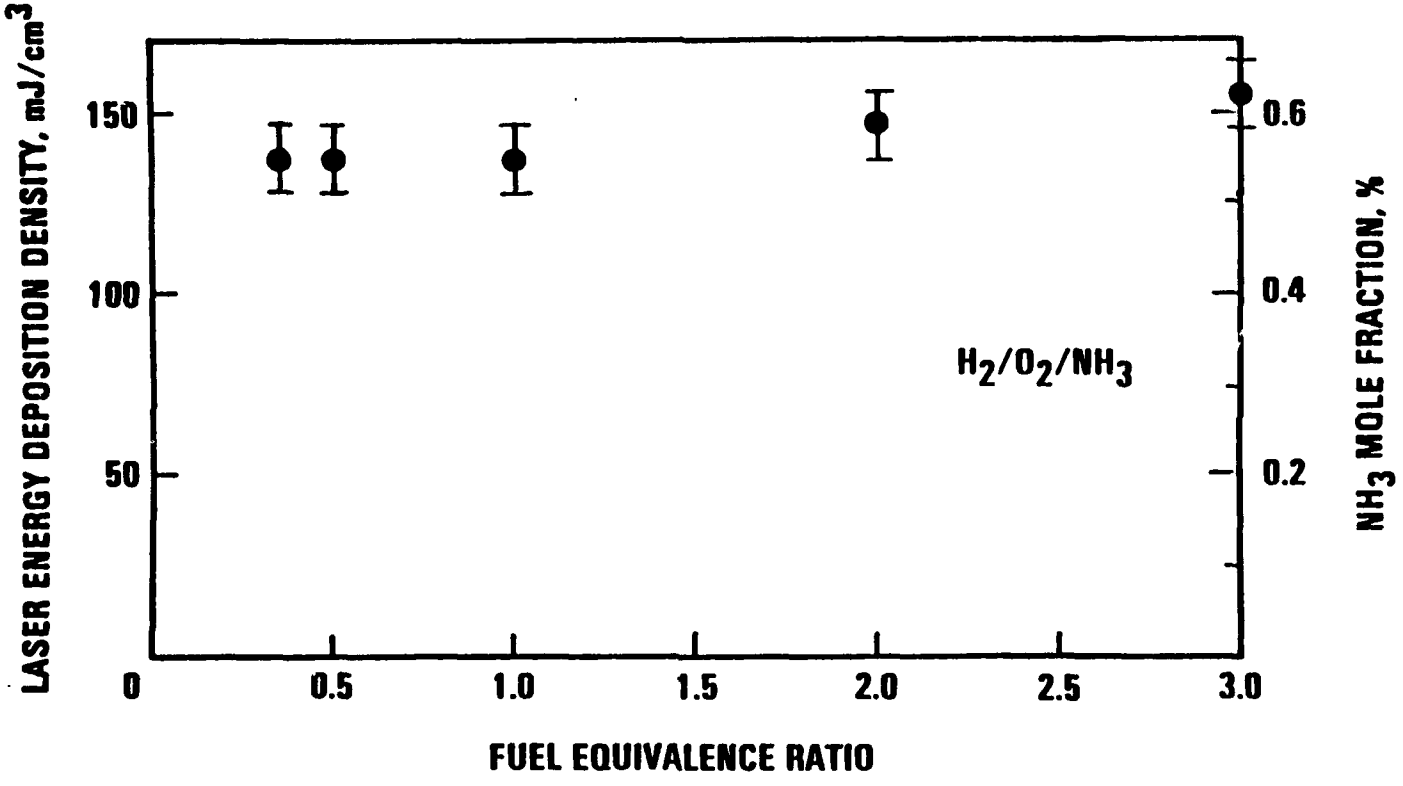
LASER ENERGY DEPOSITION DENSITY, mJ/cm3
150
100
50
0
0.5
1.0
1.5
2.0
2.5
3.0
FUEL EQUIVALENCE RATIO
H2/O2/NH3
0.6
0.4
0.2
NH3 MOLE FRACTION, %

FIGURE 7.

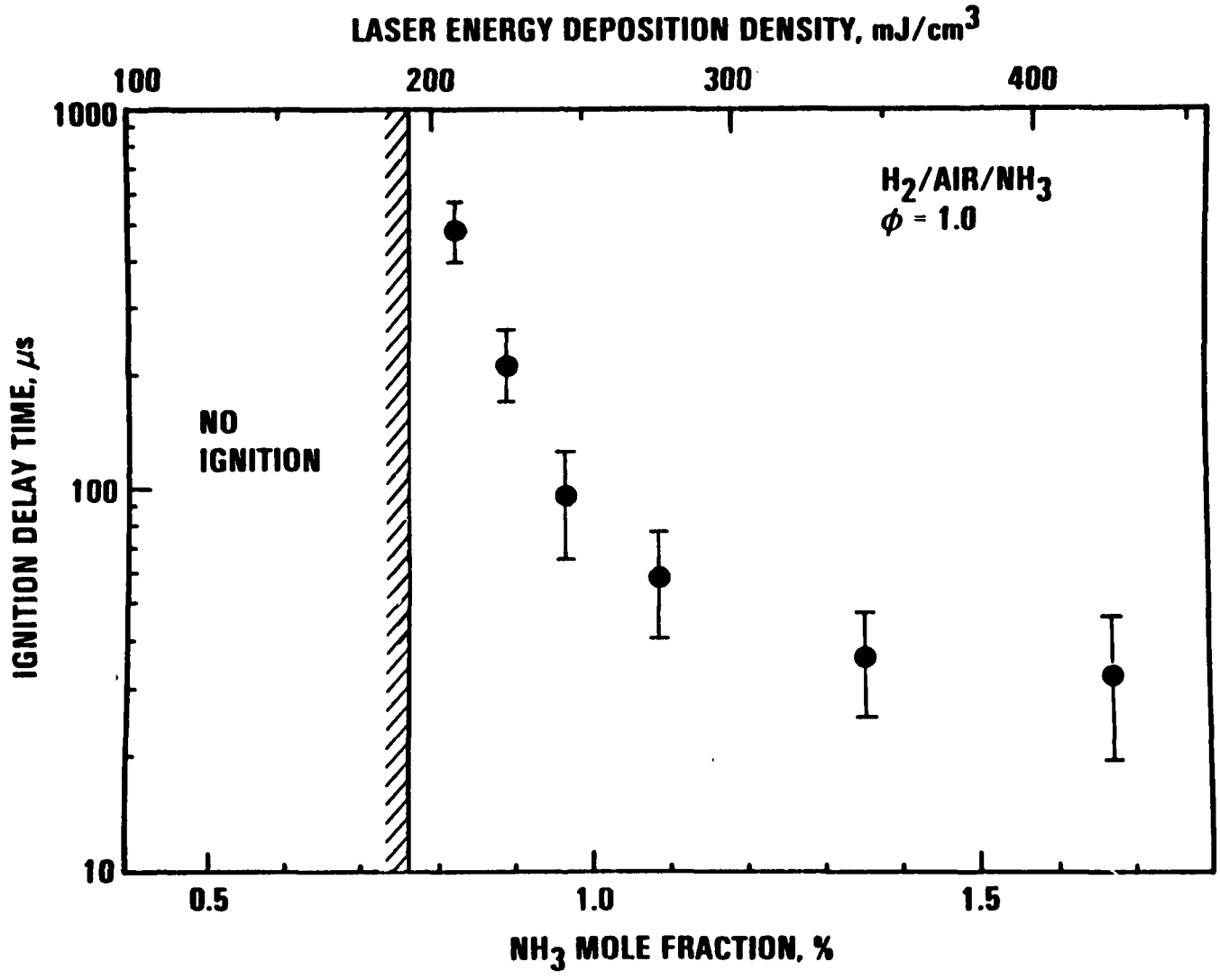
LASER ENERGY DEPOSITION DENSITY, mJ/cm3
100
200
300
400
1000
100
10
IGNITION DELAY TIME, μs
NO
IGNITION
H2/AIR/NH3
φ = 1.0
0.5
1.0
1.5
NH3 MOLE FRACTION, %

FIGURE 8.

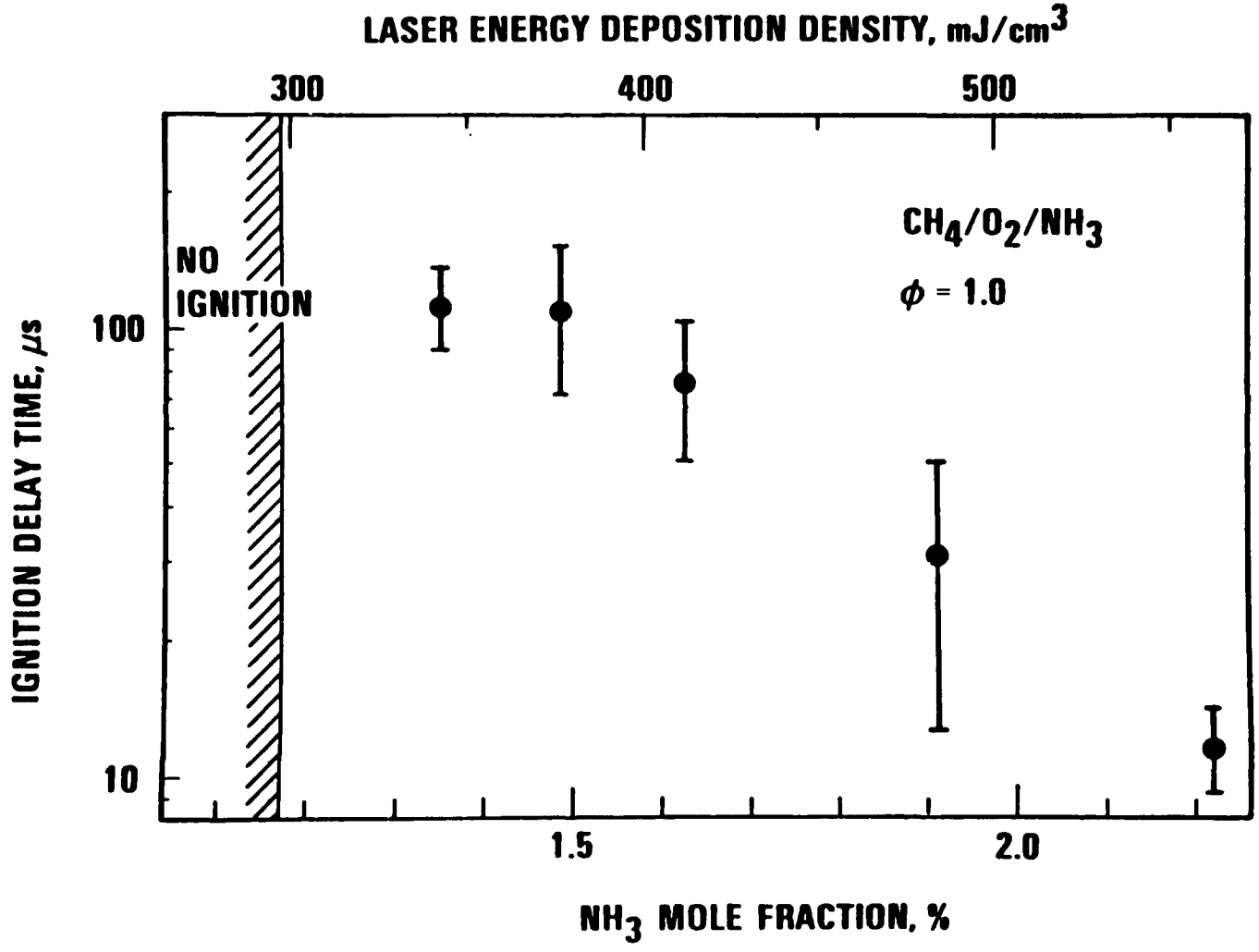
LASER ENERGY DEPOSITION DENSITY, mJ/cm3
300
400
500
NO
IGNITION
CH4/O2/NH3
φ = 1.0
100
10
IGNITION DELAY TIME, μs
1.5
2.0
NH3 MOLE FRACTION, %

FIGURE 9.

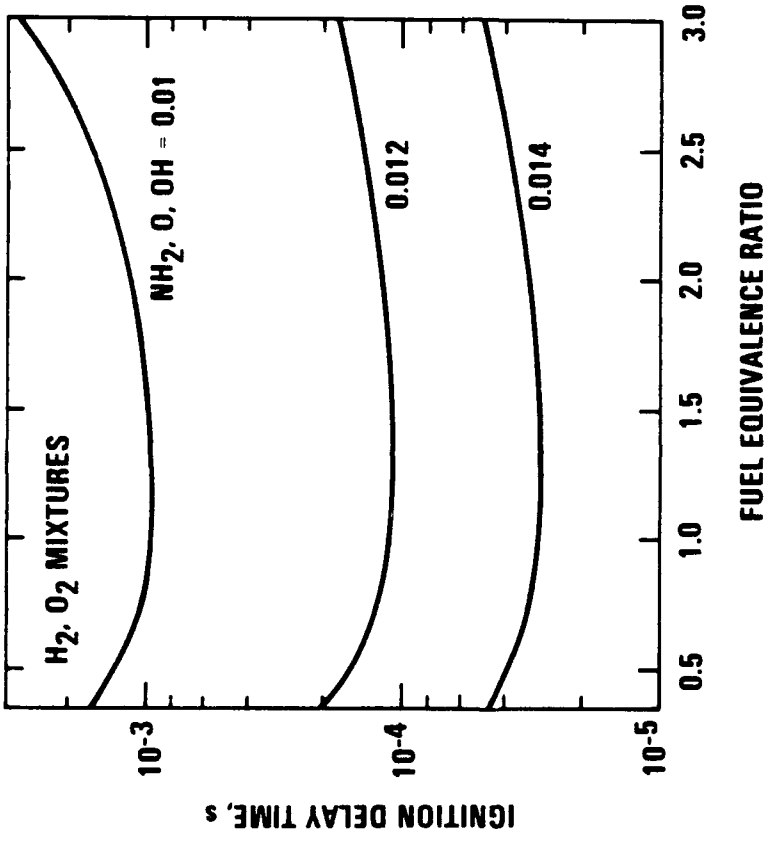
IGNITION DELAY TIME, s
10^{-3}
10^{-4}
10^{-5}
0.5
1.0
1.5
2.0
2.5
3.0
FUEL EQUIVALENCE RATIO
H_2, O_2 MIXTURES
NH_2, O, OH = 0.01
0.012
0.014

FIGURE 10.